Amplitude and Phase Noise in Modern CMOS Circuits

A DISSERTATION

SUBMITTED TO THE DEPARTMENT OF ELECTRICAL ENGINEERING

AND THE COMMITTEE ON GRADUATE STUDIES

OF STANFORD UNIVERSITY

IN PARTIAL FULFILLMENT OF THE REQUIREMENTS

FOR THE DEGREE OF

DOCTOR OF PHILOSOPHY

Reza Navid

June 2005

I certify that I have read this dissertation and that, in my opinion, it is fully adequate in scope and quality as a dissertation for the degree of Doctor of Philosophy.

Professor Robert W. Dutton

I certify that I have read this dissertation and that, in my opinion, it is fully adequate in scope and quality as a dissertation for the degree of Doctor of Philosophy.

Professor Thomas H. Lee

I certify that I have read this dissertation and that, in my opinion, it is fully adequate in scope and quality as a dissertation for the degree of Doctor of Philosophy.

Professor Bruce A. Wooley

Approved for the University Committee on Graduate Studies.

ABSTRACT

Understanding noise in submicron MOS devices is an ongoing challenge in the area of mixed-signal modeling. Experimental observations show that the classical long-channel MOSFET noise formulation underestimates the drain current noise of short-channel devices by a factor often referred to as the excess noise factor. The numerical value of this factor is still a matter of controversy, raising questions regarding the future of CMOS analog design. In order to predict the effects of this excess noise on amplitude and phase noise in future CMOS circuits, it is crucial to have a reliable MOSFET noise model and an accurate phase noise formulation.

In this dissertation we first present the semi-ballistic MOSFET noise model which is based on the transport properties of ballistic MOSFETs. Unlike most existing models, this model is not based on the long-channel formulation. Thus it does not require continual revision as we discover emerging short-channel effects. We first show that the dominant physical phenomenon responsible for noise in ballistic devices is the shot noise generated by the potential barrier next to source. We then use results of historic studies on vacuum tubes to show that noise in short-channel MOSFETs is partially-suppressed shot noise. Using this model, we study the overall noise performance of future MOSFETs and discuss its implications for the future of circuit and device engineering for analog applications.

We then discuss the effects of device noise on phase noise of electrical oscillators and present the time-domain formulation of phase noise, a method that is especially accurate for switching-based oscillators. The advantage of having an accurate phase noise formulation is twofold. It can be used to predict phase noise for a given device noise level and to calculate the device noise from phase noise measurements. The latter application is called indirect device noise characterization through phase noise measurement, a method that we introduce in this work. The time-domain phase noise formulation can also be used to investigate the properties of phase noise, especially at close-in frequencies. We explore all of these applications.

To validate our semi-ballistic MOSFET noise model we use detailed hydrodynamic device simulations and show that the predictions of our model for the behavior of noise versus temperature and noise versus biasing voltage are consistent with simulation results. The accuracy of our phase noise formulation is then verified by presenting experimental data on the phase noise of ring oscillators with various device sizes. Finally, we present an asymmetrical ring oscillator, especially-designed for MOSFET noise characterization. The accurately-predictable phase noise of this oscillator allows indirect characterization of device noise through phase noise measurements. We show that this method of extracting device noise parameters is much easier than direct noise measurements and, further, that these parameters substantiate the validity of our semi-ballistic MOSFET noise model. Our findings provide insight about the future of analog CMOS design, as well as guidelines for low-noise circuit design and device engineering.

ACKNOWLEDGMENTS

This doctoral dissertation would not have been possible without the help and support from many mentors, colleagues, friends and family members over the past four years. I would like to take this opportunity to express my gratitude to them to the extend which is possible through words.

First I would like to thank Prof. Robert Dutton, my Ph.D. adviser, for his invaluable support throughout my graduate study at Stanford. From the day I first met him on the visit day of 2001 till today, he has provided me with continuous encouragement and support. I am grateful to him for generating an environment in which I could concentrate on my work without excessive distractions of financial support and other tangential matters. His many industrial and academic liaisons have been a tremendous help for the completion of this work. Prof. Dutton's experience and vision has been a constant help to keep this project on the right path.

Prof. Thomas Lee, my associate advisor, also deserves special thanks. I cannot remember a single time that I walked into his office that a ten-minute discussion didn't save me weeks of hard work and literature search. The breadth and depth of his knowledge of electrical engineering and his understanding of the historic works have never failed to surprise me. I would like to express my appreciation for many enlightening discussions that I have had with him. He has also generously let me use Stanford's SMIrC laboratory for my measurements for which I am very grateful.

I would like to thank Prof. Bruce Wooley for accepting to be on my thesis reading committee and for his help regarding access to National Semiconductor's fabrication process. Special thanks also goes to Prof. Donald Cox for accepting to be my oral exam's committee chairman.

I am grateful to the fabulous members of Stanford TCAD group whose help has been essential for the completion of this work. I would like to thank Fely Barrera for her friendly assistance on administrative matters. Special thanks also go to the other members of the Stanford TCAD group: Tze Wee Chen, Changhoon Choi, Jung-Hoon Chun, Minghui Han, Choshu Ito, Jae Wook Kim, Hai Lan, Bih Le, Xiaoxiang Liu, Yang Liu, Yi-Chang Lu, Parastoo Nikaeen, Miho Nishi, Shinji Onga, Eric Pop, Justin Snapp, Olof Tornblad, Georgios Veronis and Dan Yergeau.

I would also like to thank the members of the research groups of Prof. Tom Lee, Prof. Simon Wong and Prof. Bruce Wooley with whom I have had many helpful and enjoyable discussions. The presence of these smart people have made working at Stanford an enjoyable and unforgettable experience.

Many colleagues have assisted me in this project. Special thanks go to Christoph Jungemann who is now with Technische Universitaet Braunschweig. During his one-year stay in Stanford, and ever since, he has been a constant source of help and support. Without him, many of the hydrodynamic device simulation results would not have been possible. I would like to thank Arjang Hassibi for many hours of discussion and for his generous help on most of the graphical demonstrations presented in this work. My special gratitude also goes to Dr. Omer Oralkan, Dr. Shwetabh Verma, Ali Javey, Dr. Sunderesan Mohan, Samuel Martin, Prof. Ali Hajimiri, Hossein Kakavand, Sam Kavusi, Ali Agah, Dr. Theresa Kramer, Scott Kulchycki, Prof. Ali Niknejad, Dr. Eric Pop, Prof. Jaijeet Roychowdhury, Dr. Patrick Yue and Sina Zahedi, among other colleagues. They have been of tremendous help for the completion of this work.

I would also like to take this opportunity to thank the entire staff of the Center for Integrated Systems of Stanford University which is the home to the Stanford TCAD group. The friendly staff of CISX and CIS have made four years of working in this center an experience to remember. I would also like to thank National Semiconductor for the fabrication of the integrated circuits.

During my four-year stay in Stanford, I have had the privilege of befriending many great people at Stanford and in the Bay area. The presence of these friends have made my stay a rich and memorable experience, both professionally and socially. Also my friends in other places in the US and back home have been a continuous source of support and encouragement. Special thanks go to Payman Shanjani, Jafar Savoj, Amin Firouzshahian, Ali Faghfuri, Pouya Kavousian, Shahriyar Azizpour, Mehdi Javanmard, Sam Kavusi, Ali Kiaei, Alireza Nojeh, Arjang Hassibi, Parastoo Nikaeen, Rostam Dinyari, Shayan Behzadi, Reza Azadegan, Abbas Abbaspour, Pouya Valizadeh, Masoud Agah, Pedram Mohseni, Maysam Ghovanloo, Shahram Taghavi, Omid Momtahen, Okhtay Taghizadeh, Vahbod Pourahmad, Shadi Oveisgharan, Yashar Ganjali, Abtin Keshavarzian, Shahriyar Matloub, Mona Jarrahi, Omer Oralkan, Kambiz Kaviani, Scott Kulchycki, Yi Lu, Mehdi Mohseni, Mohsen Bayati, Alireza Khalili, Amir Amirkhani, Bita Nezamfar, Neda Beheshti, Negin Nejati, Arash Altoontash, Sina Zahedi, Hossein Kakavand, Jia Li, Sina Sohangir, Azita Emami, Babak Heidari, Ali Motamedi, Hesam Aslani, Masoud Sharif, Eric Pop, Greg Cooley, Johnny Madrid, Mehdi Soltan, Hamid Rategh, Amirali Talasaz, Amin Nikoozadeh, Mahan Esfahani, Yaser Khalighi, Pouya Sarabandi, Nima Asgharbeygi, Alireza Kashef, Navid Hasanpour, Ali

Javey, Ali Mani and Dara Ghahramani. I have learned many things from these people through discussion on topics which often had nothing to do with electrical engineering.

During these years, my involvement in several student and social organizations have enriched my life as a graduate student and made it possible to know many fabulous people. I would like to thank the members of Persian Student Association, Islamic Society of Stanford University, KZSU (Stanford's student-operated radio), Stanford's Technical Communications Program, Stanford Outing Club and LANIC4All. I have been a proud member of all of these organizations.

This dissertation would not have been possible without the support and encouragement from my family. I would like to thank my brother and my sisters. Without their help and inspiration, I could not have completed this work.

My parents deserve special thanks for the completion of this dissertation. Without their encouragement, support and sacrifice, I would not have made it to Stanford and could not have finished this dissertation. I would like to take this opportunity to express my deepest gratitude for what they have done for me. This is the extent to which my appreciation can be expressed through words and I believe it comes tremendously short of what is due. This work is dedicated to my parents.

TABLE OF CONTENTS

LIST OF TABLES

List of Illustrations

CHAPTER 1:

INTRODUCTION

Understanding noise in electronics is an important problem for integrated systems. The performance of many of these systems is affected by noise in various ways. For example, electrical noise is one of the key factors that determines the maximum possible communication speed in communication systems. Electrical noise also determines how many users can share the same transmission media. In high-precision measurement systems, electrical noise dictates the maximum achievable precision. At the circuit level, the dynamic range of a circuit is limited on one side by its noise. At the device level, the minimum achievable noise figure is one of the most important parameters for an active device. Because of all these practical considerations, noise in electronic systems has been under investigation for several decades.

Noise in electrical systems can be divided into two components in general: amplitude noise and phase noise. Amplitude noise is a measure of random fluctuations of electrical signal around its nominal value. These random, unwanted fluctuations make it difficult to detect the desired signal and degrade the performance of the system when working with small-amplitude signals. Electrical engineers normally define a parameter called noise figure to characterize amplitude noise for a given system. The formal definition of noise figure is the signal-to-noise ratio at the input of the system divided by the signal-to-noise ratio at its output [1].

Unlike amplitude noise, which is present in all systems, phase noise is only observed in oscillatory systems. The phase noise of an oscillatory system is a measure of random deviations of its oscillation frequency from a nominal value. These deviations are due to the various noise sources in the system which modulate its oscillation frequency. The formal definition of phase noise is based on the distribution of signal power around the nominal frequency and will be discussed in Chapter 3.

Amplitude and phase noise affect the performance of electrical systems in different ways. Fig. 1 shows the effect of these two noise components on the performance of an RF receiver. This figure

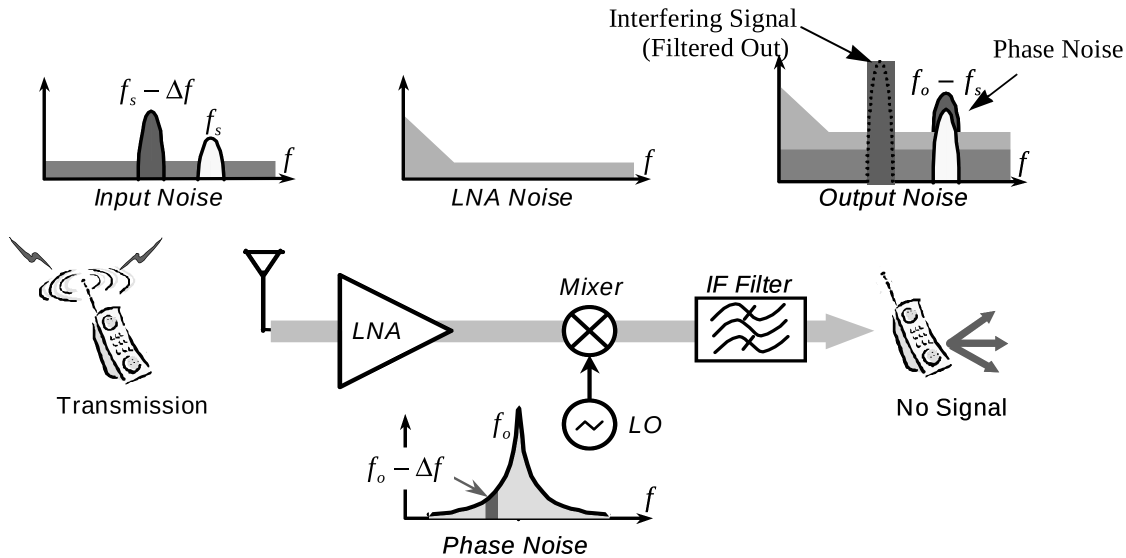

Fig. 1: Front-end of an RF receiver and the effect of amplitude and phase noise on its performance.

shows the front-end blocks where noise has the most serious influence. Amplitude noise (e.g. LNA noise) adds to the original noise floor of the input signal degrading the signal-to-noise ratio at the output of the LNA and consequently at the output of the IF filter. The effect of phase noise of the local oscillator is also graphically shown in this figure. As can be seen, the frequency instability of the local oscillator results in non-zero power at some offset frequency, Δf, from the nominal oscillation frequency (in the absence of phase noise, the spectrum of the LO would be a delta function at f_o). The signal power located around f_o-Δf can be modulated by an interfering signal at f_s-Δf, generating a noise component at f_o-f_s. Unfortunately, this noise component cannot be filtered out by the IF filter because it has the same frequency as the IF signal. Thus, phase noise adds another component to the noise at the output of IF filter. The combination of these two noise sources degrades the signal-to-noise ratio at the output of IF filter and can potentially mask the input signal, as can be seen in this figure.

Both amplitude and phase noise in electrical systems are generated by noise sources in individual electronic elements. As we will discuss shortly, there is a nonzero amount of noise associated with all these elements. The analysis of noise in electrical systems starts with a careful characterization of these noise sources using physical and sometimes empirical models. Once these noise sources are sufficiently characterized, the analysis of noise at the circuit and system levels is performed using well-developed mathematical methods. Accurate characterization of device noise appears to be the most challenging part of electrical noise analysis.

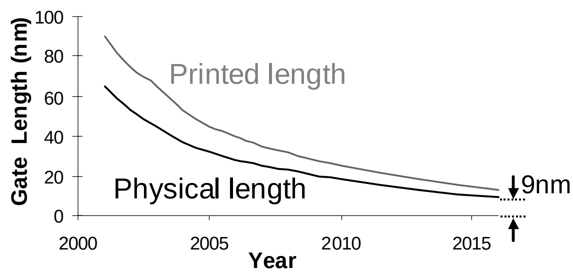

Fig. 2: Future MOSFET device technologies up to 2017 (ITRS 2002 update).

Today, MOSFETs are the most popular active devices for commercial applications. Therefore, having an accurate noise formulation for these devices is crucial for analog applications. Extensive research in this area has brought us a classical formulation of MOSFET noise which can accurately predict noise in long-channel MOSFETs. However, experimental observations show this formulation may underestimate the drain current noise of short-channel MOSFETs. Several studies have tried to explain this phenomenon. As we will see in Chapter 2, these studies have not yet led to a final answer.

Noise in short-channel MOSFETs might continue to increase as we shrink transistors. According to the 2002 International Technology Roadmap for Semiconductors, transistors as small as 9 nm in physical gate length will be available by 2017 (Fig. 2). As can be seen in Fig. 3, the majority of noise in typical CMOS technologies is due to the intrinsic MOS noise. Thus, it is important to have a clear understanding of noise in these devices to predict scalability and limits for future low-noise CMOS design. In this work, we focus on the noise properties of future MOSFETs and present a physics-based noise model for these devices.

One of the major difficulties of noise modeling for electronic elements is model verification. Measuring amplitude noise is usually a difficult process; it requires careful de-embedding of parasitic elements as well as accurate control of environmental parameters. Fortunately, measuring phase noise in electrical oscillators is a relatively easy process, as we discuss in Chapter 3. This is because the phase noise measurement is a comparative measurement between the power at the fundamental frequency and the power at some offset from it. Therefore, many of the parasitic elements are not important in this measurement. Furthermore, only the physical parameters of the elements which are **inside** the oscillator loop are important for phase noise. Thus it is easier to control the environmental parameters in this kind of measurement.

In this work, we introduce indirect noise characterization through phase noise measurement. To

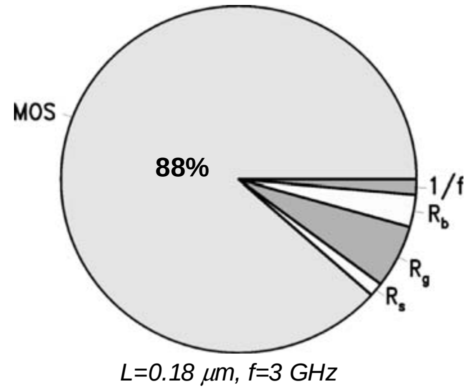

Fig. 3: Relative significance of various noise sources in a typical 0.18 micron CMOS technology [2].

provide an accurate characterization, we first present an accurate phase noise formulation for the specific oscillator topology used in our experiment (Chapter 3). The advantage of our phase noise formulation is twofold; it can be used for indirect noise characterization and it can be used for predicting phase noise in oscillators if the device noise in known. For this formulation to be most useful, we present Chapter 3 as a self-sufficient chapter. We also present some of the implications of our phase noise formulation such as the minimum achievable phase noise of *RC* oscillators and the properties of close-in phase noise in this chapter.

The connection between Chapter 2 and Chapter 3 will become clear in Chapter 4 where we verify our model using simulation and experiment. In this chapter, we first verify our MOSFET noise model using device simulations. Our phase noise formulation is then verified using experimental work. Finally, we use indirect characterization of device noise to verify our device noise model using phase noise measurement. Note that the absolute accuracy of this method remains inferior to amplitude noise measurements because of the approximations involved in the phase noise formulation. Nevertheless, this method provides a relative accuracy which suffices in many practical cases. Furthermore, as we will see in Chapter 4, special oscillator structures can be designed for which phase noise is predictable with higher accuracy.

Our formulation of device noise provides insight about the future of MOSFET noise, while our phase noise formulation can be used for device noise characterization or as an independent tool for studying oscillators. Chapter 5 discusses these applications and summarizes our findings on amplitude and phase noise in CMOS circuits. These findings can help designers understand the origins of noise in future CMOS circuits and provide them with guidelines for designing low-noise devices and circuits.

CHAPTER 2:

AMPLITUDE NOISE IN MOSFETS

For the decades following the pioneering work of J. B. Johnson [3], the study of noise in electrical devices has been an exciting research topic. During these years, the emergence of each new device has stimulated researchers to investigate its noise behavior. After the commercialization of MOSFETs in the early 60s, extensive investigations were launched that helped designers understand major MOSFET noise sources in less than a decade. These investigations revealed that there are two partially-correlated noise sources in every MOSFET: channel thermal noise [4] and induced gate noise [5]. By 1970, the classical formulation of MOSFET noise was finalized. This formulation was subsequently validated through measurements which substantiated its accuracy for existing MOSFETs.

In 1986, Jindal [6] and Abidi [7] suggested that the classical noise model underestimates noise in short-channel devices. Since then, several studies have tried to replicate those results or theoretically explain this phenomenon. As can be seen in Fig. 4, these investigations have led to different (and sometimes conflicting) results for MOSFET noise behavior. Today, these studies generally agree on one fact: If noise in short-channel MOSFETs is higher than classically predicted, it is by factors much smaller than reported in early investigations such as [7].

Understanding noise in short-channel MOSFETs is thus an ongoing challenge. Most existing short-channel noise models are based on the aforementioned classical formulation, modified to accommodate emerging short-channel effects. Unfortunately, these models often need continual revision because MOSFET scaling is an ongoing process. Furthermore, they usually fail to clearly predict noise performance of future devices. In this chapter, we present a new noise model for short-channel MOSFETs. The advantage of our model is that it is not founded on the classical formulation of MOSFET noise. Rather, it is based on a noise model that we directly derive for future ballistic MOSFETs[1].

The organization of this chapter is as follows. We first present some basic definitions which will be helpful for studying amplitude and phase noise in electrical systems. We then briefly discuss noise in electrical elements and present the classical formulation of noise in MOSFETs. This formulation is followed by a brief survey of existing short-channel noise models. We then present a model for noise in ballistic MOSFETs which is subsequently modified to fit today's short-channel devices. Finally, we use our simple model to predict the overall noise performance of future devices.

2.1. EXISTING MOSFET NOISE MODELS

2.1.1. Basic definitions

Electrical noise is a measure of random fluctuations of current or voltage at the terminals of an electrical element. These fluctuations originate from the discrete nature of charge carriers and their random movement[2]. At any non-zero temperature, charge carriers undergo a random motion that induces a voltage noise, $v_n(t)$ and/or a current noise, $i_n(t)$, on device terminals. These functions are mathematically referred to as random processes. In this subsection, we briefly discuss the properties of such functions.

A random process $x_n(t)$ (which can be current or voltage noise) is a function of time whose value at any given moment is a random variable. Such a process can be studied in either the time or frequency domain. To study this process in the time domain, we need the probability distribution function (PDF) of $x_n(t)$ for all t and the conditional PDF of $x_n(t)$ if the value of x_n is known at t_1, t_2, t_3,..., t_n, for any given n. Thus, we need an infinite number of PDFs to fully characterize a general random process in time domain.

In practice, we can use several simplifying assumptions to facilitate the characterization of random processes. Many practical random processes, including those studied in this work, are wide-sense stationary Gaussian[3] processes which are sufficiently characterized by values of their mean, mean square, and covariance.

---

1. As MOSFET scaling continues, carriers face progressively fewer scattering events in the channel. Ultimately, MOSFETs are expected to become so small that a carrier would travel from source to drain without scattering. Such a movement is called a ballistic movement and these devices are known as ballistic devices.

2. Current and voltage fluctuations can also originate from other sources such as electromagnetic interference and power supply noise. We will not study this kind of noise.

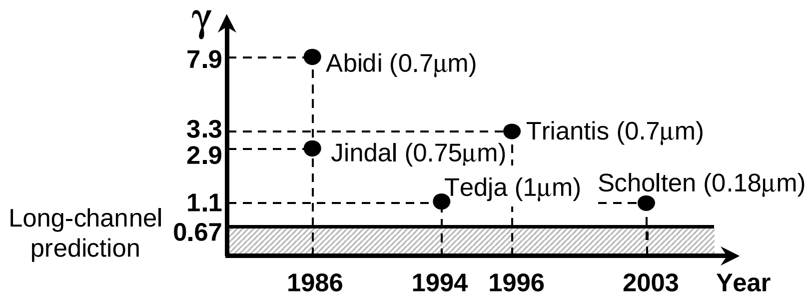

Fig. 4: Some reported values of measured noise factor in short-channel MOSFETs compared to the long-channel prediction. The numbers given in the parentheses are channel lengths of the devices under investigation.

To characterize a random process in the frequency domain, we need the definition of power spectral density (PSD) which is based on Fourier transform. Unfortunately, the Fourier transform of $x_n(t)$ is often undefined because the total energy of noise in many cases is infinite. To circumvent this difficulty, the definition of PSD is based on the Fourier transform of a windowed version of $x_n(t)$. The formal definition of the unilateral PSD, which will be used in this work, is as follows:

$$\overline{S_x(\omega)} = \begin{cases} \lim\limits_{T_w \to \infty} \dfrac{2\overline{|X_w(j\omega)|^2}}{T_w} & \omega \geq 0 \\ 0 & \omega < 0 \end{cases} \tag{1}$$

where $X_w(j\omega)$ is the Fourier transform of $x_w(t)$, a windowed version of $x_n(t)$ that is the same as $x_n(t)$ for $-\frac{T_w}{2} < t < \frac{T_w}{2}$ and zero otherwise.

It is important to understand the physical meaning of the PSD. The PSD at any frequency gives the signal power that is concentrated in 1 Hz of bandwidth around that frequency. The unit of PSD is x_{un}^2/Hz, where x_{un} is the unit of $x_n(t)$. It can be shown that for wide-sense stationary processes, the PSD is the Fourier transform of the autocorrelation function [8]. This theorem is known

3. A process is called wide-sense stationary if its mean, $\overline{x_n(t)}$, and mean square, $\overline{x_n^2(t)}$, are independent of t and its covariance, $\overline{x_n(t_1)x_n(t_2)}$, is only a function of t_1-t_2 (not t_1 or t_2). A process is called Gaussian if the PDF of $x_n(t)$ and all of its conditional PDFs are Gaussian.

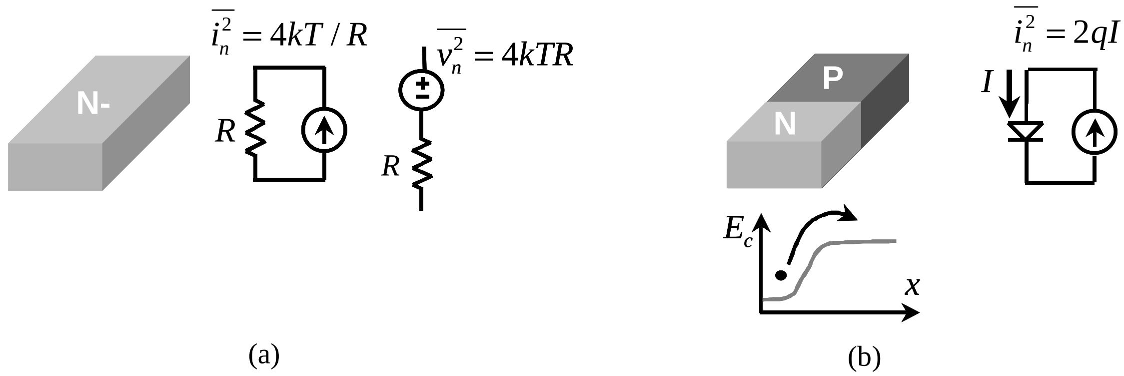

Fig. 5: Noise PSD in equilibrium is dictated by the fluctuation-dissipation theorem and Nyquist formula (a). Under non-equilibrium conditions, noise formulation is much more complicated. A famous non-equilibrium case is the appearance of shot noise in the presence of potential barriers such as PN junctions (b).

as the Wiener-Khinchin theorem. By definition, if the PSD of a process is independent of frequency, the process is called a process with white spectrum. For such a process the autocorrelation function is a delta function which means that the process has no memory of its past. Therefore, a process with white spectrum is a memory-less process and vice versa. To characterize a wide-sense stationary Gaussian, memory-less random process with zero mean, it is sufficient to have its PSD at a single frequency.

The discussion presented in this subsection will prove useful for studying amplitude and phase noise in electrical systems. However, the reader is strongly encouraged to consult [8] for a thorough discussion of random processes and random functions.

2.1.2. Noise in electrical elements

To analyze noise in an electrical element we must quantitatively characterize the fluctuations of the electrical signal (current and/or voltage) which can be sensed at its external terminals. For the purpose of this characterization, electrical systems can be divided into those in thermal equilibrium and those in non-equilibrium. Thermally-equilibrated systems are those in which there is no electrical current or energy flow. In general, a thermally-equilibrated system can have a potential difference between its terminals. For example, a MOSFET with v_S=v_D=v_B is in thermal equilibrium for most practical purposes regardless of the voltage on its gate terminal.

Formulation of noise in equilibrated systems is relatively straightforward and is based on the fluctuation-dissipation theorem of thermodynamics. According to this theorem, dissipative properties of a system provide sufficient information to characterize its fluctuation properties under equilibrium conditions [9]. Thus, the equilibrium noise properties of a system are fully known if one can calculate or measure its dissipative properties. For example, the noise of a resistor in equilibrium can be modeled by a voltage (current) noise source in series (parallel) with the resistor with a white PSD of $4kTR$ $(4kT/R)$ (Fig. 5). In general, the PSD of the noise voltage that appears at any open terminal of an equilibrated system is white and is given by $4kTR$, where R is the real part of the impedance seen from this terminal. The PSD of the current noise which would flow into this terminal (if it were shorted externally) is white too and is given by $4kT/R$. This result is known as the Johnson-Nyquist formula, which was first suggested by the experimental work of Johnson [3] and subsequently derived by the theoretical work of Nyquist [10]. The Johnson-Nyquist formula, which can also be derived using Brownian motion analysis [11], is considered a special case of the fluctuation-dissipation theorem [9].

The formulation of noise under non-equilibrium conditions is generally more complicated because a full understanding of dissipative properties is no longer sufficient for noise calculations [9][4]. The Johnson-Nyquist formula cannot be proved for non-equilibrium systems using either the Nyquist approach [10] or with Brownian motion analysis [11]. However, experiments show that non-equilibrium noise in *macroscopic* resistors is the same as its equilibrium value and is given by the Johnson-Nyquist formula. It is important to note that this result does not necessarily hold for microscopic resistors; it specially breaks down in mesoscopic conductors as will be discussed shortly [12][13].

Although a general formulation of noise in non-equilibrium is not available, this formulation can be performed in special cases. A famous case is illustrated in Fig. 5. It can be shown that if the injections of carriers across a potential barrier are mutually independent, fluctuations of current have a white spectrum with a PSD of $2qI$, where q is the quantum of charge and I is average rate of charge flow (current) [8]. Thus, the noise of the device can be modeled by a current noise source in parallel with the barrier with a PSD of

$$\overline{S_i(\omega)} = 2qI. \tag{2}$$

This noise source is known as shot noise and is observed in PN junctions, BJTs and cathode tubes. We will use this formula for our formulation of noise in ballistic MOSFETs.

---

4. This means that we can improve our understanding of carrier transport in a non-equilibrated system by studying its noise behavior, something that is not possible for an equilibrated system. This is a very useful insight.

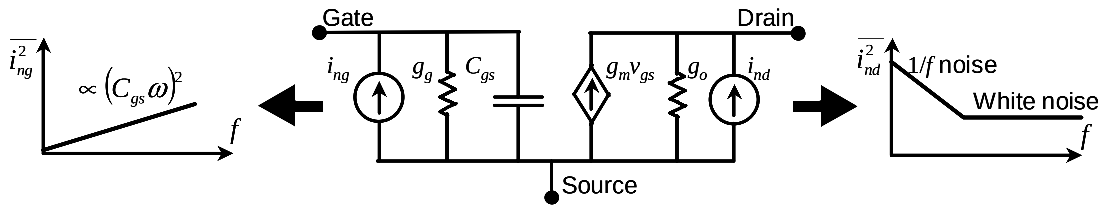

Fig. 6: The equivalent circuit of a MOSFET working in the saturation region, and the PSD of its noise sources.

2.1.3. Classical formulation of MOSFET noise

According to the classical formulation, high-frequency noise in MOSFETs originates from the random thermal motion of carriers in the channel. For noise analysis, it is usually assumed that the source (which is also connected to body) is the common terminal. The purpose of MOSFET noise analysis is to characterize quantitatively the noise currents that would flow in the drain and gate terminals if they were ac-shorted to the source terminal. These noise currents are called drain and gate noise. From a circuit point of view, these noise currents can be modeled by two noise current sources connected between drain and source, and gate and source, respectively. These noise sources are partially correlated because of their shared origin. For full characterization of MOSFET noise, we must calculate the PSD of these two sources as well as their correlation factor (a complex number in general).

Fig. 6 shows a noise equivalent circuit for a MOSFET working in the saturation region along with the PSD of its noise sources. As can be seen in this figure, the drain noise PSD increases at low frequencies due to the $1/f$ noise that is observed in nearly all non-equilibrated devices. The appearance of this noise in MOSFETs is usually linked to traps. The properties of this noise will not be studied in this work; for a comprehensive discussion, please see [9].

Fig. 6 also shows that the PSD of the gate noise increases at high frequencies. This increase is due to the capacitive coupling of channel carrier fluctuations to the gate. We will not discuss this noise source or its correlation to the drain noise here; it is left for future work. Instead, we focus on the fluctuation properties of the high-frequency portion of the drain noise, hereafter briefly referred to as drain noise and denoted by i_{nd}.

The classical approach for the formulation of drain noise PSD is graphically shown in Fig. 7. In this approach, the channel is first sliced into small pieces of resistance dR. These slices are then replaced by their noisy model and the noise contribution of each slice at the output terminal is calculated using analytical or numerical means. Subsequently, these contributions are summed up,

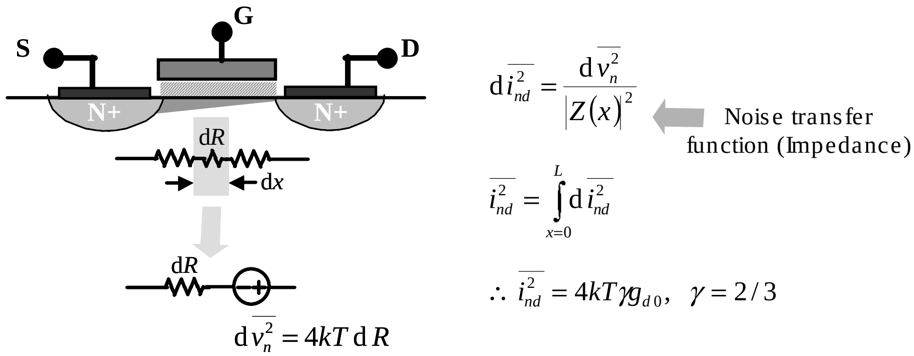

Fig. 7: Classical formulation of MOSFET noise.

assuming independence, to give the total device noise. This formulation leads to the famous Klaasen and Prins equation which gives the PSD as [14]

$$\overline{S_{ind}} = \frac{4kT}{L_c^2 i_D} \int_0^{v_D} g^2(v)dv\,. \tag{3}$$

Here, k is Boltzmann's constant, T is the absolute temperature, L_c is channel length, i_D and v_D are the dc drain current and voltage, respectively and $g(v)$ is the channel conductance at a point in channel with potential v with respect to the source. Performing the integration for an ideal MOSFET, we find PSD of the drain noise as [15][16]

$$\overline{S_{ind}} = 4kT\gamma g_{d0}\,, \tag{4}$$

where γ is a constant whose numerical value is 2/3 for devices working in saturation and g_{d0} is the output conductance of the device for v_D=0 (with the value of v_G unaltered).

The classical formulation of noise in MOSFETs is, in fact, based on a more general approach called the impedance field method (IFM) [17]. In this method, we first divide the device into small volumes (segments in 1-D analysis). We then calculate the contribution of the noise of each segment at the output terminals using an impedance transfer function. The validity of this method is not limited to MOSFETs; it can be used to prove the Johnson-Nyquist noise formula as well as to calculate noise under non-equilibrium condition. This method is usually used in device simulators to numerically calculate terminal noise currents [18].

2.1.4. Existing short channel noise theories

Although the classical formulation accurately predicts drain noise in long-channel MOSFETs, it is believed to underestimate noise in short channel devices (e.g. [6][7]). To characterize the excess noise in short-channel MOSFETs, a noise factor is normally defined as

$$\gamma = \frac{\overline{S_{ind}}}{4kTg_{do}}. \tag{5}$$

Fig. 4 shows some reported values of measured noise factor for short-channel MOSFETs compared to the long-channel prediction. For several years, researchers have proposed various methods to explain this excess noise and predict its power. In this subsection, we present a brief survey of these methods.

Excess noise in short channel devices is sometimes explained using detailed multidimensional device simulations (e.g. [19] [20]). These simulations confirm the existence of excess noise in short-channel MOSFETs and suggest that most of this noise is associated with the source end of the channel [19]. Multidimensional simulations can be done using various orders of transport models[5]. Bonani and colleagues use the drift-diffusion model and show that it fails to capture excess noise in short-channel devices even in 3-D simulations [20]. To capture excess noise, higher order transport models such as the hydrodynamic model must be used. Therefore, using the right transport model appears to be the crucial factor for noise analysis in short-channel MOSFETs.

In another effort to explain excess noise, Goo and colleagues use the classic impedance field method (IFM) for a 1-D analysis with device parameters extracted from 2D simulations. For parameter extraction, they employ both hydrodynamic and drift-diffusion transport models and compare the results [18]. They show that the hydrodynamic transport model gives much better results compared to the drift-diffusion model. This observation reinforces that the key issue in modeling noise in submicron devices is a thorough understanding of transport mechanisms.

The data presented by Goo shows that although his approach is accurate at high gate voltages with respect to source, it loses its accuracy at small gate voltages [18]. This result can be explained by looking at carrier transport in MOSFETs. At small gate voltages, smaller perpendicular electric field leads to higher mobility and fewer scattering events. This phenomenon makes the devices behave closer to the ballistic limit. As the device deviates more dramatically from the long-channel model, it becomes more difficult to predict its behavior using long-channel-based analysis. This observation and the importance of transport models call for a noise model based on ballistic transport in MOSFETs, which is the purpose of this chapter.

Excess noise is also sometimes explained using carrier velocity fluctuations [22]. These fluctua-

5. For a discussion about transport models, including drift-diffusion and hydrodynamic models, please see [21].

tions are normally associated with the small number of scattering events in the channel. Franca-Neto suggests that carrier velocity fluctuations are the outcome of having only “some of the carriers” move across the device without scattering (while others experience scattering inside the channel). This velocity fluctuation then results in an excess noise in short channel devices. Although the physical argument given in [22] is different from the one we present in this work, the end results are somehow related. In both cases, having a small number of scattering events in the channel is introduced as the origin of excess noise because scattering is an equilibrating mechanism.

In an effort to provide a compact model for excess noise, several studies try to revise the classical formulation by considering short-channel effects. Some of these studies explain excess noise based on elevated electron temperature (e.g. [16][23]). These studies usually manage to capture some excess noise in short-channel MOSFETs but suffer from a significant drawback; they imply that the phenomenon responsible for excess noise is associated with the drain end of the channel where electron temperature is maximum. This implication does not agree with quasi-2-D numerical simulation results for HEMT devices which clearly show that the source end of the channel is responsible for most of the excess noise [19].

Several other compact models based on second-order device considerations have also been proposed recently [24]-[27]. All of these methods are based on a revision of the long-channel noise formulation to account for emerging short-channel effects. Existing noise models often treat today’s MOSFETs as imperfect long-channel devices.

Modeling of noise in MOSFETs does not have to depend on the long-channel noise formulation. It is interesting that the noise properties of ballistic devices are relatively easy to model. If we consider today’s MOSFETs as imperfect ballistic devices (semi-ballistic devices), we can obtain a MOSFET noise model based on the ballistic MOSFET noise formulation. The following section presents such a model. Note that noise modeling in ballistic transistors has already been reported by other authors (e.g. [28]) using detailed quantum mechanical simulations. Here we present a simple model which is most suitable for predicting overall device performance, as we will see shortly.

2.2. Ballistic and Semi-Ballistic MOSFET Noise Models

2.2.1. Noise in ballistic MOSFETs

Although true ballistic MOSFETs are not available yet, their electrical properties are already

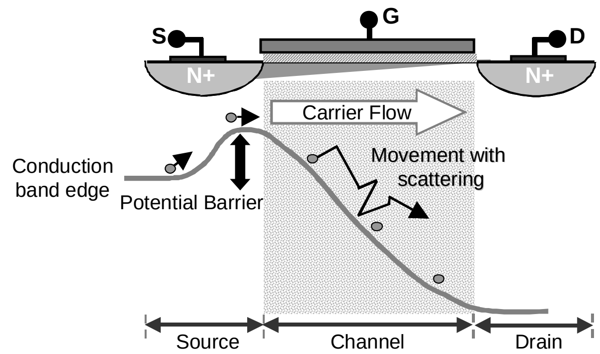

Fig. 8: Two current-limiting mechanisms in every MOSFET are the potential barrier next to source and the channel resistance.

under extensive research. Comprehensive work has been done by Lundstrom and colleagues on the deterministic properties of ballistic devices (e.g. [29]). However, less attention has been paid to the noise properties of these devices. The rest of this subsection presents a simple model for noise in ballistic MOSFETs.

To investigate the noise properties of ballistic MOSFETs, a clear understanding of current flow in MOSFETs is crucial. A careful look at carrier transport in MOSFETs shows that there are two obstacles for current flow in every MOSFET: the potential barrier next to the source and the channel resistance (Fig. 8). The potential barrier next to the source is the up-curvature of the conduction band edge produced by the gradient in impurity concentration in that region. The properties of this barrier and its bias dependencies are discussed in [29]. Carriers are injected from the source to the channel at a rate, f_{inj}, that depends upon the barrier height and carrier concentration at the boundary of source and channel, among other physical parameters. Subsequently, these carriers travel through the channel to reach the drain. The nonzero resistance of the channel implies that the carriers get scattered by various sources in the channel, especially near the silicon surface. The rate, f_{tra}, at which the carriers cross the channel depends upon the average number of scattering events experienced by a carrier on its way from source to drain, as well as, on the physical properties of the scattering phenomena. Therefore, in every MOSFET there are two obstacles for current flow: limited source injection rate and the channel resistance.

Because these two obstacles are in series, the dominant obstacle will dictate the current flow in a given device. As can be seen in Fig. 9, carrier flow in MOSFETs is analogous to the flow of a liquid in a series connection of two pipes with different cross-sections, where the rate of liquid flow is dictated by the cross-section of the thinnest pipe regardless of the order in which the pipes are

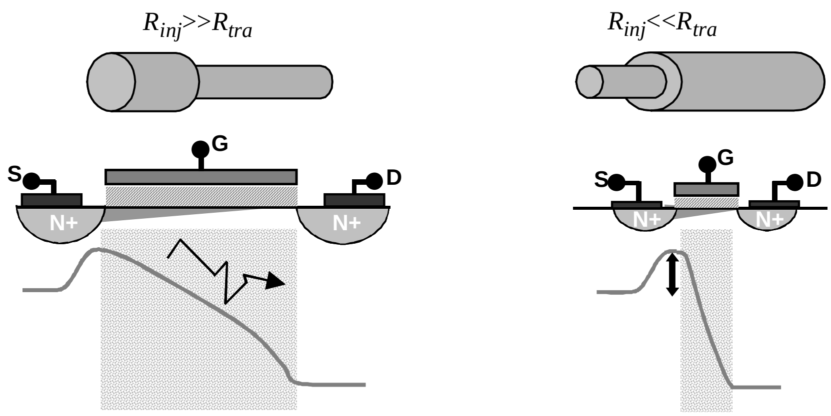

Fig. 9: The two extreme cases of carrier transport in MOSFETs are the long-channel device (left) and the ballistic device (right).

connected. In the case of the long-channel MOSFET, $f_{inj}>>f_{tra}$, causing channel resistance to dictate carrier flow and electrical current in the device. In ballistic MOSFETs, $f_{inj}<<f_{tra}$, and the source injection rate dictates current. Whichever of these obstacles dictates current will also dictate the electrical properties such as noise.

In a long-channel MOSFET, the injection rate of carriers from the source is so high that the details of carrier flow in the region next to the source are of little importance and can be neglected for device analysis. This approximation justifies the long-channel MOSFET formulation that only focuses on channel region. In a ballistic MOSFET, on the other hand, current flow is mainly limited by the source barrier (Fig. 9). For characterization of the electrical properties of these devices, we need to focus on the details of carrier transport in the region next to source.

To understand the noise properties of ballistic devices we consider an ideal ballistic MOSFET in which the carriers instantaneously reach the drain after their injection. In such a device, carrier injections across the barrier will be nearly mutually independent because the injection of each carrier will not affect the electrostatic fields of the device long enough and strongly enough to have a sensible effect on the probability of the next injection. As we discussed earlier in this chapter, such a situation leads to the appearance of shot noise. Therefore, the drain noise of this device can be modeled by a white noise current source with a PSD of $2qI_D$ connected between source and drain.

In practice, the injection of carriers is never completely mutually independent because of second-order effects. This phenomenon generally causes the partial suppression of shot noise as will be discussed in the next subsection. Nevertheless, the fictitious device introduced in this subsection is a powerful tool for developing a model for noise in short channel devices.

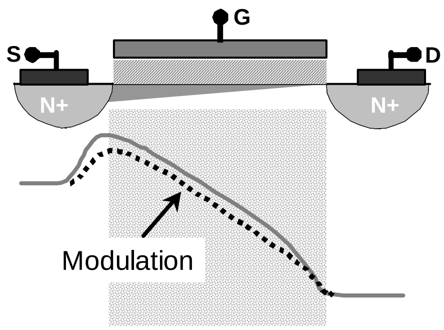

Fig. 10: In semi-ballistic devices the injection of each carrier modulates the height of the potential barriers because it affects the electrostatic fields of the device. This phenomenon causes a negative feedback which partially regulates current flow and partially suppresses shot noise.

2.2.2. Noise in semi-ballistic MOSFETs

Carrier transport in semi-ballistic devices is not entirely controlled by the source injection rate. In these devices, carrier flow is affected by both carrier injection and channel resistance because each injected carrier has to undergo channel scattering to reach the drain. This process alters the electrostatic fields in the device until the injected electron is absorbed and device fields relax to their steady-state condition. More specifically, the height of the barrier is modulated upward by the injection of each electron, Fig. 10, reducing the probability of next injection for some period of time. This process generates a negative feedback which regulates the carrier flow. Such a regulation makes the noise power smaller than $2qI_D$, a phenomenon that is referred to as partial suppression of shot noise.

Partial suppression of shot noise can be explained using the following example. Imagine a system in which carriers are injected independently across a potential barrier at an average rate of f_{inj} carriers per second. For such a system the dc current is given by $I_{dc}=qf_{inj}$ and its noise PSD is $2qI_{dc}$. To see how negative feedback can suppress shot noise, assume that the injection of carriers is regulated by negative feedback that restricts the carrier injection for $T_{inj}=1/f_{inj}$ after each injection while maintaining the same dc current. In this situation, all injections have to be exactly f_{inj} seconds apart because if two of them are further apart, two others have to be less than T_{inj} apart to maintain an average injection rate of f_{inj}, a situation that is not permitted because of our first assumption. Since all injections are T_{inj} seconds apart, the PSD of current is a train of delta functions at the harmonics of f_{inj}. This frequency is normally a very large number and experimentally undetectable. For example, for a typical current flow of 1 μA, f_{inj} evaluates to

1e-6/1.6e-19=6.25e12 Hz or 6.25 THz. Therefore shot noise is fully suppressed in this system. Although this is an extreme example, it illustrates what happens in systems with limited negative feedback such as our semi-ballistic device.

We can qualitatively analyze partial suppression of shot noise in semi-ballistic MOSFETs using historical studies on vacuum tubes. As discussed in [30], current flow in vacuum tubes can be limited by two mechanisms: the injection of carriers from the cathode (cathode efficiency) and the space charge region next to this electrode. In early vacuum tubes, the materials used for the cathode had a low injection efficiency. The current flow in these devices were mainly limited by carrier injection from cathode and the dominant noise phenomenon in the device was shot noise because carrier injections from the cathode are nearly mutually independent. With the emergence of high efficiency materials for the cathode, current in modern tubes is not limited by cathode efficiency. In these tubes, the cathode injects electrons at such a high rate that current flow is mainly limited by the space-charge region. In this space-charge limited regime, the injection events of carriers through the space charge region are not mutually independent anymore because the injection of each carrier alters the fields in the space charge region which in turn reduces the probability of the next injection. This phenomenon is discussed in detail in [30] and it is shown that in this situation the PSD of current noise is given by

$$\overline{S_i} = 2k_s qI, \tag{6}$$

where I is the dc current and $k_s<1$ is the shot noise suppression factor which is a function of physical parameters of the device.

A semi-ballistic MOSFET resembles a vacuum tube in that there exist two current-limiting mechanisms in both devices. In a semi-ballistic MOSFET, the source barrier is analogous to cathode efficiency in cathode tubes while channel resistance resembles the space-charge region. By causing a negative feedback, this resistance suppresses noise to the value given in (6), in exactly the same way that the space charge region does it in modern vacuum tubes (Fig. 11)[6]. The suppression factor, k_s, appears to be a better parameter for noise characterization of short-channel MOSFETs than the γ factor commonly used in literature because of its more intimate connections to the underlaying physics.

6. It is interesting that in fully-space-charge-limited tubes, current noise PSD is given by (4) with γ=0.6438 (it is called θ in that formulation). This number is very close to the noise factor of long-channel MOSFETs even though this equation is derived in a totally different way for cathode tubes [30].

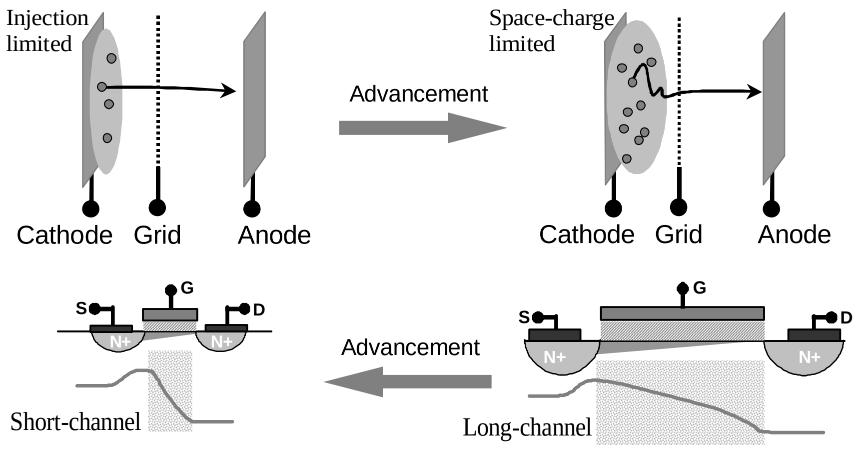

Fig. 11: Current flow in early vacuum tubes were limited by cathode efficiency, resembling a ballistic MOSFET. With the emergence of better cathode materials, modern tubes are space-charge limited. These devices are similar to today's semi-ballistic MOSFETs in which channel resistance is equivalent to the space-charge region. MOSFETs and vacuum tubes have evolved in opposite directions throughout history. This observation helps us understand the noise properties of short-channel MOSFETs using historical studies on vacuum tubes.

Based on this simple model, we can develop a compact noise model for short-channel MOSFETs. Using the power law formula for drain dc current, we have $i_D = I_1(v_{GS} - v_T)^{\alpha}$, where α and I_1 are empirical parameters. Combining this equation with (6), current noise is compactly modeled as

$$\overline{S_{ind}} = I_{n1}(v_{GS} - v_T)^{\beta} \tag{7}$$

where β and I_{n1} are empirical parameters. Note that the numerical value of β is not necessarily the same as α because k_s drops with increasing v_{GS}. This phenomenon will be discussed in Chapter 4.

Equation (6) suggests that in contrast to long-channel MOSFETs, which only show thermal noise, the dominant non-equilibrium noise source in short-channel MOSFETs is shot noise. As we will see in Chapter 4, this phenomenon is already significant in today's short-channel devices. The appearance of shot noise in non-equilibrated small conductors is not unprecedented; it has already been discovered in mesoscopic and other small-size conductors.

Mesoscopic conductors are those whose lengths are between those of microscopic and macroscopic systems. These limits are bounded on one side by the deBroglie wavelength of the electron, and on the other by the length scales of various scattering mechanisms. In these conductors the appearance of shot noise in non-equilibrium is both theoretically predicted [12] and experimentally observed [13]. Non-equilibrium noise in a mesoscopic conductor with one scattering site in

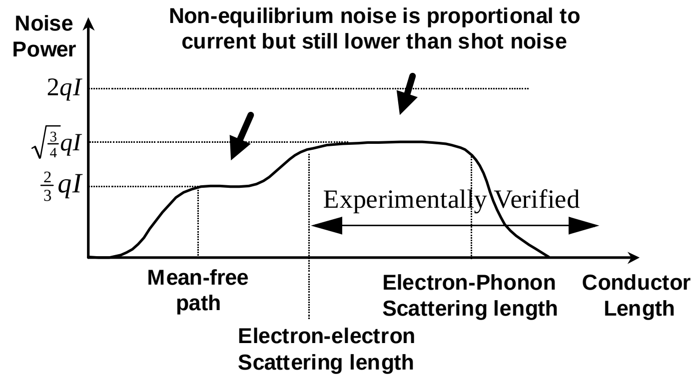

Fig. 12: Partially-suppressed shot noise in small conductors.

its channel contains a partially-suppressed shot noise term. A detailed simulation shows that this term progressively gets more heavily suppressed as the number of non-elastic scattering sites in the channel increases [31][7]. In the limit, when there are a large number of inelastic scattering sites located in the channel, the mesoscopic conductor turns into a macroscopic, dissipative conductor for which non-equilibrium noise is the same as the equilibrium noise and is given by the Johnson-Nyquist formula. This explains why the noise power in a macroscopic resistor is often the same under equilibrium and non-equilibrium and obeys the Johnson-Nyquist formula.

Partially suppressed shot noise also exists in non-equilibrium noise of small conductors. Fig. 12 shows the non-equilibrium noise in conductors of sizes comparable to electron-electron scattering and electron-phonon scattering lengths [32]-[36]. As can be seen, noise in these devices is smaller than shot noise but still proportional to current. From a pure physics point of view, the appearance of partially-suppressed shot noise in short-channel MOSFETs, mesoscopic conductors and small conductors can probably be traced back to a common origin.

It is worth mentioning here that the existence of a shot noise component in drain current noise has already been proposed for modeling purposes [37]. However, the existence of this noise is not associated with the dominance of source barrier over the channel resistance in short-channel devices. The argument presented in this section provides a theoretical ground for the appearance of shot noise and facilitates the prediction of the overall performance of future MOSFETs as we discuss in the next subsection.

7. The main reason for this phenomenon is the Pauli exclusion principle for electrons. This is why shot noise is never suppressed for photons; the Pauli exclusion principle does not hold for photons.

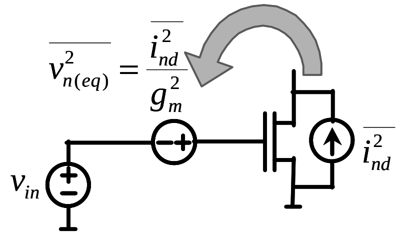

Fig. 13: A very useful parameter for noise analysis is the input-referred noise whose power can be readily compared to the input signal power.

2.2.3. Overall noise performance of short-channel MOSFETs

Our short-channel noise model can be used to predict the overall noise performance of future MOSFETs and to provide prescriptions for optimizing the noise behavior of these devices. For a rigorous analysis, we first define an appropriate figure of merit for noise. The figure of merit that is usually used by circuit designers is the input-referred noise power. Unlike the drain noise, input-referred noise power may be directly compared to the input signal and therefore plays a significant role for determining amplifiers' noise figure [1]. As can be seen in Fig. 13, the input-referred noise in a MOSFET is given by

$$\overline{v_{n(eq)}^2} = \frac{\overline{i_{nd}^2}}{g_m^2}. \tag{8}$$

According to (8), predicting the overall noise performance of future devices involves the prediction of their drain noise and their transconductance. Experiments show that for typical current densities in MOSFETs, the numerical value of shot noise, $2qI$, is larger than the numerical value of long-channel thermal noise, $4kT\gamma g_{do}$. This observation suggests that noise in MOSFETs might increase as these devices are scaled down towards the ballistic limit because ballistic MOSFETs show shot noise. On the other hand, shot noise is also observed in BJTs while these devices have better noise characteristics than MOSFETs. This second observation makes it unclear whether the appearance of shot noise in MOSFETs will have a deteriorating or enhancing effect on their noise performance.

For an accurate analysis, we need to carefully compare short-channel MOSFETs to BJTs. In ballistic MOSFETs, both noise and transconductance are dictated by the potential barrier next to source. In this situation, the dominant noise phenomenon is shot noise which is very similar to what happens in BJTs. The potential barrier also dictates the transconductance in ballistic MOS-

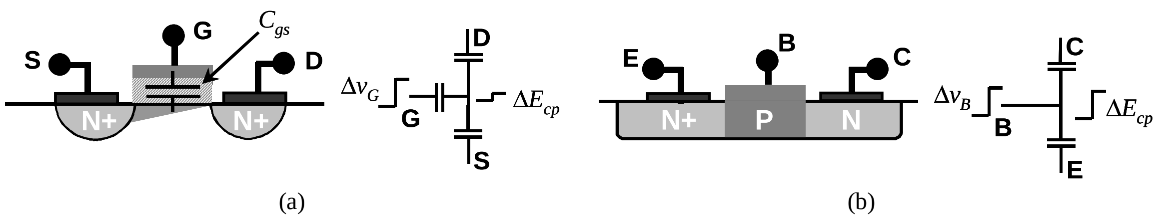

Fig. 14: Current modulation in both ballistic MOSFETs, (a), and BJTs, (b), is through the modulation of the barrier height, E_{cp}. However the g_m of a MOSFET is often smaller than that of its corresponding BJT because part of the gate voltage is dropped across C_{gs}.

FETs. As discussed in [29], the modulation of current in ballistic MOSFETs is through the modulation of the height of this barrier, which is in turn modulated by the gate voltage. This phenomenon is again similar to that in BJTs where collector current is modulated by the modulation of the emitter-base barrier height through base voltage. Thus ballistic MOSFETs resemble BJTs in many respects.

Unfortunately, the transconductance of a ballistic MOSFET is often smaller than that of its corresponding BJT. Although the modulation of current in both cases is through the modulation of the barrier height, this modulation is smaller in ballistic MOSFETs because of the indirect control of channel voltage through C_{gs}. As shown in Fig. 14, this capacitor drops part of the input voltage making the transconductance of ballistic MOSFETs inferior to that of BJT. Therefore, a ballistic MOSFET has the noise of a BJT and the transconductance of a MOSFET, the worst of two worlds. This is an unfavorable combination for low-noise analog design.

Whether future commercial MOSFETs will deteriorate in noise performance and how fast this deterioration will occur are still open questions. Investigations show that present MOSFETs are working at fifty percent of the ballistic limit which means that current in these devices is 50 percent of the expected current in a ballistic device with the same physical dimensions. This percentage has been the same for the past 10-15 years [38]. Although MOSFETs continue to scale, higher perpendicular field in small devices causes more scattering in the channel which has kept them at the same percentage of the ballistic limit for the past 10-15 years. This observation explains why the noise factor has not increased much during the past few years.

Our model can also explain the wide range of reported values for γ. Noise factor is in fact a function of the relative strength of the two current limiting mechanisms and not the absolute value of channel length. It should even be possible to design a high-noise-factor transistor with a long channel through careful engineering.

During the past decade, careful device engineering which has tried to optimize various device parameters, might have led to accidental optimization of noise in short-channel devices. It is not certain, however, whether this trend will continue. In any case, our noise model suggests that future MOSFETs should be designed in a way that avoids the dominance of source injection rate over the channel resistance. This prescription does *not* mean that more scattering should be added to the channel to achieve this goal; rather, better source engineering is required to guarantee an ample injection of carriers from source. This condition seems to be possible to satisfy today because we have stayed at fifty percent of the ballistic limit for such a long time. Ultimately, ultra short MOSFETs or new devices will emerge with more ballistic carrier transport. At that stage, more study will be necessary to guarantee optimum performance.

2.3. SUMMARY

A MOSFET noise model has been presented based on the study of noise in ballistic MOSFETs. The advantage of this model is that it progressively gets more accurate as the devices scale to smaller sizes and work closer to the ballistic limit. Furthermore, it provides a clear prediction of noise in future devices. Drain current noise in short-channel devices is shown to be best modeled by a partially-suppressed shot noise term. Based on this observation a compact model for noise in short-channel MOSFETs is presented. Overall noise performance analysis of future MOSFETs shows that, in the ballistic limit, these devices will have the transconductance of a MOSFET and the noise of a BJT, an unfavorable combination. Based on the proposed model, practical guidelines for noise optimization in future MOSFETs are presented. In the next chapter, we turn into the analysis of phase noise in electrical oscillators and discuss its relation to device noise.

CHAPTER 3:

PHASE NOISE IN OSCILLATORS

Due to its practical importance in communications, the frequency stability of electrical oscillators has been the object of extensive research. Several methods have been proposed for estimating the phase noise of these oscillators, often using approximations and numerical approaches that provide significant insight about the behavior of phase noise (e.g. [45][57][58]). Unfortunately these methods are often based on frequency-domain analysis, which unnecessarily complicates the formulation of phase noise, a formulation that can be performed through time-domain jitter analysis with fewer approximations and sometimes even analytically. Furthermore, they sometimes lead to erroneous conclusions about the behavior of phase noise (especially at close-in frequencies relative to the center frequency) because the approximations are not valid for the entire spectrum.

To discuss the effects of device noise on phase noise, we present a time-domain formulation of phase noise in this chapter, a formulation that is specifically accurate for switching-based oscillators. The advantage of having an accurate phase noise analysis method is twofold. This method can be used to predict phase noise for a given device noise level or to back-calculate the device noise from phase noise measurements. These measurements are normally easier to perform than direct device noise characterization. Compared to a frequency-domain formulation, the time-domain formulation of phase noise is more accurate at small offset frequencies because of the fewer approximations used in this method. Thus, the properties of close-in phase noise can also be studied using this formulation.

To provide a rigorous treatment of phase noise, we start with a discussion of the formal definition of phase noise. We then present our time-domain phase noise formulation for switching-based oscillators. As specific examples of time-domain phase noise analysis, we calculate the minimum achievable phase noise for relaxation (including ring) oscillators after showing that one of the fundamental principles of thermodynamics sets a lower limit on the phase noise of RC type oscillators. For the sake of completeness, phase noise in coupled RC oscillators is also discussed. Finally, we discuss the properties of close-in phase noise using a time-domain phase noise formulation.

To get the most benefit from our phase noise formulation and its implications, we present this chapter as a self-sufficient part, independent of previous chapters. The relevance of our phase noise formulation to MOSFET noise characterization will become clear in Chapter 4.

3.1. THE FORMAL DEFINITION OF PHASE NOISE

Despite its practical importance in communications, the formal definition of phase noise remains a matter of controversial. At least two distinct definitions are introduced by various authors. One of these definitions involves the power spectral density (PSD) of phase [40], the other is based on the PSD of the signal itself [39]. The choice of definition appears to be irrelevant at large offset frequencies (hereafter referred to as far-out phase noise) because the PSD of phase can be approximated by the PSD of the signal at far-out frequencies [42]. However, the numerical value of phase noise at small offset frequencies (the close-in phase noise) strongly depends on the definition. Furthermore, as we will see shortly, depending on which definition we use, some well-known properties of the far-out phase noise, such as the superposition of phase noise, can be violated at close-in frequencies. To decide which definition is more appropriate, we need to understand how frequency instability affects the performance of electrical systems.

An electrical oscillator is responsible for generating a periodic signal with a stable oscillation frequency. In an ideal oscillator, this frequency remains constant over time. In a real oscillator, however, the frequency of oscillation is modulated by electronic noise, present in all real systems. Because of this electronic noise, the oscillation frequency randomly fluctuates with time. These frequency fluctuations degrade the performance of the system in which the oscillator is used.

To evaluate the performance of a communication system in the presence of noise, we need to characterize the frequency fluctuations of its oscillator. This characterization can be performed using time-domain or frequency-domain analysis and different measures can be defined correspondingly. From a practical point of view, the best measure is the one that best facilitates the performance assessment of the communication system. Thus, depending on which kind of system is under consideration, different measures of frequency instability might be favorable. One instability measure often referred to in the literature is phase noise. In this section, we first present the existing definitions of phase noise as a measure of frequency instability. We then discuss the effect of frequency instability on the performance of various types of communication systems. In light of this discussion, we choose an appropriate definition of phase noise for our study.

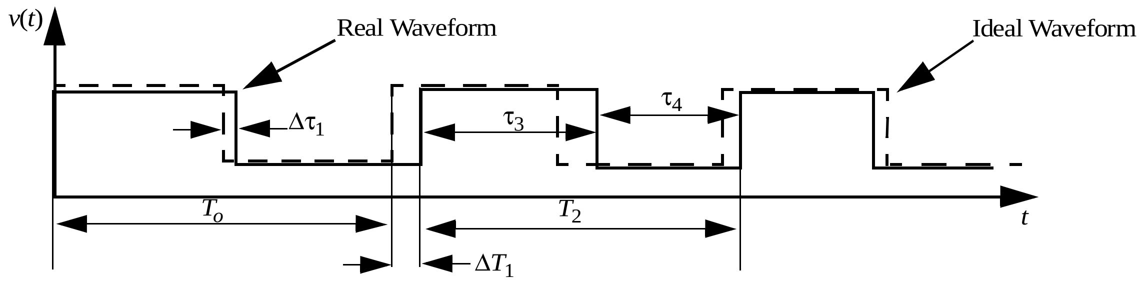

Fig. 15: Real and ideal waveforms for a rectangular oscillatory signal with parameter definitions.

3.1.1. Existing definitions of phase noise

Fig. 15 shows an ideal periodic square-wave signal along with a signal, which has nonzero frequency instability. The nominal oscillation period for this signal is denoted by T_o. In the presence of noise, the real duration of the ith period is a random variable denoted by T_i. For stationary oscillators, the expected value of this random variable is independent of i and, by definition, is the nominal period of oscillation. Demir et al. explain the properties of stationary oscillators [39]. The duration of the ith half-period of oscillation is denoted by τ_i. Thus

$$T_i = \tau_{2i-1} + \tau_{2i} \, . \tag{9}$$

We define jitter in the ith period, ΔT_i, as the difference between the actual and the nominal duration of this period, $\Delta T_i = T_i - T_o$. The period jitter, $\overline{\Delta T^2}$, is the variance of ΔT_i. For a stationary oscillator, this is independent of i. The cycle-to-cycle jitter, $\overline{\Delta T_{i,j}^2}$, is defined as the expected value of $\Delta T_i \Delta T_j$, which is normally only a function of i-j and not of i or j alone[8]. Similarly, we define half-period jitter and half-cycle-to-cycle jitter as the variance of $\Delta\tau_i$ and the expected value of $\Delta\tau_i \Delta\tau_j$, respectively. In most practical situations, having $\overline{\Delta T_{i,j}^2}$ for all (i-j) provides enough information for the characterization of frequency instability in the time domain.

The characterization of the frequency instability in the frequency domain is more complicated and is based on the definition of phase noise. At least two distinct definitions are used by various authors: one based on the PSD of the phase [40] and the other based on the PSD of the signal itself

8. This definition of cycle-to-cycle jitter is different from the one used by some other authors. This definition best suits our analysis, as we will see shortly.

[39].

According to the first definition, phase noise is the PSD of the phase. The main advantage of this definition is that it keeps the phase noise independent of the amplitude noise. However, this choice of definition also generates some mathematical and practical difficulties. For example, phase is not a stationary random variable and its PSD is mathematically undefined[9]. Although it is possible to define a generalized PSD for phase, this would complicate the already involved mathematics for two reasons. First, the total power of the generalized PSD would be infinite, making it impossible to normalize. Second, the generalized PSD would grow without bound around zero frequency. Such an ill-behaved function is hard to work with, especially when close-in phase noise is of interest.

According to the second definition, the phase noise is the PSD of the signal itself, normalized to the power of the fundamental tone. Using this definition, the phase noise can be calculated analytically and is a well-behaved function around zero offset frequency [39][41]. However, the PSD of the signal is a function of both jitter and amplitude noise.

It has been shown that the behavior of phase noise at large offset frequencies is independent of the choice of definition [42]. At small offset frequencies, however, these two definitions provide significantly different values for phase noise. To decide which definition is more appropriate for a specific application, we first need to study the effect of frequency instability on the performance of communication systems.

3.1.2. Phase noise in communication systems

RF communication systems normally require an accurate time reference because of their multi-user nature. In these systems, several users share the same communication channel, necessitating modulation/demodulation of the messages. Reliable modulation and demodulation is highly dependent upon the accuracy of the frequency of the oscillators used in these systems. On the other hand, in high-speed digital communication systems, the necessity of having an accurate time reference stems from the desire to reach higher data rates. In both cases, the frequency instability of the carrier or clock degrades the performance of the system. However, because of the different nature of these systems, different sets of tools are required to assess performance.

Fig. 16 shows a typical RF communication system. The desired signal and an interfering one are located at ω_{RF} and $\omega_{RF}+\Delta\omega$, respectively. Note that the presence of a high-power interfering signal

9. Note that phase can be made stationary if it is kept between 0 and 2π. We do not consider this interpretation of phase here because it causes discontinuity and is rarely used for phase noise analysis.

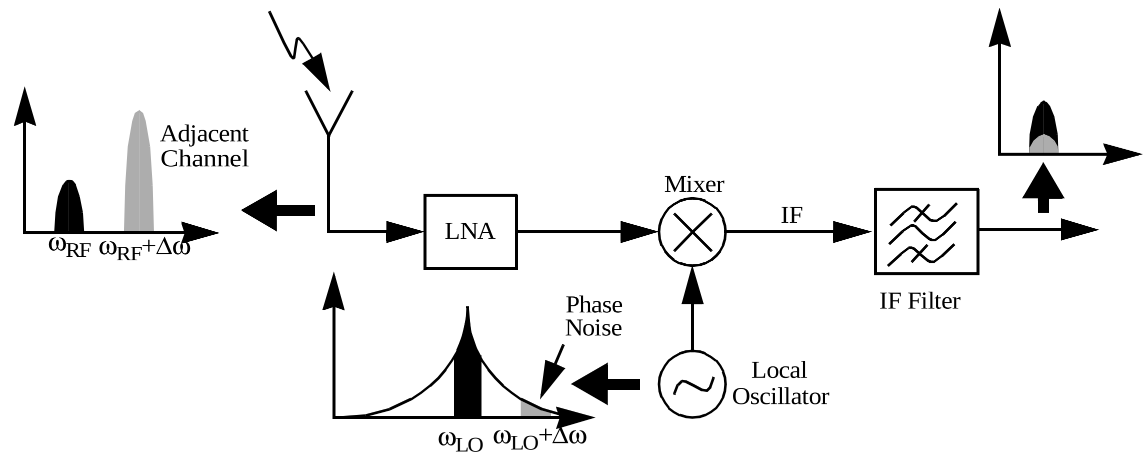

Fig. 16. The front-end of a typical RF receiver.

is the result of using the same transmission medium for several users. This interfering signal is multiplied by the local oscillator signal in the mixer. Thus the noise of the local oscillator is modulated by this interfering signal and appears at the output of the mixer. At the output of the mixer, the noise power at IF is proportional to the magnitude of the PSD of the local oscillator signal in the vicinity of $\omega_{LO}+\Delta\omega$. Since the IF signal power is proportional to the total power of the local oscillator at the output of the mixer, the degradation of the signal-to-noise ratio due to phase noise is proportional to the phase noise of the local oscillator if we adopt the second definition of phase noise. Therefore, the performance assessment of RF communication systems is greatly simplified if we adopt this definition.

In high-speed digital communication systems, the frequency instability of the clock increases the bit error rate. The bit error rate in these systems is solely a function of jitter and is independent of amplitude noise. Since the amplitude noise affects the PSD of the signal but not that of phase, it might seem that the first definition of phase noise is more convenient for these systems. However, the analysis of bit error rate in communication systems is most easily performed in the time domain. Consequently, the choice of the definition of phase noise is of little importance for these systems.

The second definition of phase noise also facilitates experimental work. The measurement of the PSD of the signal using a spectrum analyzer is a routine measurement procedure. On the other hand, the process of measuring the PSD of phase is usually much more involved. Furthermore, as we will see in the next section, the analytical calculation of the PSD of the signal is relatively straightforward.

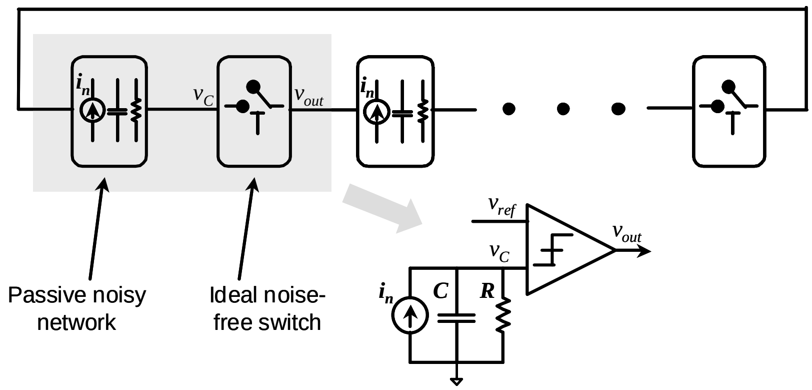

Fig. 17: A simplified model for a typical switching-based oscillator.

The comparison of the two definitions of phase noise reveals that defining the phase noise in terms of the PSD of the signal, normalized to the total power, facilitates its measurement and analytical calculations and is usually more helpful for assessing the performance of RF communication systems. The main drawback of adopting this definition is that the amplitude noise affects the PSD of the signal. In practice, the effect of this amplitude noise can usually be suppressed using a limiting amplifier and should be distinguished from effects of jitter, which are impossible to suppress. To circumvent this problem, we need to perform phase noise analysis **after** taking into account the effect of the limiting amplifier. We believe that the benefits of defining the phase noise as the normalized PSD of the signal outweighs this complexity.

3.2. Time-Domain Formulation of Phase Noise

In this section we introduce a formulation of jitter entirely in the time domain. Phase noise is subsequently calculated using pre-derived mathematical relationships between jitter and phase noise as will be discussed shortly. This method is especially appropriate for switching-based oscillators. We first provide a brief definition for this class of oscillators and then describe our formulation.

In switching-based oscillators, Fig. 17, the energy injecting elements act like ideal switches, *i.e.* they have a countable number of states between which transitions may be considered instantaneous. Relaxation oscillators can be modeled as switching based oscillators. For this class of oscillators, phase noise is most easily calculated by first calculating the jitter in the time domain. Since the oscillator's feedback path is broken by the active devices (modeled by ideal switches in

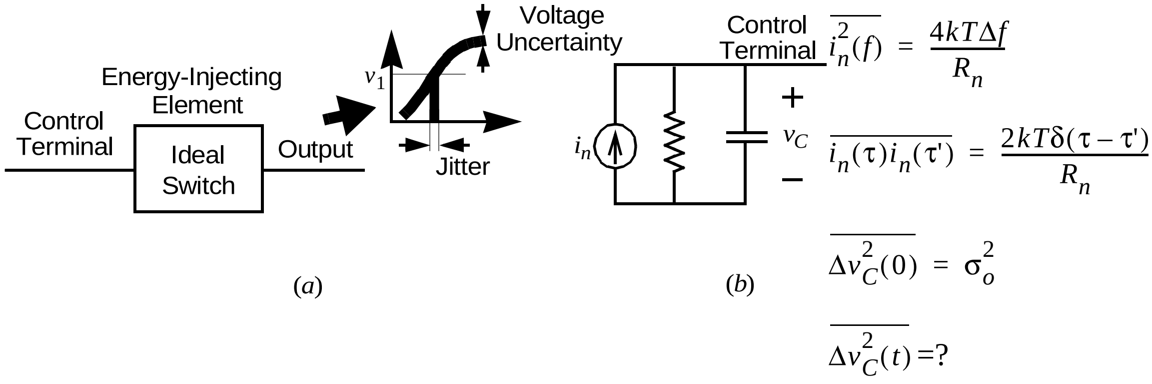

Fig. 18: (a) Switching time jitter in switching-based oscillator (b) Noise circuit model of the passive network connected to the input of each switch and problem definition for calculation of voltage uncertainty on the control terminal.

Fig. 17) during the non-switching time interval, the calculation of jitter for these oscillators is relatively simple. Once the jitter is determined, phase noise can be calculated using available mathematical relationships presented in Appendix A. In the rest of this section we elaborate on how these calculations are performed.

Fig. 18a shows part of a switching based oscillator. The energy injecting element switches when the voltage of the control terminal reaches v_1. We use the first crossing approximation, which assumes that the switching takes place when the voltage reaches v_1 for the first time [43]. Using a linear approximation, the variance of the switching time jitter is found to be proportional to the variance of the control terminal voltage and inversely proportional to the square of the rate of change of voltage at this node.

The variance of the control terminal voltage can be calculated by knowing the total resistance and total capacitance on this node as well as the stochastic properties of the noise sources connected to this node. Fig. 18b shows the noise circuit model of the passive network connected to the input of each switch. The problem definition is also given in the inset of this figure. The variance of the capacitor voltage at t=0 is assumed to be a Gaussian random variable with zero mean and a variance of σ_o^2. We are interested in calculating the variance of this voltage at some later time t. The voltage on the capacitor at time t is given by

$$\Delta v_C(t) = \frac{e^{-\frac{t}{RC}}}{C}\int_0^t e^{\frac{\tau}{RC}} i_n(\tau)d\tau + \Delta v_C(0)e^{-\frac{t}{RC}}. \tag{10}$$

Since i_n is a Gaussian process with zero mean, (10) dictates that Δv_C is also a Gaussian process with zero mean [44]. Consequently, the fluctuation properties of Δv_C are completely conveyed by its variance. Using (10) we can find the variance of Δv_C at time t:

$$\overline{\Delta v_C^2(t)} = \frac{e^{-\frac{2t}{RC}}}{C^2}\int_0^t\int_0^t e^{\frac{\tau+\tau'}{RC}}\,\overline{i_n(\tau)i_n(\tau')}\,d\tau d\tau' + \sigma_o^2 e^{-\frac{2t}{RC}}, \tag{11}$$

in which $\overline{i_n(\tau)i_n(\tau')}$ is the autocorrelation function of the noise source. Let us assume that the noise source is white with the autocorrelation function given in the onset of Fig. 18b. Using this autocorrelation function in (11) and performing the integration, the variance of Δv_C is found to be[10]

$$\overline{\Delta v_C^2(t)} = \frac{kTR}{CR_n}\left(1 - e^{-\frac{2t}{RC}}\right) + \sigma_o^2 e^{-\frac{2t}{RC}}. \tag{12}$$

Note that if R_n=R the variance of v_C converges to kT/C as $t \to \infty$ and becomes independent of R and σ_o^2.

Under the linear approximation, the variance of the switching time jitter is simply the variance of Δv_C divided by the square of the capacitor's voltage rate of change:

$$\overline{\Delta T_s^{\,2}} = \overline{\Delta v_C^2(t)}\left|\frac{\partial v_C}{\partial t}\right|^{-2}. \tag{13}$$

The total period jitter in the oscillator is then calculated by adding up all of the individual switch time jitters, which are assumed to be independent in the absence of colored noise.

Once the period jitter is calculated, phase noise can easily be calculated. In most cases (including relaxation oscillators) the output of the switching oscillator can be approximated by a stochastic square wave signal with mutually-independent, Gaussian-distribution period jitter. As presented in Appendix A, the phase noise of such a signal has a nearly-Lorentzian shape around each harmonic. The phase noise around the first harmonic at an offset frequency of Δf is given by

$$PN(\Delta f) = \frac{f_o^3\overline{(\Delta T_o)^2}}{\left(\pi f_o^{\,3}\overline{(\Delta T_o)^2}\right)^2 + (\Delta f)^2}, \tag{14}$$

10. The presented derivation is simplified for brevity. A rigorous derivation shows that the final result is, nevertheless, correct [44].

where f_o and Δf are the center and offset frequency, respectively, and $\overline{(\Delta T_o)^2}$ is the variance of the period. This equation predicts that the phase noise has a $1/f^2$ shape for sufficiently large offset frequencies, which is consistent with the previously reported measurement results (e.g. [45][46]).

Note that (14) is valid only if period jitters of different cycles are mutually independent. In the presence of colored noise this condition is usually violated and hence (14) would lose its validity. We will discuss those cases later in this chapter.

In the following section, we first present a physical argument about the minimum achievable phase noise of RC oscillators, a discussion that will be of great value in assessing the feasibility of using certain oscillators for a particular application. We will then use time-domain phase noise analysis to formulate the minimum phase noise of specific oscillator topologies.

3.3. Minimum Achievable Phase Noise of RC Oscillators

The significance of phase noise in RF systems limits the usefulness of *RC* oscillators[11] because of their typically inferior phase noise properties compared to inductor-based and distributed oscillators. RF designers need to improve these properties in order to benefit from the attractive integrated nature of *RC* oscillators, a virtue that has made them popular for clock-recovery circuits [59] and on-chip clock distribution [60]. Several investigations have focused on improving the frequency stability of *RC* oscillators (*e.g.* [51]). However, the literature does not include a study of the possible theoretical limits on the phase noise of *RC* oscillators for a given power. Such a study will help assess the feasibility of designing low-phase noise *RC* oscillators and will reduce the lingering uncertainty about the future of RFIC design.

In this section we first show that one of the fundamental principles of thermodynamics imposes a lower limit on the phase noise of *RC* oscillators. After establishing this, we use a time-domain phase noise formulation to calculate the minimum achievable phase noise for a few oscillator topologies. This discussion helps to understand this method and provides useful insight about the future of *RC* oscillators.

Nonzero phase noise in an oscillatory signal indicates that the period of oscillation is not truly constant. To stabilize this period (and hence to build a low-phase-noise oscillator), we should

11. In this chapter, lumped, inductorless oscillators, including ring and other relaxation oscillators, are all referred to as *RC* oscillators.

make the period of oscillation dependent on a reliable physical phenomenon, one which can force the oscillation period to be traceable to a physical constant with the dimension of time. In inductor-based oscillators (like the Colpitts) this constant is $\sqrt{LC}$ where L is the inductor and C is the capacitor. In transmission-line-based oscillators the ratio of l/v establishes the time constant in which l is the length of the transmission line and v is the velocity of electromagnetic wave inside the transmission line. In RC oscillators the product of RC is usually the time constant. There is, however, a fundamental difference between this latter case and the first two cases. The fluctuation-dissipation theorem of thermodynamics states that a nonzero amount of thermal noise is associated with any resistor[12]. Thus, in contrast to lossless-inductor-based and lossless-transmission-line-based oscillators, the time constant of RC oscillators is inherently noisy because of the resistor dissipation. This noise component will affect the period of oscillation in a random fashion and result in nonzero phase noise. Consequently, even if the rest of the circuit is noise-free, the resistor noise imposes a lower limit on the phase noise of RC oscillators.

To provide a quantitative prediction of this minimum achievable phase noise, we use simple models for relaxation oscillators. For the formulation of minimum achievable phase noise of relaxation oscillators, only the equilibrium noise current of the feedback resistor (given by $4kT/R$) is taken into account. For the special case of ring oscillators, we assume that the only noise sources in the circuit are those associated with MOSFETs. To find the minimum achievable phase noise, the power spectral density of this noise source is predicted by the long channel MOSFET noise theory. In order to provide a quantitative analysis of minimum achievable phase noise, we first use the time-domain phase noise analysis method for switching-based oscillators introduced earlier in this chapter.

3.3.1. Phase noise in RC relaxation oscillators

Fig. 19 shows a typical RC relaxation oscillator. The oscillator is composed of a Schmitt trigger comparator in an RC feedback loop. We first derive the basic equations governing the behavior of this oscillator and then present an analysis for jitter and phase noise. Since we are interested in the minimum achievable phase noise, we take into account only the equilibrium resistor noise (whose

12. The fluctuation-dissipation theorem is strictly applicable to the thermal equilibrium state of the resistor. Nonetheless, experimental observations show that a resistor's nonequilibrium noise is also finite and, in most cases, has the same value as that of the thermal equilibrium noise. The power spectral density of this noise source is given by Nyquist formula which will be used for quantitative analysis in this paper.

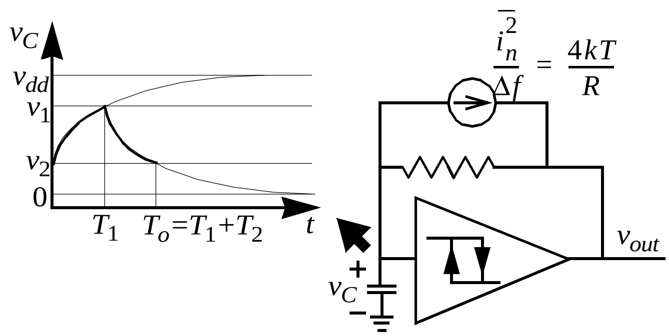

Fig. 19: Typical relaxation oscillator and the respective waveform.

density is given by $4kT/R$) and neglect all other noise sources associated with the comparator and all non-equilibrium noise sources (such as $1/f$ noise).

The oscillator of Fig. 19 works as follows: during the first half of the period, the capacitor voltage changes exponentially from v_1 to v_2 (the two comparison levels). The duration of the first half of the period is found to be

$$T_1 = RC \times \ln\left(\frac{v_{dd} - v_1}{v_{dd} - v_2}\right). \tag{15}$$

Similarly, the duration of the second half of the period is

$$T_2 = RC \times \ln\left(\frac{v_2}{v_1}\right), \tag{16}$$

and the frequency of oscillation is given by

$$f_o = \frac{1}{T_o} = \frac{1}{T_1 + T_2} = \frac{1}{RC \times \ln\left(\frac{v_{dd} - v_1}{v_{dd} - v_2} \times \frac{v_2}{v_1}\right)}, \tag{17}$$

where T_o is the nominal period of oscillation.

The absolute minimum power dissipation of this oscillator (neglecting the power consumed by the comparator) is dictated by the amount of charge transferred to the capacitor as its voltage moves between v_1 and v_2 in each cycle:

$$P_{min} = v_{dd} C (v_2 - v_1) f_o. \tag{18}$$

The nonzero minimum power dissipation is another distinct property of *RC* oscillators. For lossless *LC* and transmission-line-based oscillators, the minimum power dissipation is zero; the energy can be exchanged losslessly between two energy-storage elements.

The jitter is generated by the fluctuations of v_C which are in turn caused by the resistor noise. The probability density function of the fluctuations of v_C at any given time t can be found using the circuit model of Fig. 18b. Since the switching takes place when the capacitor voltage reaches the decision levels, v_1 and v_2, this voltage is accurately known at the beginning of each half-period. Using (12) with $\sigma_o^2 = 0$ and $R_n = R$ we get

$$\overline{\Delta v_C^2(t)} = \frac{kT}{C}\left(1 - e^{-\frac{2t}{RC}}\right). \tag{19}$$

Using $t = T_1$ or T_2 in this equation, we can find the variance of Δv_C at the end of the first and second half-periods, respectively.

The switching time jitter at the end of each half period can be found using (13):

$$\overline{\Delta T_1^2} = \left|\frac{\partial v_C}{\partial t}\right|_{t = T_1}^{-2} \overline{\Delta v_C^2} = \left(\frac{RC}{v_{dd} - v_2}\right)^2 \overline{\Delta v_C^2} \tag{20}$$

and

$$\overline{\Delta T_2^2} = \left|\frac{\partial v_C}{\partial t}\right|_{t = T_o}^{-2} \overline{\Delta v_C^2} = \left(\frac{RC}{v_1}\right)^2 \overline{\Delta v_C^2}, \tag{21}$$

where the linearization is justified due to the fact that the noise level is normally small. The variance of the period is the sum of (20) and (21) because ΔT_1 and ΔT_2 are uncorrelated variables based on the following argument. The switching takes place when v_C equals v_1 or v_2. Consequently, at the beginning of each half cycle the value of v_C is known accurately. Since the only noise source taken into account is white, the uncertainty of v_C at the end of each half cycle is completely independent of the one at the end of previous half cycle. This ensures that ΔT_1 and ΔT_2 are in fact independent and the variance of the period jitter is the sum of (20)and (21):

$$\overline{\Delta T_o^2} = kTR^2C\left(\frac{1}{(v_{dd} - v_2)^2} + \frac{1}{v_1^2}\right)\left(1 - e^{-\frac{T_o}{RC}}\right), \tag{22}$$

in which we have assumed a duty cycle of 50% so that we can replace $2t$ in (19) by T_o.

After eliminating R between (17) and (22) we get

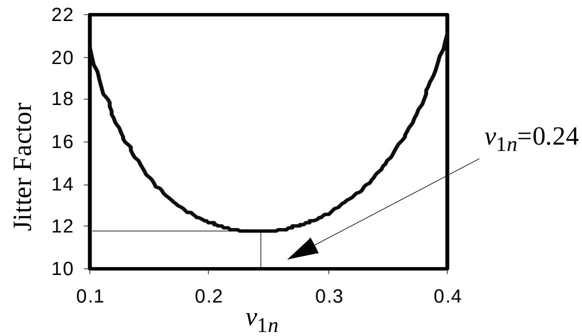

Fig. 20: Normalized jitter vs. normalized decision level v_{1n}

$$\overline{\Delta T_o^2} = \frac{kT}{2Cf_o^2v_{dd}^2} \cdot \frac{(1-2v_{1n})}{v_{1n}^2\left[\ln\left(\frac{1}{v_{1n}}-1\right)\right]^2(1-v_{1n})^2}, \tag{23}$$

where $v_{1n} = v_1/v_{dd}$ is the normalized decision level. We have assumed v_2=v_{dd}-v_1, which ensures a duty cycle of 50%. The second part of (23), called the jitter factor, is only a function of v_{1n} and can be plotted versus this parameter. Fig. 20 presents such a plot and it shows that the jitter factor is minimized for $v_{1n} \approx 0.24$. For constant values of temperature, capacitance, oscillation frequency and bias voltage, jitter (and hence phase noise) assumes its minimum value for $v_1 \approx 0.24v_{dd}$ and $v_2 \approx 0.76v_{dd}$. Hereafter, we will use these values to find the minimum achievable phase noise. The minimum power dissipation and minimum period jitter are then found to be

$$P_{min} \approx 0.52Cf_ov_{dd}^2 \tag{24}$$

and

$$\overline{\Delta T_o^2} = 2\overline{\Delta T_1^2} \approx \frac{5.9kT}{Cf_o^2v_{dd}^2} \approx \frac{3.1kT}{P_{min}f_o}. \tag{25}$$

Using (25) in (14) the phase noise at offset frequencies much larger than $\pi f_o^3\overline{(\Delta T_o)^2}$, which are the only practically important frequencies, is found to be

$$PN_{min}(\Delta f) \approx \frac{5.9f_okT}{Cv_{dd}^2(\Delta f)^2} \approx \frac{3.1kT}{P_{min}}\left(\frac{f_o}{\Delta f}\right)^2. \tag{26}$$

It is instructive to compare this equation to the one presented in [47] for differential *LC* oscilla-

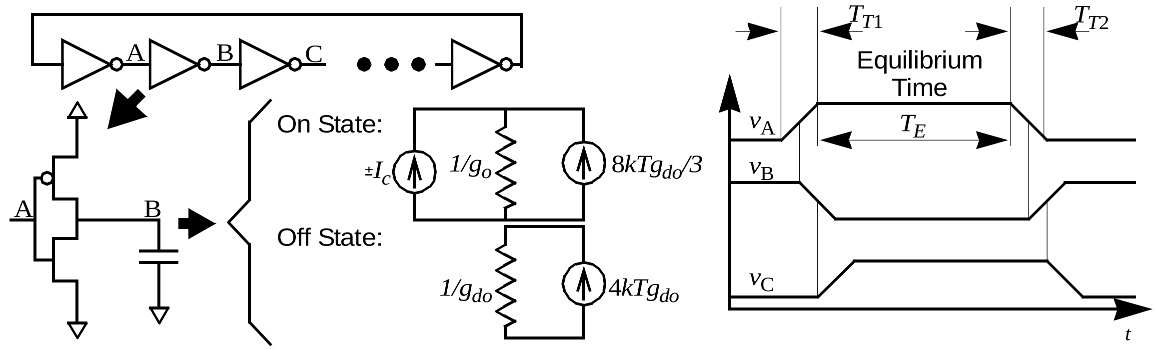

Fig. 21: A ring oscillator modeled as a switching-based oscillator. Dominant noise sources are also demonstrated.

tors derived using Leeson's formula. This comparison shows that the phase noise of a differential *LC* oscillator is smaller than that of an *RC* oscillator by roughly a factor of Q^2. Equation (13) in [47] reduces to (26) with Q=1, except for a numerical constant which is determined by the oscillator's topology. This is also consistent with the discussion presented in [47] regarding definitions of Q in various oscillators.

Equation (26) also shows that the phase noise is inversely proportional to the minimum power dissipation, which is in turn proportional to the capacitor value and the square of the bias voltage. We will see that this result holds for ring oscillators as well.

3.3.2. Phase noise in ring oscillators

To calculate the phase noise in ring oscillators, we model them as switching-based oscillators. In this model, each inverter is assumed to have only two distinct states for noise calculations. In its *on* state, T_T, it delivers (or sinks) a constant current, I_C, independent of its input and output voltages. Its output resistance is $1/g_o$ in this state and its equivalent noise resistance is $3/(2g_{do})$, as predicted by the long channel theory of MOSFET noise [48]. Here, g_o and g_{do} are the device output conductance values in the saturation region and for zero v_{ds}, respectively. For simplicity, the two transistors in each inverter are assumed to be properly sized to be equivalent. In its *off* state, T_E, the inverter is in equilibrium and can be replaced by a resistor of $1/g_{do}$ because its output conductance is dominantly determined by the conducting device (Fig. 21).

In this model, the interstage noise effects are neglected. That is, variations of the voltage on node A do not affect the voltage on node B regardless of the inverter's state. For simplicity we assume that the electrical properties of NMOS and PMOS transistors are identical. Furthermore, each inverter is assumed to switch when its input voltage reaches $v_{dd}/2$ (Fig. 21). These assumptions do not affect the general validity of the derivation.

To calculate phase noise one first finds the variance of the control voltage right before the switching moment. Since we have assumed that the switching takes place when the voltage reaches $v_{dd}/2$, the value of the control voltage is a deterministic variable after each switching. We can then use (12) with $\sigma_o^2 = 0$ repeatedly for various regions of one half-period, starting with the second half of R_{T1}, to find the variance of voltage at the new switching time. Fortunately certain simplifications are possible in the case of our model. According to (12), if the equilibrium time, T_E, is much longer than the time constant C/g_{do}, the variance of the control voltage at the end of this time interval is kT/C. This condition is usually well satisfied because g_{do} is a relatively large number. The approximation further improves for ring oscillators with many inverters.

During the first half of T_{T2}, the output impedance of the inverter is $1/g_o$ which is normally large. Consequently, we can assume that $T_{T2}/2$ is much smaller than C/g_o in this region and we can replace the exponential terms in (12) by their series expansion. The variance of control voltage at the switching time is then given by

$$\overline{\Delta v_C^2} = \frac{kT}{C}\left(1 + \frac{2T_{T2}g_{do}}{3C}\right), \tag{27}$$

where we have used $t = \frac{T_{T2}}{2}$, $\overline{\sigma_o^2} = \frac{kT}{C}$, $R_n = \frac{2}{3g_{do}}$, $R = \frac{1}{g_o}$ and $t \ll RC$ in (12). Since we assumed that current is constant during the *on* state, (27) can be rewritten as

$$\overline{\Delta v_C^2} = \frac{kT}{C}\left(1 + \frac{2g_{do}}{3}\frac{v_{dd}}{I_C}\right), \tag{28}$$

and using (13) the variance of the switching time jitter is

$$\overline{\Delta T_s^2} = \frac{kTC}{I_C^2}\left(1 + \frac{2g_{do}}{3}\frac{v_{dd}}{I_C}\right). \tag{29}$$

Since there are $2N$ independent switching events in each period, the total period jitter will be

$$\overline{\Delta T_o^2} = \frac{2NkTC}{I_C^2}\left(1 + \frac{2}{3}\frac{g_{do}v_{dd}}{I_C}\right), \tag{30}$$

where N is the number of inverters in the oscillator. The nominal period of the signal from this oscillator is equal to the sum of all delays from individual inverters:

$$T_o = \frac{NCv_{dd}}{I_C}. \tag{31}$$

After eliminating I_c between (30) and (31) and using the long-channel expression for g_{do} in (30), the period jitter is found to be

$$\overline{\Delta T_o^2} = \frac{2kTT_o^2}{NCv_{dd}^2}\left(1 + \frac{4}{3}\frac{v_{dd}}{v_{gs} - v_T}\right). \tag{32}$$

For calculation of the minimum phase noise for ring oscillators, we assume the optimum case of $v_{gs} \approx v_{dd}$, $v_T \approx \frac{v_{dd}}{2}$ and note that $P_{min} = f_o NCv_{dd}^2$. We can then find the minimum jitter and minimum phase noise, just as we did for other relaxation oscillators:

$$\overline{\Delta T_o^2} \approx \frac{7.33kT}{NCv_{dd}^2 f_o^2} = \frac{7.33kT}{p_{min} f_o} \tag{33}$$

and

$$PN_{min}(\Delta f) \approx \frac{7.33 f_o kT}{NCv_{dd}^2(\Delta f)^2} = \frac{7.33kT}{P_{min}}\left(\frac{f_o}{\Delta f}\right)^2. \tag{34}$$

3.3.3. Phase noise in coupled oscillators

Coupled oscillators are used for several applications, including high-resolution delay circuits and multi-phase clock generators in digital systems [49]. Phase noise in these oscillator topologies (in their most general form) has been studied elsewhere and it is shown that the phase noise of a network of M optimally-coupled, identical oscillators is M times smaller than that of each individual oscillator working by itself [50].

The time-domain analysis presented here supports this result. In a set of M coupled oscillators, if the random noise delays the transition at any of the nodes in any of the oscillators beyond the nominal transition time, the transitions in the corresponding node in other oscillators accelerate the transition through coupling. In an optimally-coupled set of oscillators, the final jitter in each of the oscillators is the average of what the jitter would be in an individual oscillator working by itself. Since the jitters in individual oscillators are independent random variables, the variance of their average is $1/M$ of the jitter in each single oscillator working by itself. This finding, combined with (14), dictates that the phase noise of a set of M optimally-coupled oscillators is $1/M$ of the phase noise in each oscillator.

The coupling of oscillators reduces the phase noise at the expense of higher power dissipation. A network of M coupled oscillators exhibits M times smaller phase noise compared to single oscillators while it also consumes M times more power. Equations (25) and (34) show that a suppression factor of M in the phase noise of individual oscillators is already achievable through increasing the power consumption by the same factor. The use of coupling is thus not particularly useful for phase noise suppression because it does not reduce the minimum achievable phase noise.

3.4. Close-in Phase Noise in Electrical Oscillators

One of the advantages of time-domain analysis of phase noise is that it is based on fewer approximations compared to frequency-domain analysis. The results of this method are valid over a wider range of spectrum. This characteristic makes it possible to study the properties of phase noise at close-in frequencies using time-domain analysis. As we will see shortly, some of these properties are distinctly different from those of far-out phase noise.

"Close-in" is defined at small offset frequencies relative to the oscillation frequency, where the phase noise spectrum does not have a $1/f^2$ shape. The analysis of phase noise at these frequencies is usually more complicated than that of the far-out phase noise mainly because close-in phase noise is, by definition, affected by low-frequency colored noise, such as generation/recombination noise and $1/f$ noise.

The analysis of close-in phase noise is often regrettably avoided in the literature on the ground that phase-locked-loops, which are used in most communication systems, suppress the phase noise at small offset frequencies. However, with the emergence of submicron MOSFETs with $1/f$-noise corner frequencies on the order of 100 MHz, close-in phase noise can have a noticeable effect on the overall performance of future communication systems[13]. Furthermore, a deep understanding of phase noise demands its characterization at all offset frequencies.

In this section, we use a simple, practical relaxation oscillator to study the properties of close-in phase noise. We first present the analytical formulation of the phase noise of the signal shown in

13. The spectrum of phase noise generated by $1/f$-noise has a $1/f^3$ shape. Thus, a large $1/f$-noise corner frequency causes a large $1/f^3$ corner frequency in phase noise spectrum. By definition, this extends close-in phase noise region to larger offset frequencies.

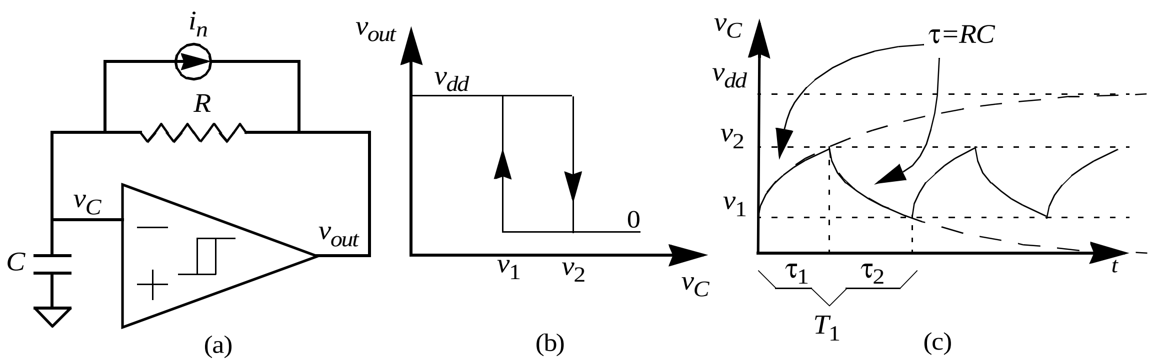

Fig. 22: (a) A typical *RC* relaxation oscillator. (b) The Schmitt comparator transfer function. (c) The capacitor voltage waveform.

Fig. 15. This signal can represent the output of a relaxation oscillator as well as the output of an arbitrary oscillator after passing it through a limiting amplifier. Thus, many of the phase noise properties of this signal are generally applicable to all kinds of oscillators. We first introduce a relaxation oscillator whose output can be represented by the signal given in Fig. 15. We then present the analytical formulation of phase noise due to white noise and low-frequency colored noise. Unless otherwise stated, our formulation assumes that the signal of Fig. 15 is generated by the simple relaxation oscillator shown in Fig. 22. This assumption does not affect the generality of the final results. Using these formulations, we discuss various properties of close-in phase noise as well as various ways of suppressing the effect of low-frequency, colored noise on phase noise. This discussion provides useful insight about the frequency stability of electrical oscillators and practical guidelines for designing low-phase-noise oscillators. Some of the formulations provided in subsection 3.4.1 are already briefly presented in previous parts when we studied the minimum achievable phase noise of this oscillator in absence of colored noise. These parts are repeated here for completeness.

3.4.1. Formulation of jitter in relaxation oscillators

The relaxation oscillator of Fig. 22 is composed of a Schmitt trigger comparator in an *RC* feedback loop. The details of the operation of this oscillator were explained earlier in this chapter. In this section we assume that the output of this oscillator has a duty cycle of fifty percent.

For the analysis of jitter and phase noise of this oscillator, we assume that the only noise source of the system is i_n, which is in parallel with the resistor (the comparator is noise-free). The jitter is the result of the uncertainty of the capacitor voltage at the end of each half period, which is in turn the result of the resistor noise. The value of the capacitor voltage at the start of each half period is a deterministic variable because the comparison levels v_1 and v_2 are assumed to be noise-free. We define the series of random variables Δv_i to characterize the uncertainty of the capacitor voltage at the end of the ith half-period. Using (10), these random variables as functions of the noise source and circuit parameters are given by

$$\Delta v_i = \frac{e^{-\frac{T_o}{2RC}}}{C}\int_0^{\frac{T_o}{2}} e^{\frac{x}{RC}} i_n\left(x + \frac{(i-1)T_o}{2}\right) dx , \tag{35}$$

where we have approximated the duration of the ith half-period by its nominal value. Using this equation, we can calculate the fluctuation properties of Δv_i's:

$$\overline{\Delta v_i} = 0 \tag{36}$$

and

$$\overline{\Delta v_i \cdot \Delta v_j} = \frac{e^{-\frac{T_o}{RC}}}{C^2}\int_0^{\frac{T_o}{2}}\int_0^{\frac{T_o}{2}} e^{\frac{x+y}{RC}} \overline{i_n\left(x + \frac{(i-1)T_o}{2}\right) i_n\left(y + \frac{(j-1)T_o}{2}\right)} dxdy . \tag{37}$$

The random variable $\Delta\tau_i$ characterizing the fluctuations of the duration of the ith half period is merely Δv_i divided by the slope of the capacitor voltage at the transition time if we use the linear approximation. Consequently, we can write the half-cycle-to-cycle jitter as

$$\overline{\Delta\tau_i \cdot \Delta\tau_j} = \frac{e^{-\frac{T_o}{RC}}}{S_i S_j C^2}\int_0^{\frac{T_o}{2}}\int_0^{\frac{T_o}{2}} e^{\frac{x+y}{RC}} \overline{i_n\left(x + \frac{(i-1)T_o}{2}\right) i_n\left(y + \frac{(j-1)T_o}{2}\right)} dxdy , \tag{38}$$

where S_i is the slope of the capacitor voltage at the end of the ith half-period (a signed number). Evaluation of this integral is possible only after knowing the fluctuation properties of i_n.

3.4.2. Formulation of phase noise generated by white noise

In the case of white noise, $\overline{i_n(t) i_n(t')} = i_{nw}\delta(t - t')/2$, where i_{nw} is the amplitude of the single-sided PSD of the white noise source. Equation (38) dictates that in this case the half-cycle-to-cycle jitter is zero for any $i \neq j$. That is, the variations of the duration of all half-periods are mutually independent. By setting $i = j$ in (38), the half-period jitter is found to be

$$\overline{\Delta\tau_i^2} = \frac{Ri_{nw}}{4S_i^2C}\left(1 - e^{-\frac{T_o}{RC}}\right) \tag{39}$$

where, for simplicity, we have assumed that the slope of the waveform is the same for all falling and rising edges. Using (9) we can calculate the period jitter as

$$\overline{\Delta T_i^2} = \frac{Ri_{nw}}{2S_i^2C}\left(1 - e^{-\frac{T_o}{RC}}\right). \tag{40}$$

The variance of the duration of k consecutive periods, called cumulative jitter, is k times this number and grows linearly with k (or, equivalently, with the total duration under consideration). This result is essential for the formulation of phase noise presented in this sub-section. Although our proof of the linear dependency of cumulative jitter on k is limited to the circuit of Fig. 22, it is generally a valid approximation if the following conditions are satisfied. First, all of the noise sources in the system should be white, and second, all poles of the system should be significantly higher in frequency than the offset frequency at which we calculate phase noise. The proof of this supposition is presented in Appendix B.

Knowing that the variance of the cumulative jitter grows linearly with time, we can analytically calculate the PSD of the signal given in Fig. 16. This analysis is performed in Appendix A for Guassian distributed jitter, and it is shown that the spectrum of phase noise around the first harmonic can be approximated by

$$PN(\Delta f) = \frac{f_o^3\overline{(\Delta T)^2}}{\left(\pi f_o{}^3\overline{(\Delta T)^2}\right)^2 + (f - f_o)^2}. \tag{41}$$

Equation (41) indicates that the phase noise around the first harmonic can be approximated by a Lorentzian function. Stratonovich [41] shows that the phase noise of a noisy sinusoidal signal can also be approximated by such a function. In fact, this result is quite general and applies to any periodic signal (regardless of its shape) as long as the square root of the period jitter is much smaller than the period and the cumulative jitter grows linearly with time. The first of these conditions is satisfied in any circuit that one could practically call an oscillator. The second condition was discussed earlier.

Equation (41) shows that the far-out phase noise drops as $1/(\Delta f)^2$ when $\Delta f = f - f_0$ is the offset frequency. This far-out phase noise behavior is well-known from measurement results [51] and other theoretical work [42] and is independent of the choice of definition for phase noise. The phase noise, however, becomes flat in the vicinity of the carrier. This latter result is dependent upon the choice of definition for phase noise.

3.4.3. Formulation of phase noise generated by colored noise

In the presence of colored noise, the formulation of phase noise becomes complicated because the autocorrelation of the i_n is no longer a delta function and cycle-to-cycle jitter can be non-zero for $i \neq j$. In this subsection, we assume that the autocorrelation function of colored noise is Lorentzian. The effect of $1/f$ noise can be captured by modeling it as the sum of several Lorentzian sources.

The power spectral density and autocorrelation function of a single Lorentzian-shape current noise source are given by $S_i(\omega) = i_{nl}/(1+\omega^2\theta^2)$ and $\overline{i_n(t)i_n(t')} = i_{nl}/(4\theta)\exp(-|t-t'|/\theta)$, respectively, where i_{nl} is the amplitude of the single-sided PSD at ω=0, and θ determines how fast the autocorrelation function drops with time. Using this autocorrelation function, (38) reduces to:

$$\overline{\Delta\tau_i^2} = \frac{i_{nl}R^2}{4S_i^2(R^2C^2-\theta^2)}\left(-\theta-\theta e^{-\frac{T_o}{RC}} + RC - RCe^{-\frac{T_o}{RC}} + 2\theta e^{-\frac{T_o}{2RC}-\frac{T_o}{2\theta}}\right) \tag{42}$$

and

$$\overline{\Delta\tau_i \cdot \Delta\tau_j} = \frac{i_{nl}R^2}{4S_iS_j(R^2C^2-\theta^2)}\left(-\theta-\theta e^{-\frac{T_o}{RC}} + \theta e^{-\frac{T_o}{2RC}-\frac{T_o}{2\theta}} + \theta e^{-\frac{T_o}{2RC}+\frac{T_o}{2\theta}}\right)e^{\frac{-|i-j|T_o}{2\theta}} \tag{43}$$

for any $i \neq j$.

The above equations can be combined with (9) to calculate the period jitter and cycle-to-cycle jitter. This calculation shows that period jitter can be minimized by equalizing the slope of the signal at all transitions (rising and falling edges). This result is consistent with previous findings [51] and can be explained intuitively. The change in the duration of each half-period due to noise can be compensated by the change in the duration of the adjacent half period because the fluctuation properties of the noise source vary slowly with time, and the S_i's have different signs at the end of two consecutive half-periods. In the fully symmetric case, $S_{2i-1} = -S_{2i}$, and the effect of low-frequency colored noise is greatly suppressed.

In the fully asymmetric case $S_{2i-1} = \infty$ and S_{2i} is finite. Since we are usually interested in the effect of low frequency colored noise on close-in phase noise, we have $\theta \gg T_o$ and $\theta \gg RC$. The calculations of cycle-to-cycle jitter using these relationships for the fully unsymmetrical case leads to

$$\overline{T_i \cdot T_j} \approx A_\theta e^{\frac{-|i-j|T_o}{\theta}}, \tag{44}$$

where A_θ is given by

$$A_\theta = \frac{i_{nl}R^2}{4S_{2i}^2(R^2C^2 - \theta^2)}\left(-\theta - \theta e^{-\frac{T_o}{RC}} + \theta e^{-\frac{T_o}{2RC} - \frac{T_o}{2\theta}} + \theta e^{-\frac{T_o}{2RC} + \frac{T_o}{2\theta}}\right). \tag{45}$$

Equation (44) is exact only for $i \neq j$.

Equation (44) shows that the cycle-to-cycle jitter drops in a manner similar to a Lorentzian auto-correlation function. This result is essential for the phase noise formulation presented in this sub-section. Although our proof of this phenomenon is limited to the circuit of Fig. 22, it can be a reasonable approximation for many other circuits if the following conditions are satisfied. First, the only noise source of the circuit should be a Lorentzian noise, and second, the lowest-frequency pole of the system should be much larger than the offset frequency at which we calculate phase noise (Appendix B). Thus the validity of the phase noise formulation presented in this chapter is not limited to the circuit of Fig. 22.

The phase noise of a signal with cycle-to-cycle jitter given in (44) is calculated in Appendix A as

$$PN(j\omega) = \frac{\displaystyle\sum_{k'=0}^{\infty} \frac{\left(-\frac{\omega^2 E_\theta}{2}\right)^{k'}}{k'!} \frac{f_o^3\left(D_\theta + \frac{2k'T_o}{\omega^2\theta}\right)}{\left(\pi f_o^{\,3}\left(D_\theta + \frac{2k'T_o}{\omega^2\theta}\right)\right)^2 + (f - f_o)^2}}{\displaystyle\sum_{k'=0}^{\infty} \frac{\left(-\frac{\omega^2 E_\theta}{2}\right)^{k'}}{k'!}}, \tag{46}$$

which is in fact the sum of several Lorentzian functions. C_θ, D_θ and E_θ are given by

$$C_\theta = -2A_\theta \frac{e^{-\frac{T_o}{\theta}}}{\left(1 - e^{-\frac{T_o}{\theta}}\right)^2}, \tag{47}$$

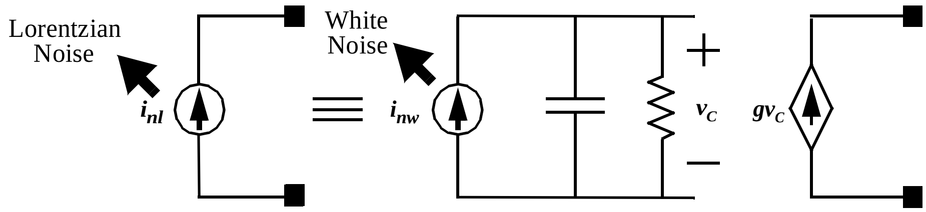

Fig. 23: White-noise equivalent network for a Lorentzian noise source.

$$D_\theta = A_\theta\left(1 + \frac{2e^{-\frac{T_o}{\theta}}}{\left(1 - e^{-\frac{T_o}{\theta}}\right)}\right) \tag{48}$$

and

$$E_\theta = 2A_\theta \frac{e^{-\frac{T_o}{\theta}}}{\left(1 - e^{-\frac{T_o}{\theta}}\right)^2}. \tag{49}$$

In the presence of multiple independent noise sources in a system, the total cycle-to-cycle jitter will be the sum of the cycle-to-cycle jitters generated by individual sources. It is easy to show that in this case the cumulative jitter is also the sum of the cumulative jitter generated by individual sources. After calculating the accumulated jitter, we can calculate the phase noise using the method presented in Appendix A.

3.4.4. The characteristics of close-in phase noise

In this section we use our phase noise formulation to discuss the properties of close-in phase noise. We first examine the general shape of the phase noise spectrum in the presence of various kinds of noise sources and discuss the validity of some of the generally-accepted beliefs about this spectrum. We then explain the differences between the properties of the close-in phase noise and that of the far-out phase noise. Our analysis shows that some of the approximations, which are valid for far-out phase noise, are not acceptable for close-in phase noise. Finally, we discuss various ways of suppressing the effect of low-frequency, colored noise on phase noise.

Contrary to popular belief, the spectrum of the phase noise is not necessarily Lorentzian in the absence of colored noise. According to our formulation, the phase noise has a Lorentzian shape in the vicinity of the oscillation frequency only if we assume that the cumulative jitter grows linearly

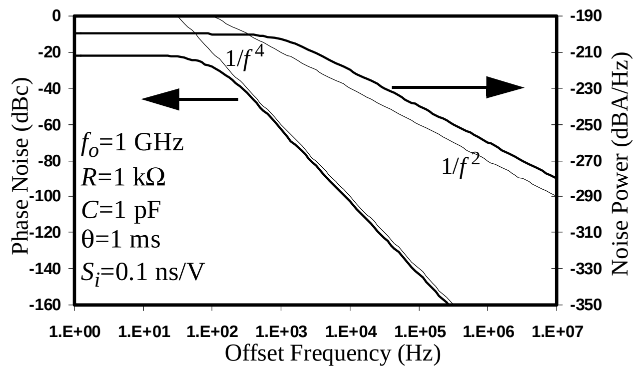

Fig. 24: Phase noise spectrum generated by a Lorentzian noise sources

with time. As discussed earlier, the validity of this assumption requires that not only all of the noise sources in the system be white but also all poles of the system lie significantly beyond the offset frequency at which we calculate the phase noise. This second condition is not necessarily satisfied for circuits containing only white noise sources. In fact, from a circuit-theory point of view, a colored noise source can often be constructed using a network of white noise sources and noise-free electronic components. Fig. 23 shows the reconstruction of a Lorentzian noise source as an example. The construction of $1/f$ noise sources is straightforward if we notice that a $1/f$ spectrum is the sum of several independent Lorentzian sources. Using such construction networks, we can start from an arbitrary oscillatory system and replace the colored noise sources with their white-noise equivalent networks to arrive at a system with only white noise sources. We would expect the phase noise spectrum of this system to have a Lorentzian shape if the absence of colored noise sources were a sufficient condition for having a Lorentzian-shape phase noise spectrum. That is, we would expect the phase noise to be Lorentzian in all systems. However, this result is experimentally shown to be invalid [51].

The fallacy of this result can also be shown using our phase noise formulation. This formulation in the presence of colored noise sources shows that the phase noise of a system with one Lorentzian noise source is the sum of several Lorentzian functions. Fig. 24 shows such a phase noise spectrum along with the PSD of the noise source generating this phase noise. The numerical parameters used in this simulation are given in the inset of this figure. Note that the spectrum of phase noise has a $1/f^4$ shape at far-out frequencies.

Fig. 25 shows that in the co-presence of independent Lorentzian and white-noise sources, the spectrum of phase noise eventually returns to a nearly-$1/f^2$ shape at far-out offset frequencies. This

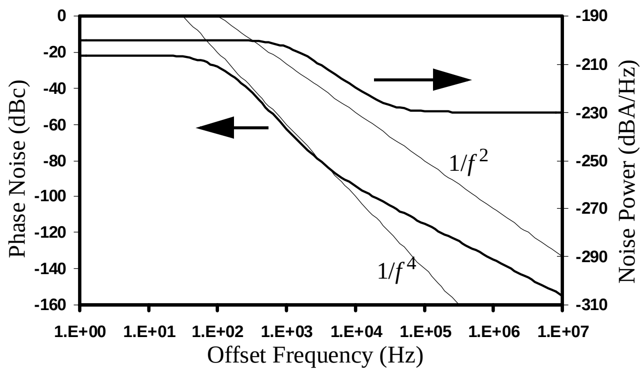

Fig. 25: The spectrum of phase noise generated by a combination of Lorentzian and white noise sources.

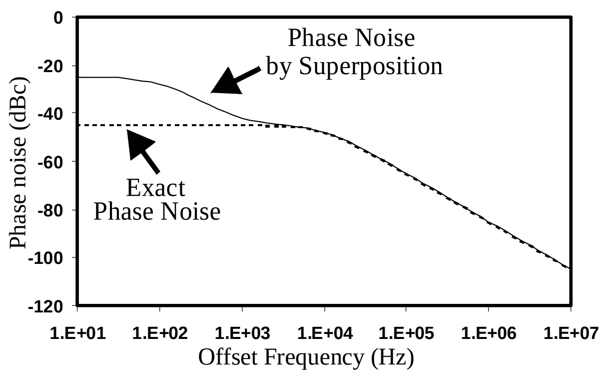

Fig. 26: Phase noise calculation using superposition.

result is expected because at high frequencies the white noise eventually dominates the Lorentzian noise. This analysis is performed using the superposition properties of cumulative jitter, as explained earlier. The numerical parameters used in this simulation are the same as the ones given in the inset of Fig. 24.

One of the generally-accepted approximations about the spectrum of far-out phase noise is superposition [51]. Unfortunately, this approximation is invalid for close-in phase noise. To see this, consider the oscillator in Fig. 22 with only one noise source $\overline{i_n(t)i_n(t')} = i_{nw}\delta(t-t')/2$. The phase noise of this oscillator is given by (41) in the vicinity of the fundamental frequency. We can rewrite the noise source as $\overline{i_n(t)i_n(t')} = i_{nw}\delta(t-t')/200 + 99i_{nw}\delta(t-t')/200$. According to superposition, the spectrum of phase noise would be the sum of the phase noise spectra generated by individual sources (with appropriate normalization). Fig. 26 shows the phase noise calcu-

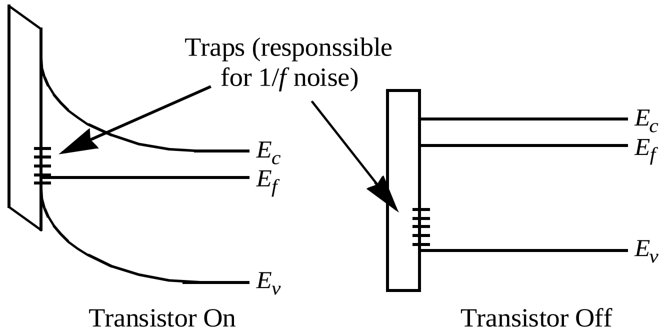

Fig. 27: Relative position of traps and the Fermi level in On and Off states.

lated using superposition and the directly-calculated phase noise. This graph clearly shows that the superposition approximation is valid only for far-out phase noise and breaks down at small offset frequencies.

Our analysis of phase noise can explain why the effect of low-frequency, colored noise on oscillators' phase noise can be suppressed by noise source switching. To suppress the effect of non-white noise, we need to force the cumulative jitter to grow linearly with time. The cumulative jitter grows linearly with time if, and only if, the jitter in each period is independent of the jitters of the previous cycles. If the system does not have a memory of the jitter induced in the previous cycles, its phase noise will be Lorentzian and the effect of the colored noise will be suppressed. The memory of the system can be reduced by periodically switching the noisy devices on and off. For example, the basic device physics for MOS devices shows that switching these devices moves the relative location of the Fermi level to the trap sites responsible for $1/f$ noise (Fig. 27) [52]. Thus, the trap sites that are located in the vicinity of the Fermi level during the 'on' state move to locations significantly higher or lower than the Fermi level due to switching and their occupancy becomes relatively deterministic during the off time. Once the device is switched back on, its noise properties are only functions of the initial conditions generated during the off time and are relatively independent of what had happened in the previous on-time. In effect, if we periodically switch the device on and off, it loses its memory of what had happened in the previous 'on' times, which means that it will have less colored noise. The experimental data supports this suppression of $1/f$ noise in switched MOS circuits [53][54]. This phenomenon is partially responsible for the experimentally-observed suppression of $1/f^3$ phase noise in single-ended ring oscillators [51].

Another way of suppressing the effect of low-frequency, colored noise on phase noise is symmetrization. Since low-frequency colored noise sources have a rich content at low frequencies, their fluctuation properties change slowly with time. Consequently, if we symmetrize the signal in terms of duty cycle and rise/fall slope, we can compensate for the effect of jitter in one half-period by its effect in the other half-period. However, the symmetrization techniques can only be useful for the noise sources which are active during the whole period. For example, this technique is effective for suppression of the effect of the noise sources associated with the tail current source in differential ring oscillators. On the other hand, this technique is ineffective for noise sources which are present only in half of the period such as MOSFET device noise in single-ended ring oscillators. In this case, the symmetrization of the waveform has an insignificant effect on phase noise because the noise of the PMOS and NMOS devices are independent, and only one of them is active in each half-period. In single-ended ring oscillators, the symmetrization can only suppress the effect of the noise of the short circuit time during which both devices conduct. It is then clear that the main mechanism of suppression of phase noise in single-ended ring oscillators is the switching effect described earlier.

The study of close-in phase noise, presented in this section, is one of the many applications of time-domain phase noise formulation. Having the advantage of being remarkably simple, this formulation can be applied to many practical problems. In the next chapter we apply this method to an asymmetrical ring oscillator to indirectly characterize MOSFET noise. The indirect characterization of MOSFET noise provides a fast and reliable method for studying noise in emerging CMOS technologies.

3.5. SUMMARY

The analysis of phase noise in electrical oscillators and its relationship to device noise have been studied. After discussing the formal definition of phase noise we presented a time-domain formulation of phase noise which is especially accurate for switching-based oscillators. We used this method to predict the minimum achievable phase noise of different types of RC oscillators after showing that a lower limit is imposed on the phase noise of such oscillators by the fluctuation-dissipation theorem of thermodynamics. We then used this method to study the properties of close-in phase noise which is crucial for analyzing the effects of low-frequency, colored noise on the frequency stability of electrical oscillators. We showed that these properties are distinctly different from those of far-out phase noise commonly studied in the literature using frequency-domain analysis. In the next chapter, we will use our time-domain phase noise formulation to indirectly characterize device noise through phase noise measurement.

CHAPTER 4:

SIMULATION AND EXPERIMENTAL RESULTS

Verification of the accuracy of noise models is arguably the most difficult problem in noise analysis. The number of parasitic elements and environmental variables that can affect the outcome of a noise measurement experiment is virtually countless. In order to obtain reliable results, these elements and variables should be de-embedded, and accounted for or controlled during the course of the experiment. Because of the complexity of such experiments, there are usually endless arguments about the validity of any experimental noise data reported in the literature.

To circumvent this problem, compact noise models are sometimes validated using detailed device simulations. In this approach, we use device simulators with various degrees of complexity to verify a compact model. These simulators are in turn validated using theoretical and experimental means. The advantage of this method is that there are fewer parasitic elements and uncertainties to be accounted for. Furthermore, environmental parameters such as temperature are much easier to control in these simulators. As we will see shortly, a graph of noise versus a wide range of temperature conditions can reveal crucial information about major noise sources in MOSFETs. Such a plot can be generated easily using device simulation while it is almost impossible to generate using experimental data.

In this chapter we first validate our compact MOSFET noise model using detailed hydrodynamic simulations. Transistors as small as 60 nm in printed gate length are used in these simulations. The results of these simulations are presented after describing the hydrodynamic device simulator used in this study.

We then turn to our phase noise formulation and verify its accuracy using previously-published phase noise data. Some of the implications of our minimum achievable phase noise formulation are also discussed in this section. To get the most benefit out of our phase noise formulation, we present this section independently of the rest of this chapter. Thus, the reader who is interested only in phase noise formulations can skip Section 4.1.

The connection between our MOSFET and phase noise formulations will become clear in Section 4.3. In this section, we experimentally validate our MOSFET noise model using indirect noise characterization through phase noise measurement. We first introduce an asymmetrical ring oscillator for which the time-domain phase noise formulation provides accurate phase noise predictions. We then use phase noise measurements to estimate the noise of the MOSFETs used in this oscillator. As discussed in Chapter 1, this method facilitates noise characterization and provides a high level of relative accuracy which suffices in many practical cases, including those presented in this work. We compare MOSFET noise for various channel lengths and under different biasing conditions to verify the predictions of our model. Finally, we discuss phase noise performance of future ring oscillators.

4.1. AMPLITUDE NOISE IN MOSFETS

4.1.1. Hydrodynamic device simulators

Device simulators are powerful tools for predicting the behavior of an electronic device before it comes into existence. A device simulator is a TCAD tool which takes impurity profiles and boundary conditions (such as terminal voltages) as inputs and provide deterministic and random fluctuations of terminal currents as outputs. Today, these simulators are commercially available with various degrees of complexity. Such simulators normally solve the Poisson equation along with a carrier transport model to find the carrier flow in the device. Once carrier flow is calculated, terminal currents can be found using the Shockley-Ramo theorem [64][65].

One of the most important parts of a device simulator is its carrier transport model which describes the relationship between electric field and carrier movement. Various carrier transport models can be used in device simulators. The origin of all of these models is the Boltzmann transport equation (BTE). The BTE is, in principle, the continuity equation for the carriers in the six-dimensional position-momentum space [21]. In the absence of generation/recombination, BTE can be written as

$$v \cdot \nabla_r f + F \cdot \nabla_p f = -\frac{\partial}{\partial t} f + \left.\frac{\partial}{\partial t} f\right|_{collision}, \tag{50}$$

where f is the probability distribution function of finding a carrier at position r with momentum p, v is carrier velocity and F is the external force. For noise analysis we also need to include carrier velocity and density fluctuation terms in this equation so that we can capture current fluctuations. These terms will be omitted in our simplified discussion here.

The BTE is a general relationship between carrier flow, external force and carrier concentration, and is thus very difficult to solve in its raw form. To find more useful relationships, we usually multiply the BTE by a function $\theta(p)$ and integrate both sides of the equation over the momentum space to arrive at simpler relationships known as balance equations. For example, defining $\theta(p)=1$ leads to balance equations for carrier density. Similarly defining $\theta(p)=p$, and $\theta(p)=E(p)$[14] leads to balance equations for momentum and energy density, respectively [21].

Using some simplifying assumptions, balance equations can lead us to the transport equations needed for device simulators[15]. The simplest set of transport equations which can be obtained using this method are the famous drift-diffusion equations:

$$J_n = nq\mu_n E + qD_n \nabla n \tag{51}$$

and

$$J_p = pq\mu_p E - qD_p \nabla p\,, \tag{52}$$

where μ and D are the mobility and diffusion constant, respectively, while n and p stand for electron and hole concentrations.

Drift-diffusion equations, although very helpful in many practical applications, have a significant deficiency. These equations ignore carrier heating and non-local transport effects. Therefore this model fails when the gradient of carrier temperature is non-zero [21], a situation which is observed in short-channel MOSFETs.

To obtain a more accurate transport model for small devices, we need to treat balance equations with more accurate approximations to arrive at a new transport model known as the hydrodynamic model [21]. The hydrodynamic model captures many non-local effects and is more accurate than drift-diffusion equations when applied to small-scale devices[16]. Eventually, this model will also fail for very small devices where Monte-Carlo simulators have to be used. Monte-Carlo simulators track the movement of individual carriers one by one and provide the most reliable numbers among all device simulators. Unfortunately, these simulators are very slow and thus cannot be used as everyday tools.

In this work we use a hydrodynamic simulator which is specially tailored for noise simulation.

---

14. $E(p)$ is the energy of a particle with momentum p.

15. For a thorough discussion, please consult [21].

16. A drawback of this model is that it involves relaxation rates which are normally very hard to estimate accurately; they are often treated as fitting parameters. This deficiency does not affect the validity of our results on the behavior of MOSFET noise.

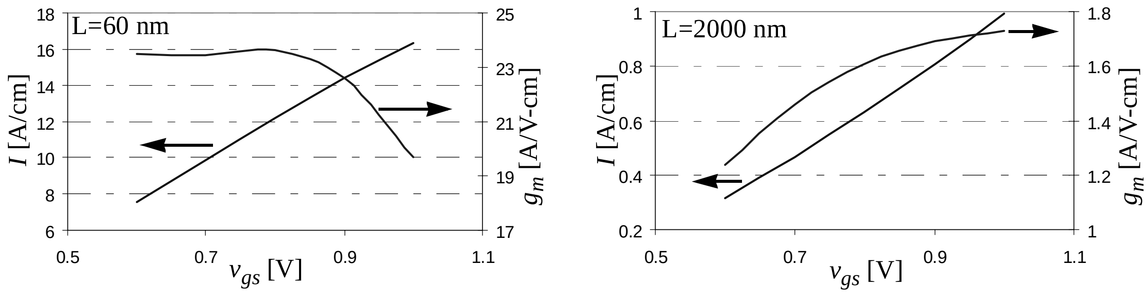

Fig. 28: Dc characteristics of long-channel and short channel devices used in hydrodynamic simulations. Drain voltage is kept constant at 1 V.

In this simulator, carrier fluctuation terms are first calculated using lengthy Monte-Carlo simulations for various impurity levels and electric fields. These numbers are then stored in a lookup table for later use by a hydrodynamic simulator. It is shown that this method gives good accuracy for noise analysis and has the advantage of being reasonably fast because the fluctuation terms are calculated only once using the Monte-Carlo simulator. The details of this simulator is discussed in [61] and [62].

4.1.2. Hydrodynamic simulation of noise in MOSFETs

For the hydrodynamic simulations presented in this work we have selected bulk devices with channel lengths ranging from 60 nm to 2000 nm. The two ends of the length range represent short-channel and long-channel MOSFETs, respectively. While they do not operate like ideal short and long-channel MOSFETs, these devices are good representatives of the two extremes. As discussed earlier, the hydrodynamic transport model fails at very small channel lengths preventing us from looking at shorter devices.

The devices used in this work are the same as the device used and discussed in [63] which is scaled (using bulk doping as a parameter) to have a constant off-current of 5e-3 A/cm at 1.0 V drain and 0 V gate bias at room temperature. We have not changed the source/drain structure with gate length. Unless otherwise stated all data are for v_{gs}=0.8 V, v_{ds}=1 V and temperature=300 K.

Fig. 28 shows the dc characteristics of short and long channel devices used in this study. In 60 nm devices, current depends almost linearly on v_{gs} resulting in a nearly constant transconductance, as we expect from short-channel devices. The slight drop in transconductance at large gate voltages is due to the strong perpendicular field which degrade carrier mobility. In 2000 nm devices, the transconductance increases with increasing gate voltage as expected for long-channel MOSFETs. Although the device does not exactly follow the square law relationship, it is a good

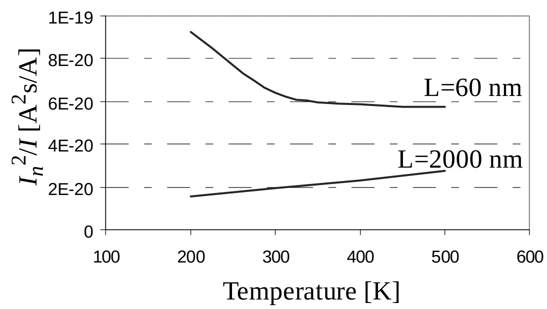

Fig. 29: Noise PSD normalized to the device current versus temperature for long and short-channel devices. Source and drain voltages are kept constant at 0.8 V and 1 V, respectively.

representative of long-channel MOSFET behavior.

The temperature dependency of drain current noise PSD reveals crucial information about the major noise phenomenon in MOSFETs. For example, if the major noise mechanism is thermal noise, its noise power usually increases with temperature. Such a device often shows inferior noise performance at high temperatures. On the other hand, if the major noise mechanism is a non-thermal effect, the noise-temperature dependency will be different. For instance, if the major noise source is shot noise, the noise power will be independent of temperature as long as the current flow is constant. Thus a graph of noise versus temperature is very useful for determining the dominant noise phenomenon in MOSFETs.

Fig. 29 shows a graph of noise PSD versus temperature for the 60 nm and 2000 nm devices studied in this work. The graphs are generated using a hydrodynamic simulation. To have a fair comparison, noise PSD is normalized to device current. This is equivalent to using wider devices at high temperatures so that the total device current levels remain constant. For long-channel devices, this normalization compensates for the change of g_{do} with temperature. Fig. 29 shows that normalized noise has a strong component that is almost linearly proportional to temperature in long-channel devices[17]. This observation suggests that the dominant noise source in these devices is thermal noise, as expected. On the other hand, noise power drops at high temperatures in short-channel devices suggesting a non-thermal effect in these devices. As we explained earlier, the dominance of the potential barrier next to source leads to the appearance of shot noise in these devices which results in a distinctive temperature dependency of noise in these devices.

Fig. 30 compares MOSFET noise to the long-channel prediction and full shot noise at different

17. For 2000 nm devices, the graph of Fig. 29, if extrapolated, does not intercept zero at 0 K. Thus these devices are not ideal long-channel devices, consistent with their I-V relationship.

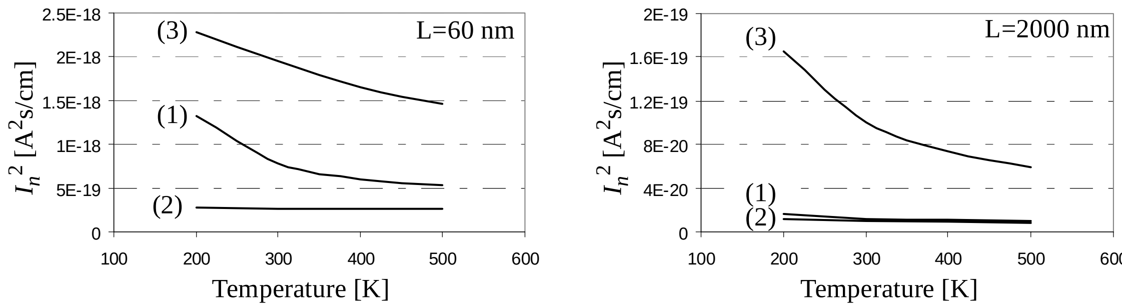

Fig. 30: Actual drain noise of a MOSFET, (1), compared to the classical prediction, (2), and full shot noise, (3) for short and long-channel devices. Source and drain voltages are kept constant at 0.8 V and 1 V, respectively.

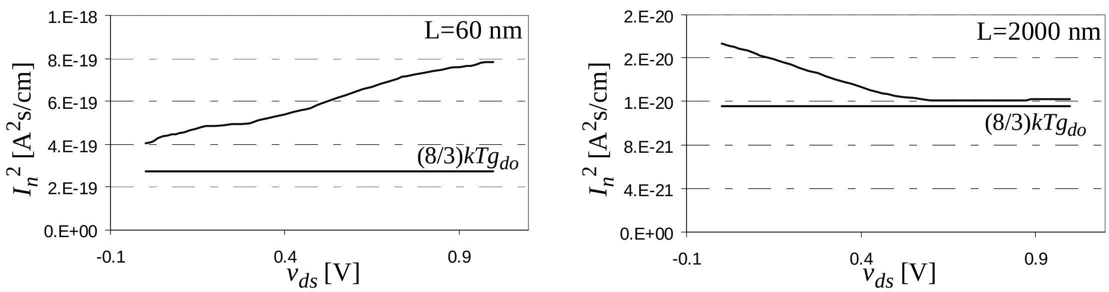

Fig. 31: Drain current noise versus drain voltage for short and long-channel devices at v_{gs} =0.8 V.

temperatures for short and long-channel devices. Note that the noise power spectral density is not normalized to current in this and the following graphs. While the drain noise of the 2000 nm-long devices closely matches long-channel predictions, the noise of the 60 nm devices drops similar to the shot noise and is always smaller than full shot noise. In these devices, drain noise drops faster than full shot noise at elevated temperatures. This is because at high temperatures, the number of scattering events in the channel increases due to lattice scattering, resulting in greater suppression of shot noise as explained in Chapter 2.

To better understand the origin of noise in MOSFETs, we also study the dependency of drain current noise on drain voltage. Fig. 31 shows drain current noise versus drain voltage for short and long-channel MOSFETs at a constant gate voltage of 0.8 V. In long-channel devices, the drain current noise decreases with increasing drain voltage, as expected from the long-channel noise formulation. On the other hand, drain current noise of the short channel device monotonically increases with drain voltage. This behavior can be explained using our MOSFET noise model. With increas-

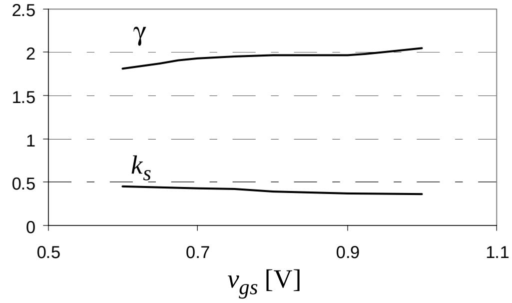

Fig. 32: Noise factor and shot noise suppression factor for a 60 nm MOSFET versus gate voltage at v_{ds}=1 V.

ing drain voltage, drain current increases which results in the increase in drain current noise due to the existence of partially-suppressed shot noise.

Fig. 31 suggests that the excess noise in short-channel MOSFETs cannot be due to carrier heating or strong electric field effects. If these phenomena were responsible for excess noise, we would expect the noise to initially drop at low drain voltages before increasing at higher drain voltages. This is because at low drain voltages, the device does not experience a strong electric field or carrier heating and thus it should behave similar to a long-channel device at small drain voltages. Since the noise of the short-channel device increases monotonically with drain voltage, it is hard to explain this excess noise based on carrier heating or strong electric field because at small drain voltages these effects are insignificant.

A comparison between the drain noise of a short-channel MOSFET (Fig. 31) and that of a carbon nanotube (Fig. 3 in [66]) reveals striking similarities. In fact, the fundamental phenomena responsible for noise in both devices are the same. In both cases nearly-independent injection of carriers from one terminal to the other terminal leads to the appearance of shot noise which is consequently partially-suppressed due to feedback.

A larger number of scattering events in the channel also results in heavier suppression of shot noise at large values of gate voltage. Fig 32 shows k_s and γ at different gate voltages. As can be seen in this figure, the shot noise suppression factor drops at high gate voltages, a behavior that can be explained by our physical argument about noise in short-channel MOSFETs. On the other hand, the dependency of γ on gate voltage cannot be easily explained. This results in a great deal of confusion when various authors report this factor (usually for different biasing conditions) and try to compare the results.

To quantitatively verify our compact model, we present in Fig. 33 a graph of noise in a

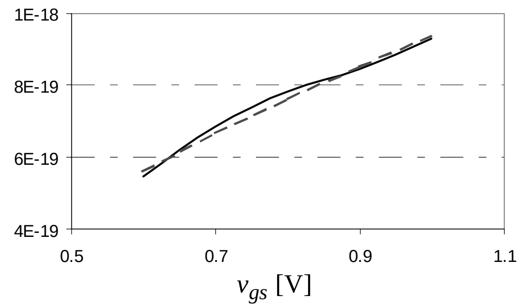

Fig. 33: Drain noise versus gate voltage compared to our compact model prediction for a 60 nm MOSFET. The dashed curve shows our compact model prediction. Drain voltage is held constant at 1 V.

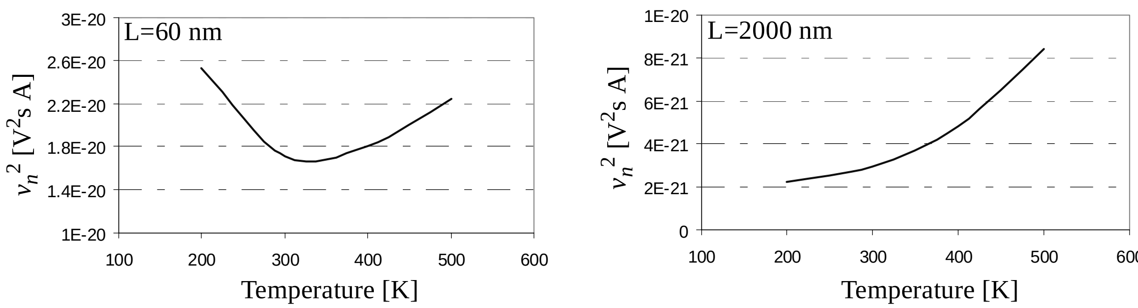

Fig. 34: Input-referred power of MOSFET drain noise versus temperature for v_{gs}=0.8 V and v_{ds}=1 V.

short-channel (60 nm) MOSFET versus gate voltage and compare it to our compact model prediction given in (7). v_T is extracted from Fig. 28 while β and I_{n1} are fitting parameters. The numerical value of β is found to be 0.65. The maximum difference between the noise power predicted by eq. (7) and the actual device noise power is less than 3 percent or 0.13 dB. It is instructive to note that the best linear fit (as suggested by the long-channel prediction) would result in an error of more than 13 percent or 0.53 dB.

Using the data extracted from these simulations, we can discuss the overall noise performance of short-channel MOSFETs. As a figure of merit we study input-referred noise in these devices[18]. Given the distinctly different noise-temperature dependency of short-channel device suggested by Fig. 29, it is instructive to look at the input referred power of drain noise versus temperature.

18. It is also possible to look at the minimum achievable noise figure of the device. However, this factor is also a function of gate noise and the correlation factor between the two noise sources which are not studied in this work.

Fig. 34 shows such a graph for short and long-channel devices. To generate these graphs, both drain noise and g_m are normalized to dc current. As discussed earlier this is equivalent to using wider devices at high temperatures so that the current level stays constant. The input-referred power of drain noise increases monotonically for long-channel devices, as expected. On the other hand, for short channel devices this power reaches a minimum at a specific temperature. For the devices studied in this work, this temperature happens to be around room temperature.

4.2. PHASE NOISE IN OSCILLATORS

We start verifying our phase noise formulation by looking at the phase noise of ring oscillators. These oscillators can usually be modeled as switching-based oscillators as discussed in Chapter 3. Table I compares the measurement results reported in [51] to the theoretical prediction of the minimum achievable phase noise (assuming long-channel MOSFET noise formulation) given by (34) for the same power. The index numbers are the same as the ones assigned in [51]. N is the number of stages and L_{min} is the channel length of the shortest transistor in the circuit. The data is presented in descending order of L_{min}. ΔPN is the difference between the minimum achievable phase noise PN_{min} and the measured phase noise $PN_{meas.}$. Hereafter, this parameter will be referred to as the “wastefulness factor”, a factor that gives a measure of the efficiency of the oscillator in terms of the power-phase-noise trade-off. Note that the simple equation given in (34) is capable of predicting the phase noise within a few dB. This confirms the accuracy of the time domain phase noise calculation method presented in this paper.

Table I shows that the wastefulness factors of these ring oscillators are smaller than 6 dB with most numbers around 2 dB. This is much better than the relaxation oscillators as we will see shortly. This table also shows that the wastefulness factor of a ring oscillator increases with decreasing L_{min}. This phenomenon can be attributed to higher short-circuit switching current in faster transistors (when PMOS and NMOS transistors conduct at the same time) or to the higher excess noise in short-channel MOS devices. The origin of this second phenomenon was discussed earlier.

It is instructive to calculate the wastefulness of practical relaxation oscillators and compare it to that of ring oscillators. The expression given in (26) provides the minimum achievable phase-noise for the idealized version of the relaxation oscillator shown in Fig. 19. Most practical relaxation oscillators are not implemented exactly in this fashion. Fig. 35 provides the schematic and the

Table 1. Experimental results vs. theoretical prediction of minimum achievable phase noise at an offset frequency of 1MHz for the ring oscillators of [51].

Index	N	L_{min} µm	f_o MHz	Power mW	$PN_{meas.}$ dBc/Hz	PN_{min} dBc/Hz	ΔPN dB	Current Starved
1	5	2	232	1.5	-118.5	-119.7	1.2	No
2	11	2	115	2.5	-126	-128	2	No
4	3	0.53	751	5.85	-114	-115.4	1.4	Yes
5	5	0.39	850	6.27	-112.6	-114.6	2	Yes
6	7	0.36	931	6.22	-111.7	-113.8	2.1	Yes
7	9	0.32	932	6.82	-112.5	-114.2	1.7	Yes
8	11	0.32	869	6.62	-112.2	-114.6	2.4	Yes
9	15	0.28	929	7	-112.3	-114.3	2	Yes
10	17	0.25	898	9.5	-112	-115.9	3.9	Yes
11	19	0.25	959	9.75	-110.9	-115.5	4.6	Yes
3	19	0.25	1330	25	-111.5	-116.7	5.2	No

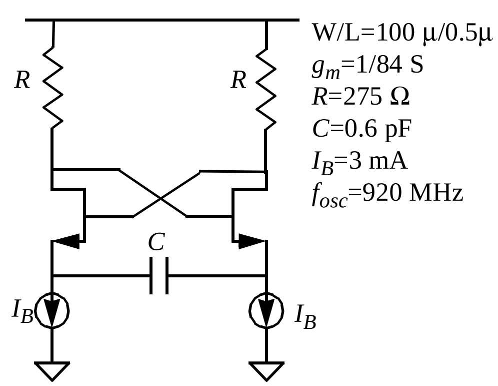

Fig. 35: The schematic and design parameters of the relaxation oscillator reported in [45].

design parameters of a CMOS relaxation oscillator reported in [45]. Although this oscillator is not exactly of the same form as the idealized relaxation oscillator given in Fig. 19, it can be modeled as such. In the case of the oscillator of Fig. 35, the charging and discharging mechanism of the capacitor is not through a resistor but rather through the current sources and the transistors. Nevertheless, these components are noisy and thus result in finite phase noise for this architecture. We compare the measured phase noise of this oscillator to the minimum phase noise predicted by (26) for the same power to get a measure of the power efficiency of the oscillator.

Fig. 36 compares the phase noise reported in [45] to the minimum achievable phase noise given

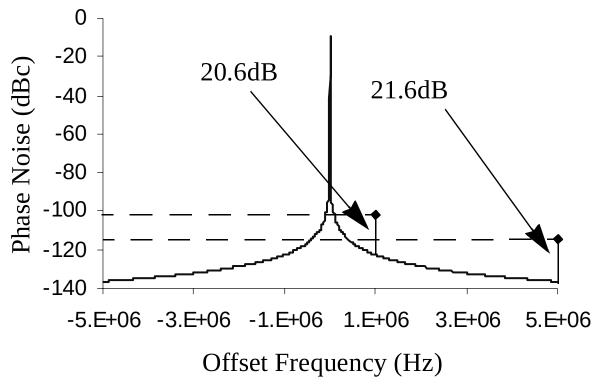

Fig. 36: Minimum achievable phase noise compared to the data reported in [45] for an oscillator with f_{osc}=920 MHz and P_{min}=19.8 mW at T=300 K.

by the second part of (26) under a constraint of constant power. To calculate P_{min}, we have assumed v_{dd}=3.3 V, which is typical for a 0.5 μm technology. The minimum achievable phase noise for this power level is -122.6 dBc/Hz and -136.6 dBc/Hz at 1 MHz and 5 MHz offset frequencies, respectively. The measured values reported in [45] are -102 dBc/Hz and -115 dBc/Hz. The wastefulness factor is around 21 dB for this oscillator at these offset frequencies.

A similar architecture is reported in [46] as a relaxation VCO, which draws 2.3 mA of current from a 6 V power supply at 115 MHz (Fig. 5a and 7 in [46]). Under constant power, (26) predicts that the minimum achievable phase noise for this oscillator is -139 dBc/Hz at an offset frequency of 1 MHz. This is again 21 dB lower than the reported value of -118 dBc/Hz given in [46]. These two examples illustrate that this particular relaxation oscillator configuration suffers a high wastefulness factor. The large wastefulness factor in these relaxation oscillators can be due to the continuous current flow in these oscillator topologies. It is also possible that the presence of other noise sources in the comparator lead to a high wastefulness factor.

4.3. Indirect Characterization of MOSFET Noise through Phase Noise Data

Experimental verification of noise models is a very costly and time-consuming process. In this section, we introduce a new indirect method for MOSFET noise characterization and use this method to experimentally validate our MOSFET noise model. Being based on phase noise measurements, this method is much faster than direct device noise characterization which requires accurate control of environmental variables and de-embedding of all parasitic elements. This is because the phase noise of an oscillator is predominantly set by the noise sources and electrical components inside the oscillation loop. Thus most off-chip parasitic elements have an insignificant effect on the phase noise of integrated oscillators. Furthermore, phase noise measurement is a comparative measurement between the signal power at the center frequency and that at a small offset frequency. Therefore, the effects of many parasitic elements such as cable loss and impedance mismach are significantly canceled out in this measurement.

In the rest of this section, we first introduce an asymmetrical ring oscillator that will be used for indirect characterization of device noise. This oscillator is designed to provide a predictable phase noise power for a given device noise level. We present experimental results for the phase noise of this oscillator and discuss its implications for noise in MOSFETs. These results substantiate the predictions of our semi-ballistic MOSFET noise model presented in Chapter 2.

4.3.1. An oscillator for indirect MOSFET noise characterization

Figure 37 shows the asymmetrical ring oscillator designed for our experiment. This oscillator satisfies most of the simplifying assumptions used in the time-domain phase noise formulation presented in Chapter 3. Therefore the phase noise of this oscillator is accurately predictable using that formulation.

As can be seen in Fig. 37, our asymmetrical ring oscillator is composed of seven inverters capacitively loaded with large metal-insulator-metal (MIM) capacitors. These capacitors are designed to be large enough to swamp the total capacitance of all internal nodes of the oscillator. Therefore the total capacitance is guaranteed to be linear and have a weak temperature dependency. Furthermore the capacitors are the same in different ring oscillators making it possible to compare the device noise of MOSFETs with various channel lengths.

The seven inverters in the oscillation loop are sized differently, hence the name asymmetrical. There are three 1X inverters and four 10X ones in the oscillation loop. With the loading capacitors being the same, the outputs of the small inverters change much more slowly than the outputs of large inverters (Fig. 37). Thus the frequency of oscillation is mainly determined by these inverters. Also, because of the faster voltage rate of change, the noise of large inverters has an insignificant effect on the phase noise of the oscillator. This is because the induced jitter at each stage is inversely proportional to the square of the voltage rate of change at its output. Even though current noise power at the output of the large inverters is approximately ten times stronger than that at the output of the small oscillators, their jitter contribution is ten times smaller because of the faster voltage rate of change. Therefore the formulations presented in Chapter 3 are valid for this oscilla-

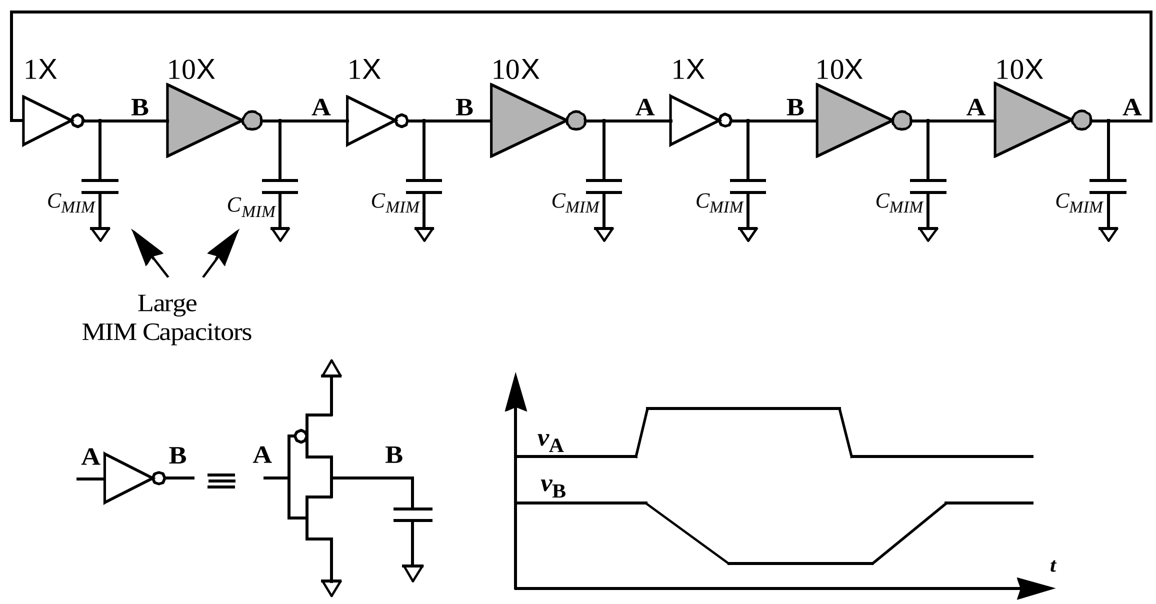

Fig. 37: An asymmetrical ring oscillator for indirect characterization of device noise through phase noise measurement.

tor with N=3.

Another feature of this oscillator is the fact that the gate to source voltage of the transistors in small inverters is nearly constant for the duration of charge or discharge of the capacitors at their outputs. This is because the large inverters are capable of charging and discharging their output nodes much faster than are the small inverters. Since these nodes are the input to small inverters, the gate to source voltage of the transistors in these inverters stays constant during most of the charge and discharge time. This means that the biasing condition of the transistors whose noise power set the oscillator's phase noise is constant during their active time. This is an important virtue of this oscillator which enables reliable indirect characterization of device noise though phase noise measurements for various biasing condition.

As can be seen, the approximations involved in the time-domain formulation of phase noise presented in Chapter 3 are closely satisfied in this oscillator. Thus we expect this formulation to provide accurate numbers for phase noise for a given device noise level. Similarly, it should be possible to back-calculate device noise power using the same equations after measuring phase noise.

To study device noise at different channel lengths, three oscillators have been designed with the same topology and the same loading capacitance but different channel lengths. We expect the shortest transistors to be semi-ballistic devices and the longest MOSFETs to follow long-channel

Table 2. Design parameters for the three asymmetrical ring oscillators.

Oscillator Number	L_{n_small} (µm)	W_{n_small} (µm)	L_{p_small} (µm)	W_{p_small} (µm)	L_{n_large} (µm)	W_{n_large} (µm)	L_{p_large} (µm)	W_{p_large} (µm)	$C_{MIM}+C_{paras.}$ (fF)
OSC1	0.18	0.28	0.18	0.56	0.18	2.8	0.18	5.6	525
OSC2	0.38	0.56	0.38	1.12	0.38	5.6	0.38	11.2	570
OSC3	0.54	0.84	0.54	1.68	0.54	8.4	0.54	16.8	625

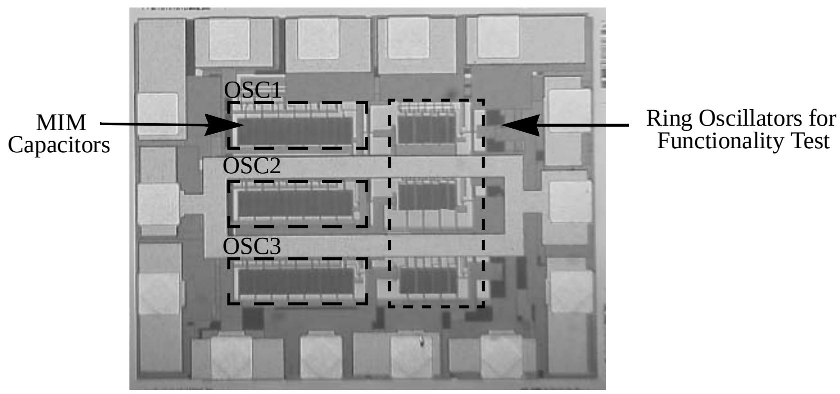

Fig. 38: Die photo of the three asymmetrical ring oscillators.

MOSFET formulation. The width-to-length ratio has been kept constant in these oscillators to ensure comparable oscillation frequencies. The transistors are built with multiple gate fingers to minimizes gate resistance noise. In all cases, the noise power of the gate resistance is at least a factor of ten smaller than the device noise, according to the published data. All inverters in all three oscillators are loaded by similar MIM capacitors of a nominal value of 500 fF. Thus the loading capacitance is, to the first order, the same in these oscillators.

Using circuit simulation, we have estimated the parasitic capacitance at internal nodes by increasing the loading capacitance to $2C_{MIM}$ and taking note of the frequency change. The effective value of the parasitic capacitance can be found using the following equation:

$$\frac{C_{parasitic} + C_{MIM}}{C_{parasitic} + 2C_{MIM}} = \frac{f_{ocs-new}}{f_{osc-old}} \tag{53}$$

where $f_{osc\text{-}old}$ and $f_{osc\text{-}new}$ are the oscillation frequencies before and after increasing the loading capacitance, respectively.

The oscillators described above are fabricated in a commercially-available 0.18 µm CMOS process technology. Figure 38 shows a photo of the die carrying these oscillators. Table 2 shows the design parameters for these oscillators. Total capacitance per node for each of the oscillators extracted from simulation is also reported in this table. In the following section we present the result of phase noise measurement on these oscillators and their implication for noise in short-channel MOSFETs.

4.3.2. Phase noise measurement results and discussion

We have measured the phase noise of the three oscillators, under various biasing conditions, using an HP8563 spectrum analyzer. Figure 39 shows the spectrum of the three oscillators with a typical supply voltage of 1.8 V after amplification using an RF amplifier. As presented in Table 2, these oscillators have the same loading capacitance and transistor width-to-length ratio while their transistor lengths are different. OSC1, OSC2 and OSC3 use 0.18 μm- 0.38 μm- and 0.54 μm-long transistors, respectively. As can be seen in this figure, the oscillators with longer transistors have a superior spectral purity and smaller phase noise. To measure the phase noise of these oscillators accurately, we use the phase noise measurement module on HP8563.

Figure 40 shows the phase noise of these oscillators with a typical supply voltage of 1.8 V. All of the phase noise measurements are performed at an offset frequency of 1 MHz from the center frequency. This offset frequency is located in the $1/f^2$ region of phase noise for all oscillators. Because the effect of $1/f$ noise is thus insignificant, the phase noise at this offset frequency is predominantly set by the power in the white region of noise spectrum.

As can be seen in Fig. 40, the phase noise of the oscillators with longer channel lengths is generally smaller, a phenomenon which is expected because of the smaller noise power in these devices. It is difficult to quantitatively estimate the effect of excess noise on the performance of these oscillators from these numbers because the oscillation frequency and the loading capacitance are also slightly different in these oscillators.

To quantify the effect of excess device noise, we compare the phase noise of these oscillators to the minimum achievable phase noise of ring oscillators derived in Chapter 3. Fig. 41 presents such a comparison. For the calculation of minimum achievable phase noise we have used the first part of (34) assuming a room temperature of 300 K and N=3, as justified earlier in this section. Multiple measurements have been performed to obtain more reliable results. The solid line connects the average values. Fig. 41 shows that the difference between the minimum achievable phase noise and the measured phase noise is larger at small channel lengths, with a difference of around 6.5 dB between the longest and the shortest transistors. Thus we estimate that the noise power of the min-

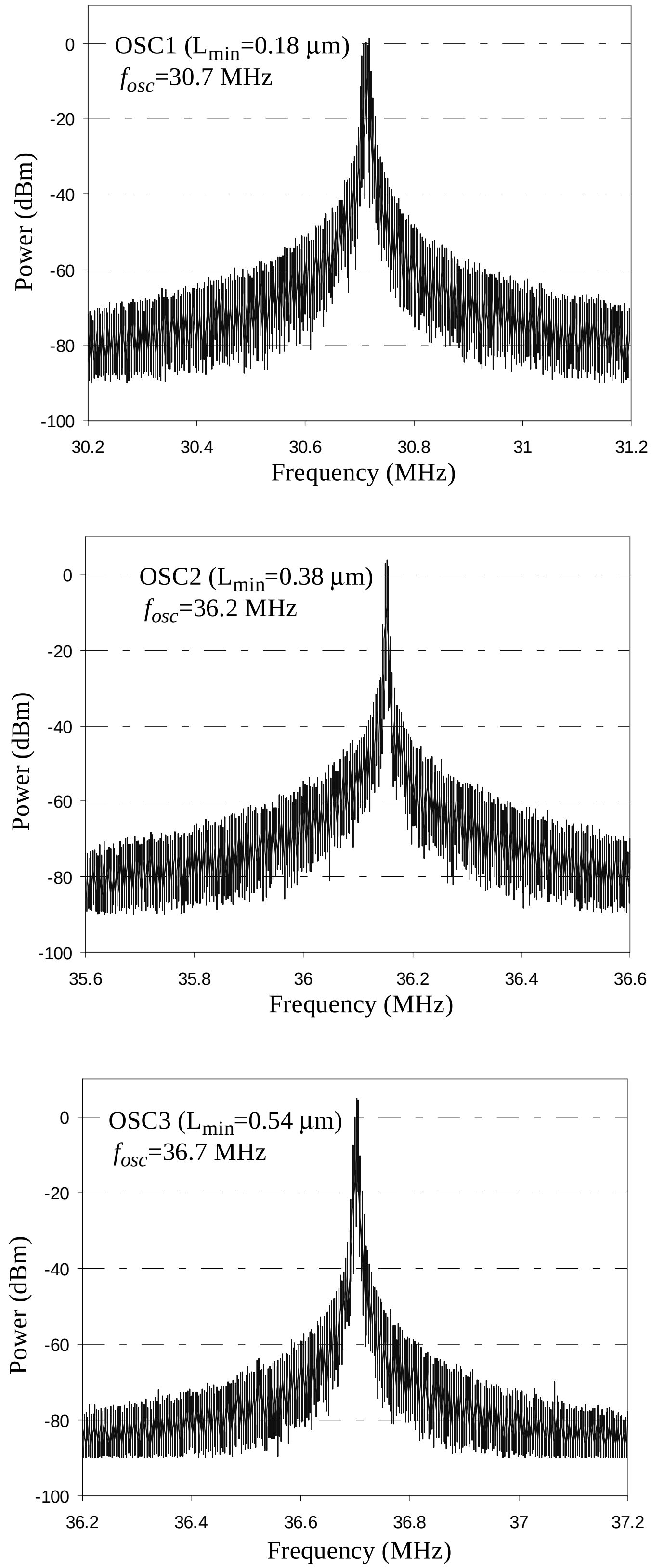

Fig. 39: The spectrum of three asymmetrical ring oscillators with different channel lengths (IF bandwidth = 300 Hz).

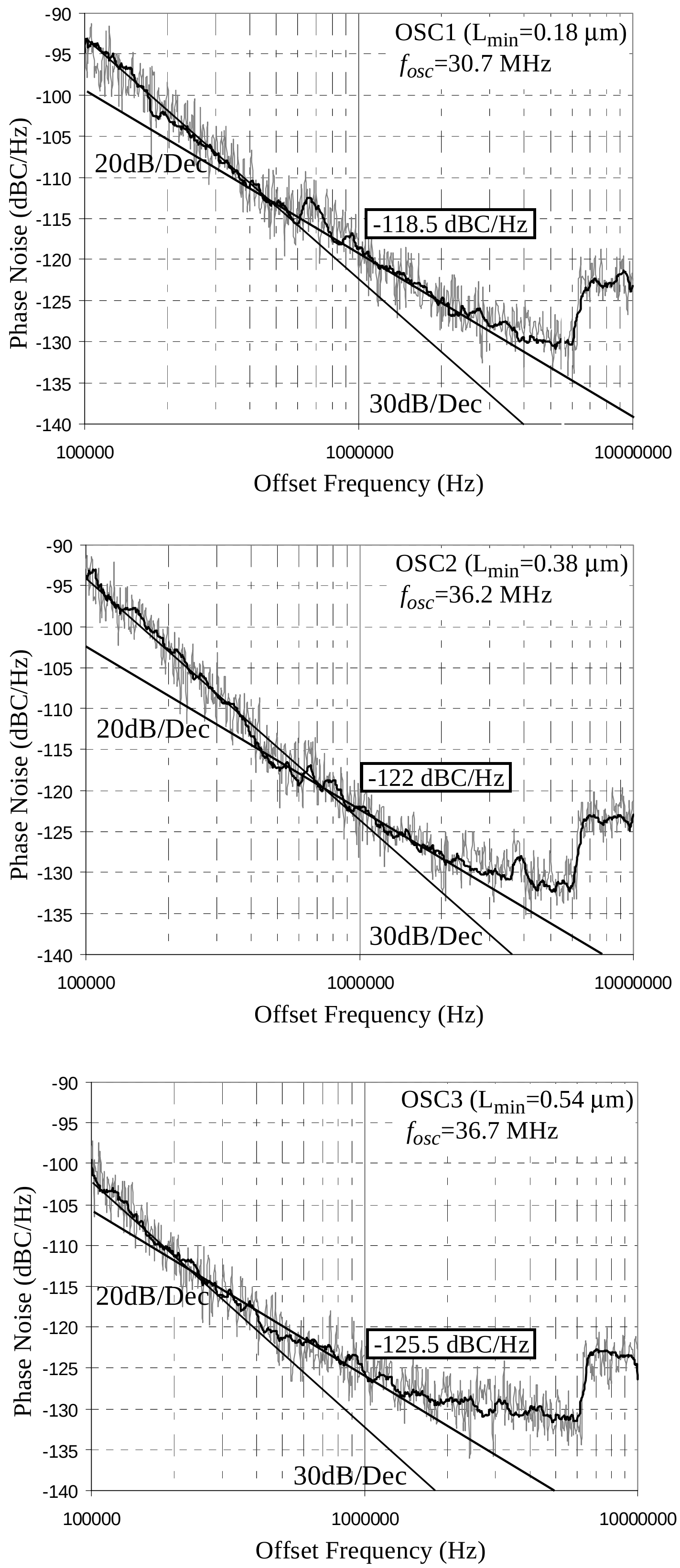

Fig. 40: Phase noise of three asymmetrical ring oscillators.

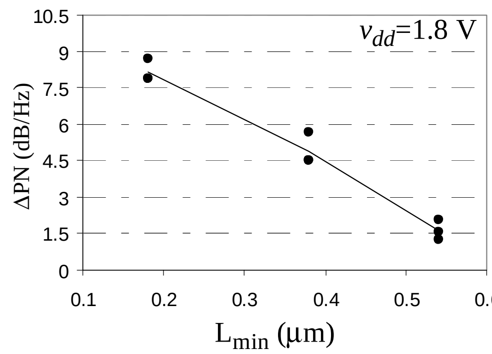

Fig. 41: The difference between minimum achievable phase noise and measured phase noise for oscillators with different minimum channel lengths.

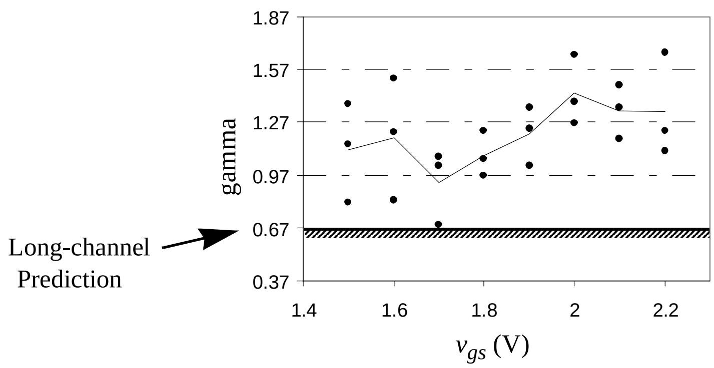

Fig. 42: Gamma factor (extracted from phase noise data) for long-channel (0.54 micron) transistors versus gate-to-source voltage. v_{ds} and v_{gs} are kept equal.

imum-channel-length transistors in this technology is almost four times the noise power of transistors with a channel length of three times minimum channel length in the same technology.

Using the time-domain formulation of phase noise, we can also calculate noise parameters of the transistors from phase noise measurement data. Re-deriving (34) and assuming an unknown gamma factor, we get

$$PN_{meas}(\Delta f) \approx \frac{2(1+4\gamma)f_o kT}{NCv_{dd}^2(\Delta f)^2}, \tag{54}$$

where γ is the gamma factor of the transistors having the dominant effect on the oscillator's phase noise and PN_{meas} is the measured phase noise. All other parameters are the same as those defined in (34). Using (54) we can use phase noise data to calculate the gamma factor of the transistors for various gate to source voltages. Fig. 42 shows the result of such experiment for long-channel (0.54 μm) devices. To change v_{GS}, we change the supply voltage of the oscillator. For the calculation of gamma, we have assumed a room temperature of 300 K and N=3, as justified earlier.

Fig. 42 shows that the gamma factor of our long-channel transistors is generally greater than the long-channel prediction of 0.67 and increases at high gate voltages. The deviation of the gamma factor from its long-channel value and its increase at high gate voltages can be partly attributed to measurement error (notice the scattered data points at each biasing condition). Furthermore, the limited accuracy of our phase noise formulation might have led to some error. For example, our formulation assumes that the NMOS and PMOS transistors are identical in this process. Although we have tried to make these devices identical by appropriate sizing, this assumption can be a source of error in gamma. This kind of error affects the absolute value of gamma but is less likely to affect the relative value of gamma at different gate voltages because the same formulation is used at all data points. The difference between the extracted gamma factor and long-channel prediction can also be an indication of short-channel effects in these transistors. It is possible that longer transistors are needed in order to arrive at the long-channel prediction of gamma.

Although we have tried to increase the accuracy of the data of Fig. 42 through multiple measurements, the variations, due to various sources of noise, are too large to draw a definite conclusion regarding the dependency of gamma factor on the supply voltage. Nevertheless, by looking at the solid line connecting the average values of the data points, one might infer that the gamma factor increases at high supply voltages. This can be due to hot electron effects at excessively high supply voltages; these transistors are designed to work at a nominal supply voltage of 1.8 V.

We can also calculate the noise parameters of short-channel transistors from phase noise measurement results. In this case, however, we cannot calculate gamma using (54) because this equation assumes long-channel I-V relationships which are not valid for short-channel devices. Furthermore, as we discussed earlier, noise mechanisms in short-channel devices are different from long-channel MOSFETs, making gamma a less relevant parameter.

As discussed in Chapter 2, the appropriate noise parameter for short-channel MOSFETs is the shot noise suppression factor, k_s. To extract k_s, we need to re-drive (34) assuming an unknown noise source of $\overline{i_n^2}$ for each MOSFET. It is easy to show that this derivation leads to

$$PN_{meas}(\Delta f) \approx \frac{2kTf_o}{NCv_{dd}^2(\Delta f)^2}\left(1 + \frac{\overline{i_n^2}v_{dd}}{4kTI_C}\right), \tag{55}$$

where I_C is the charging current and all other parameters are the same as those defined in (34). The numerical value of I_C can be found using (31). As before, we assume a room temperature of 300 K and N=3 for this calculation.

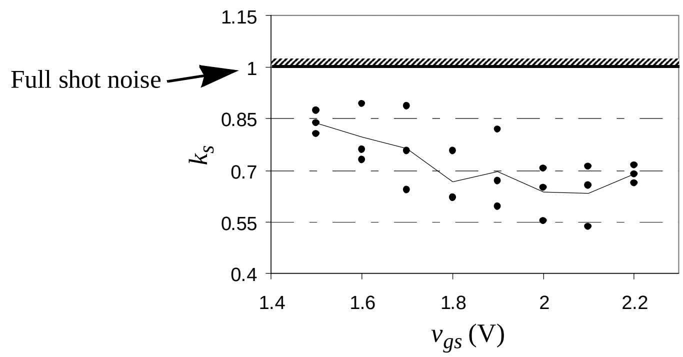

Fig. 43: Shot noise suppression factor for short-channel (0.18 micron) transistors versus gate-to-source voltage. Suppression factors are extracted from phase noise measurement data. v_{ds} and v_{gs} are kept equal.

Fig. 43 shows the extracted value of shot noise suppression factor in short-channel MOSFETs. It can be seen that the suppression factor is close to one in this case and its value drops at higher gate voltage. The apparent slight increase of k_s at v_{GS}=2.2 and 1.9 is within the error bars and thus may be artifacts. The overall drop of k_s at high v_{GS} values is consistent with our model. At high gate voltages, carriers experience more scattering in the channel causing noise power to deviate more heavily from full shot noise. This phenomenon has been discussed in detail earlier in this chapter.

It is instructive to predict the phase noise of ring oscillators assuming full shot noise for its active devices. Using (55) we can show that for $\overline{I_n^2} = 2qI$, phase noise can be written as

$$PN(\Delta f) \approx \frac{2kTf_o}{NCv_{dd}^2(\Delta f)^2}\left(1 + \frac{v_{dd}}{2v_{TH}}\right) = \frac{2kT}{P_{min}}\left(1 + \frac{v_{dd}}{2v_{TH}}\right)\left(\frac{f_o}{\Delta f}\right)^2, \tag{56}$$

where $v_{TH} = kT/q$ is the thermal voltage. Comparing (56) to (34) shows that the phase noise of oscillators built with full-shot-noise devices is always larger than that of those built with long-channel MOSFETs unless v_{dd} becomes smaller than $5.33v_{TH}$, a condition that is unlikely to be satisfied for practical reasons[19]. Thus the phase noise of long-channel-MOSFET ring oscillators will continue to be superior to those built using full-shot-noise devices. However, the phase noise of the oscillators built using full-shot-noise devices gets smaller at lower supply voltages if the power consumption is kept constant. On the other hand, the phase noise of long-channel-MOSFET ring oscillators stays constant with decreasing supply voltage if the power consumption is kept

19. At T=300 K, v_{TH}=26 mV.

constant. Thus, with the decrease of supply voltage in integrated circuits the difference is expected to get smaller. To get the best oscillation performance from the devices which have full shot noise, they should be designed with as low a supply voltage as possible while keeping the power consumption constant.

4.4. SUMMARY

Simulation and measurement results were used to verify the accuracy of the semi-ballistic MOSFET noise model and the time-domain formulation of phase noise presented in the previous chapters. We first used hydrodynamic device simulations to validate our MOSFET noise model. We then used measurement results of the phase noise of ring and other relaxation oscillators and compared the results to the predictions of our time-domain phase noise formulation. Finally, we introduced an indirect device noise characterization method through phase noise measurement. Using our time-domain phase noise formulation and an asymmetrical ring oscillator designed for this purpose, we calculated device noise parameters and showed that their behavior is consistent with the predictions of our model. We used the semi-ballistic MOSFET noise model and the time-domain formulation of phase noise to predict the phase noise of future CMOS ring oscillators.

CHAPTER 5:

CONCLUSIONS AND FUTURE WORK

We have developed a new model for noise in short-channel MOSFETs based on the transport properties of ballistic MOSFETs. Unlike most existing MOSFET noise models, our model does not rely on a long-channel noise formulation. Thus, it does not have to face continual revisions as MOSFET scaling continues and short-channel effects become more severe. According to this model, the major noise phenomenon in short channel MOSFETs is the shot noise generated by the potential barrier next to the source. This noise is partially suppressed due to the finite channel resistance in today's semi-ballistic MOSFETs. We used historical studies on vacuum tubes to avoid a re-derivation of the formulation that already exists for this noise component. Our model shows that excess noise in short-channel MOSFETs is not solely a function of channel length. Rather, it is a result of the competing effects of channel resistance and source injection efficiency. This explains the wide range of reported gamma factors at nearly all channel lengths for the past two decades. The model's prediction of temperature and bias dependencies of MOSFET noise are consistent with detailed hydrodynamic device simulation results. Our study shows that future ballistic MOSFETs are expected to have the high noise power of a BJT and the poor transconductance of a MOSFET. These findings provide useful insight for the design of future MOSFETs and for the prediction of the future of analog CMOS design.

To experimentally validate our model, we introduced a new indirect method for MOSFET noise characterization based on the phase noise of electrical oscillators. As part of our indirect MOSFET noise characterization method, we presented a time-domain formulation for phase noise. In this formulation, the analysis of jitter is performed entirely in the time domain. This analysis is then followed by the calculation of phase noise using pre-derived relationships between jitter and phase noise. When applied to ring oscillators, this time-domain phase noise formulation provides a simple formula which predicts the phase noise of these oscillators within a few dB. The advantage of having this accurate phase noise model is twofold: It can be used to study phase noise for a given device noise level and it can be used for indirect characterization of device noise from phase noise data. Both applications were explored in this work.

Using the time-domain phase noise formulation, we have studied the characteristics of close-in phase noise in ring oscillators and showed that some of the approximations which are routinely used for far-out phase noise are not acceptable at close-in frequencies. Unlike the far-out phase noise, the behavior of close-in phase noise is dependent upon the choice of definition between the two widely accepted definitions of phase noise. We compared these two definitions of phase noise and chose the definition of phase noise as the normalized PSD of the signal for this study. With this definition, phase noise has a Lorentzian spectrum if we assume that the cumulative jitter grows linearly with time. This condition is satisfied if the system does not include any colored noise sources or any poles at frequencies comparable to the offset frequency at which we calculate the phase noise. Therefore, contrary to general belief, white noise sources can, in principle, generate non-Lorentzian phase noise spectra. In practice, however, the deviation of phase noise spectrum from a Lorentzian shape is usually an indication of the presence of a colored noise source because well-designed oscillators rarely have a pole at frequencies comparable to the offset frequency at which we measure phase noise.

The suppression of the effect of low-frequency colored noise on the oscillator's phase noise is possible by switching the noise sources on and off periodically or by symmetrization of the waveform. In single-ended ring oscillators, the switching of transistors is the main suppression mechanism of the effect of $1/f$ noise on the phase noise. On the other hand, symmetrization is most effective for the noise sources which are always on, such as the tail current source in differential ring oscillators. These findings provide insight for efficient design of low-phase-noise electrical oscillators.

To experimentally validate our MOSFET noise model using an indirect device noise characterization method, we designed asymmetrical ring oscillators whose phase noise is accurately predictable using a time-domain phase noise formulation. These oscillators were built with three different channel lengths and it was shown that the phase noise of the oscillator built with short-channel devices is considerably larger than that of the oscillators built with long-channel devices for the same frequency and power consumption. Using the time-domain phase noise formulation we calculated the gamma factor of long-channel devices and shot noise suppression factor of short-channel devices from phase noise data. These calculation show that the gamma factor of long-channel devices is close to the classical prediction of 2/3 while the shot noise suppression factor is close to unity in short channel devices. The bias dependency of this parameter is shown to be consistent with the predictions of our model.

We also studied the phase noise of future ring oscillators. Our time-domain phase noise formulation predicts that the phase noise of the oscillators built with full-shot-noise active devices is always inferior to that of the oscillators built with long-channel MOSFETs. However the difference between the two is expected to shrink as lower supply voltages are used in the former category of oscillators.

Recommendation for future work

Accurate noise modeling for short-channel MOSFETs is of the utmost importance for analog circuit design. A full characterization of MOSFET noise normally includes quantitative analysis of both drain noise and gate noise. The model presented in this work predicts the drain noise by assuming a semi-ballistic carrier transport in the channel. In many applications, MOSFET gate noise is also significant in determining the overall noise performance of analog circuits. Quantitative analysis of this noise component should be possible based on the same assumptions made for drain noise modeling. This is a problem that has not been addressed in this work and awaits to be explored.

In the area of phase noise analysis, we have introduced a time-domain phase noise analysis method and developed a formulation for switching-based oscillators. This method has the advantages of being very simple and providing good intuition about the effect of various noise sources on phase noise. In principle, it should be possible to apply this analysis to other oscillators such as the Colpitts oscillator. This is because well-designed oscillators normally limit the contribution of the active devices to a small time interval in every period to minimize their noise contribution. This feature facilitates the calculation of jitter in the time domain. The development of a time-domain formulation of phase noise for non-switching based oscillators is a problem that is not addressed in this work and needs to be explored in a future study.

The analysis of phase noise with colored noise sources is another problem which is not yet fully addressed. We have developed the relationships between jitter and phase noise for white and Lorentzian jitter spectra in Appendix A. However, to formulate phase noise generated by colored noise sources such as $1/f$ noise, extraction of jitter-phase-noise relationships for such jitter spectra is necessary. This interesting problem is very important in practice for achieving a fast and accurate formulation of phase noise in circuits with colored noise sources.

Indirect characterization of device noise offers a new method and is presented in this work for the first time. We applied this method to the white portion of MOSFET noise. However, this method is much more general and can be applied to many other problems. For example, given an accurate formulation of phase noise generated by colored noise, we can use this method to indirectly characterize $1/f$ noise. Given that this noise component is highly varied and hard to model, this indirect characterization would be very useful from a practical point of view. Also, the noise of emerging devices such as carbon nano-tubes can be studied using indirect characterization of device noise through phase noise data. The oscillator that we introduced for this characterization in this work is only one of many possible circuits that can be designed for this purpose. When working with emerging active devices, other oscillators can be designed to help with this indirect device noise characterization. This is an emerging and promising method which can be of great importance as researchers continue their quest for new devices to replace MOSFETs.

APPENDIX A:

AN ANALYTICAL FORMULATION OF PHASE NOISE

In this Appendix, we present the analytical formulation of the phase noise of a noisy square wave signal with noise-free amplitude and Gaussian-distributed jitter (Fig. 44). This signal can represent both the output of a relaxation or ring oscillator and the output of a limiting amplifier fed by an arbitrary periodic signal. Such amplifiers are routinely used for suppressing amplitude noise in periodic signals. Thus, our formulation is applicable to many oscillatory systems. We consider both white and Lorentzian jitter spectra and discuss the implications of the final equations in each case. Our formulation will improve our understanding of the characteristics of phase noise at close-in frequencies and will facilitate its calculation through time-domain jitter analysis.

To find an analytical expression for the phase noise of the stochastic signal $x(t)$ shown in Fig. 22, we first treat the function $x(t)$ as the sum of rectangular pulses whose start and stop times are a set of random variables:

$$x(t) = \sum_{k=-\infty}^{\infty} u[t - kT_o - a_k] - u\left[t - \left(k + \frac{1}{2}\right)T_o - b_k\right], \tag{57}$$

where u represents a step function, T_o is the nominal period of the signal, and a_k and b_k are random variables characterizing the time fluctuations of the actual rise and fall instants of the signal in the

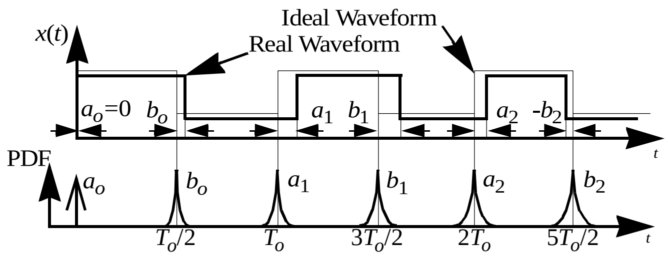

Fig. 44: The noisy signal compared to the ideal noise-free one and the probability density functions (PDF) of the transitions.

kth period with respect to the anticipated rise and fall instants (Fig. 44). The statistical properties of these random variables will be discussed shortly.

We define phase noise as the single-sided power spectral density (PSD) of the signal, normalized to the total signal power. The PSD of a stochastic signal $x(t)$ is given by

$$p(j\omega) = \lim_{T \to \infty} \frac{\overline{\left|X_T(j\omega)\right|^2}}{T}, \tag{58}$$

where $X_T(j\omega)$ is the Fourier transform of the windowed function, $x_T(t)$, which equals $x(t)$ for $|t| < T$ and is zero outside this interval. For simplicity, we set $T = nT_o$ in (58) and evaluate the limit as n goes to infinity.

Since $x(t)$ is real, $|X_T(j\omega)|^2$ can be written as

$$\left|X_T(j\omega)\right|^2 = \left[\int_{-nT_o}^{nT_o} x(t)\sin(\omega t)\,dt\right]^2 + \left[\int_{-nT_o}^{nT_o} x(t)\cos(\omega t)\,dt\right]^2. \tag{59}$$

After inserting $x(t)$ from (57), exchanging the order of integration and summation, and performing the integration, we have

$$\begin{aligned}
&\left|X_T(j\omega)\right|^2 = \\
&\frac{4}{\omega^2}\left[\sum_{k=-n}^{n} \sin\omega\left[\left(k+\frac{1}{4}\right)T_o + \frac{b_k + a_k}{2}\right]\sin\omega\left[\frac{T_o}{4} + \frac{b_k - a_k}{2}\right]\right]^2 \\
&+ \frac{4}{\omega^2}\left[\sum_{k=-n}^{n} \cos\omega\left[\left(k+\frac{1}{4}\right)T_o + \frac{b_k + a_k}{2}\right]\sin\omega\left[\frac{T_o}{4} + \frac{b_k - a_k}{2}\right]\right]^2 .
\end{aligned} \tag{60}$$

where we have also used some triangular identities.

To simplify this equation further, we note that $\left(\sum s_k\right)^2 = \sum\sum s_i s_j$. Using this identity, we convert the squared summations of (60) to double summations and combine them into one:

$$\left|X_T(j\omega)\right|^2 =$$

$$\frac{4}{\omega^2}\sum_{i,j=-n}^{n}\sin\omega\left[\frac{T_o}{4}+\frac{b_i-a_i}{2}\right]\times\sin\omega\left[\frac{T_o}{4}+\frac{b_j-a_j}{2}\right]$$

$$\left\{\sin\omega\left[\left(i+\frac{1}{4}\right)T_o+\frac{b_i+a_i}{2}\right]\sin\omega\left[\left(j+\frac{1}{4}\right)T_o+\frac{b_j+a_j}{2}\right]+\right.$$

$$\left.\cos\omega\left[\left(i+\frac{1}{4}\right)T_o+\frac{b_i+a_i}{2}\right]\cos\omega\left[\left(j+\frac{1}{4}\right)T_o+\frac{b_j+a_j}{2}\right]\right\}. \qquad (61)$$

The expression inside the curvy brackets constitutes the cosine of the difference between $\omega[(i+1/4)T_o+(b_i+a_i)/2]$ and $\omega[(j+1/4)T_o+(b_j+a_j)/2]$. Thus, we can rewrite (61) as

$$\left|X_T(j\omega)\right|^2 = \frac{4}{\omega^2}\sum_{i,j=-n}^{n}\sin\omega\left[\frac{T_o}{4}+\frac{b_i-a_i}{2}\right]\sin\omega\left[\frac{T_o}{4}+\frac{b_j-a_j}{2}\right]$$

$$\cos\omega\left[(i-j)T_o+\frac{b_i-b_j+a_i-a_j}{2}\right]$$

$$=\frac{1}{\omega^2}\sum_{i,j=-n}^{n}\cos\omega[(i-j)T_o+b_i-b_j]+\cos\omega[(i-j)T_o+a_i-a_j]$$

$$-\cos\omega\left[\left(i-j-\frac{1}{2}\right)T_o+a_i-b_j\right]-\cos\omega\left[\left(i-j+\frac{1}{2}\right)T_o+b_i-a_j\right], \qquad (62)$$

where, once again, we have used some triangular identities to arrive at the final form of (62).

The terms inside this double summation are only functions of i-j and not of i or j alone; there is no preferred time spot for the oscillator. We can then replace b_i-b_j by $c_{(i-j)}$, where $c_{(i-j)}$ is the random variable characterizing the fluctuations in the duration of the total time of (i-j) consecutive periods. By the same token, a_i-a_j, a_i-b_j and b_i-a_j can be replaced by $d_{(i-j)}$, $e_{(i-j)}$ and $f_{(i-j)}$, respectively. Hence, the expression inside the double summation of (62) is only a function of $i-j$. This summation can then be simplified as follows:

$$\left|X_T(j\omega)\right|^2 = \frac{1}{\omega^2}\sum_{k=-2n}^{2n}(2n+1-|k|)\left\{\cos\omega[kT_o+c_k]+\right.$$

$$\left.\cos\omega[kT_0+d_k]-\cos\omega\left[\left(k-\frac{1}{2}\right)T_o+e_k\right]-\cos\omega\left[\left(k+\frac{1}{2}\right)T_o+f_k\right]\right\}. \qquad (63)$$

To calculate the expected value of (63), we need to know the statistical properties of c_k, d_k, e_k

and f_k. Due to the linearity of the expected value operator, the expected value of (63) is the sum of the expected values of the individual terms. Since each term is only a function of one random variable, we do not need to have any information about the correlation factors between the random variables involved in this expression. For calculating the expected value of (63) it is sufficient to have the statistical properties of each of the c_ks, d_ks, e_ks and f_ks as stand-alone random variables. Each of these random variables is the sum of several independent, zero-mean, Gaussian-distributed random variables, each of which characterizes the jitter in one half-period of oscillation. Consequently, c_k, d_k, e_k and f_k are all zero-mean, Gaussian random variables as well. We call the variances of these random variables σ_{ck}^2, σ_{dk}^2, σ_{ek}^2 and σ_{fk}^2, respectively.

We can now find the expected value of $\left|X_T(j\omega)\right|^2$ if we note that for a zero-mean, Gaussian random variable p, the expected value of $\cos(ap+b)$ is given by $\exp(-a^2\sigma_p^2/2)\cos b$, where σ_p^2 is the variance of p. Thus, the expected value of (63) is

$$\overline{\left|X_T(j\omega)\right|^2} = \frac{1}{\omega^2}\sum_{k=-2n}^{2n}(2n+1-|k|)\left[e^{-\frac{\omega^2\sigma_{ck}^2}{2}}\cos\omega kT_o + e^{-\frac{\omega^2\sigma_{dk}^2}{2}}\cos\omega kT_o - e^{-\frac{\omega^2\sigma_{ek}^2}{2}}\cos\omega\left(k-\frac{1}{2}\right)T_o - e^{-\frac{\omega^2\sigma_{fk}^2}{2}}\cos\omega\left(k+\frac{1}{2}\right)T_o\right] \quad . \tag{64}$$

To find an analytical expression for phase noise we use (64) in (58), set $T=nT_o$ and evaluate the summation. It can be shown that the part of the summation that includes $(1+|k|)$ is finite, so it vanishes when we evaluate the limit. Consequently, the PSD can be written as

$$p(j\omega) = \frac{2}{\omega^2 T_o}\sum_{k=-\infty}^{\infty}\left\{e^{-\frac{\omega^2\sigma_{ck}^2}{2}}\cos\omega kT_o + e^{-\frac{\omega^2\sigma_{dk}^2}{2}}\cos\omega kT_o - e^{-\frac{\omega^2\sigma_{ek}^2}{2}}\cos\omega\left[k-\frac{1}{2}\right]T_o - e^{-\frac{\omega^2\sigma_{fk}^2}{2}}\cos\omega\left[k+\frac{1}{2}\right]T_o\right\} \quad . \tag{65}$$

To evaluate the summation in (65), σ_{ck}^2, σ_{dk}^2, σ_{ek}^2 and σ_{fk}^2 should be expressed as functions of k. The various c_k and d_k are random variables characterizing the fluctuations of the total time of $|k|$

consecutive periods. Their variances can be replaced by $\sigma_{ck}^2 = \sigma_{dk}^2 = \sigma_{|kTo|}^2$ where $\sigma_{|kTo|}^2$ is the variance of the duration of this time interval. The e_k and f_k are the random variables characterizing the fluctuations of the total time of k consecutive periods minus and plus a half-period respectively. The variance of these random variables can be denoted by $\sigma_{ek}^2 = \sigma_{|(k-1/2)To|}^2$ and $\sigma_{fk}^2 = \sigma_{|(k+1/2)To|}^2$, respectively.

We now make an approximation which facilitates the calculation of phase noise with a Lorentzian jitter spectrum. At small offset frequencies, the fast variations of phase are not important. Thus, we can assume that the jitter occurs entirely in the second half-period and the duration of the first half-period is a deterministic variable. With this assumption one can verify that $\sigma_{ck}^2 = \sigma_{dk}^2 = \sigma_{|kTo|}^2 \approx \sigma_{ek}^2 \approx \sigma_{fk}^2$. We can then simplify (65) to

$$p(j\omega) = \frac{4\left(1-\cos\frac{\omega T_0}{2}\right)}{\omega^2 T_o} \sum_{k=-\infty}^{\infty} e^{-\frac{\omega^2\sigma_{|kTo|}^2}{2}} \cos\omega k T_o = \frac{8}{\omega^2 To} \sum_{k=-\infty}^{\infty} e^{-\frac{\omega^2\sigma_{|kTo|}^2}{2}} \cos\omega k T_o \quad , \tag{66}$$

where the second equality is because $\cos(\omega T_o/2) \approx -1$ around the fundamental frequency. We use (66) for calculating phase noise with a Lorentzian jitter spectrum. With a white jitter spectrum, however, this approximation is not necessary; in that case, we can find phase noise in its exact form.

A.1. PHASE NOISE WITH A WHITE JITTER SPECTRUM

A white jitter spectrum is normally observed in oscillators, which have no colored noise sources and have poles only at frequencies considerably larger than the offset frequency at which we calculate phase noise (Appendix B). With this jitter spectrum, the fluctuations of the duration of different periods are mutually independent. Thus, $\sigma_{ck}^2 = \sigma_{dk}^2 = |k|\overline{(\Delta T_o)^2}$, where $\overline{(\Delta T_o)^2}$ is the variance of the duration of one period. By the same token, $\sigma_{ek}^2 = \left|k\overline{(\Delta T_o)^2} - \overline{(\Delta\tau_1)^2}\right|$ and

$\sigma_{fk}^2 = \left|k\overline{(\Delta T_o)^2} + \overline{(\Delta\tau_1)^2}\right|$, where $\overline{(\Delta\tau_1)^2}$ is the variance of the duration of the first half of the period, which is assumed independent of the variance of the duration of the second half of the period, $\overline{(\Delta\tau_2)^2}$. Using these equations in (65), we get the following closed-form expression for the PSD of the signal:

$$p(j\omega) = \left[8\sinh\frac{\omega^2\overline{(\Delta T_o)^2}}{4}\right]\cdot\frac{\left\{\cosh\frac{\omega^2\overline{(\Delta T_o)^2}}{4} - \cos\frac{\omega T_o}{2}\cdot\cosh\left[\frac{\omega^2\overline{(\Delta T_o)^2}}{4} - \frac{\omega^2\overline{(\Delta\tau_1)^2}}{2}\right]\right\}}{\omega^2 T_o\left[\cosh\frac{\omega^2\overline{(\Delta T_o)^2}}{2} - \cos\omega T_o\right]}. \quad (67)$$

The phase noise is defined as the PSD normalized to the total power of the carrier. We assume that the total power of the carrier is not greatly affected by noise. The total power of the first harmonic of this oscillator is $2/\pi^2$. The phase noise at an offset frequency of $\Delta\omega = \left|\omega - (2\pi)/T_o\right|$ is then given by

$$PN(j\omega) = \sinh\frac{\omega^2\overline{(\Delta T_o)^2}}{4}\cdot\frac{\left\{\cosh\frac{\omega^2\overline{(\Delta T_o)^2}}{4} - \cos\frac{\omega T_o}{2}\cdot\cosh\left[\frac{\omega^2\overline{(\Delta T_o)^2}}{4} - \frac{\omega^2\overline{(\Delta\tau_1)^2}}{2}\right]\right\}}{f^2 T_o\left[\cosh\frac{\omega^2\overline{(\Delta T_o)^2}}{2} - \cos\omega T_o\right]}. \quad (68)$$

Using (68) it can be shown that the phase noise has a nearly-Lorentzian shape around each harmonic. Around the first harmonic, phase noise can be approximated by

$$PN(\Delta f) = \frac{f_o^3\overline{(\Delta T_o)^2}}{\left(\pi f_o{}^3\overline{(\Delta T_o)^2}\right)^2 + (f - f_o)^2}. \quad (69)$$

Fig. 45 compares (68) to (69) around the first harmonic on a logarithmic scale. It can be seen that these two equations are equivalent up to relatively large offset frequencies.

It has been shown that the phase noise of a quasi-sinusoidal signal can also be approximated by a Lorentzian spectrum [55]. Equation (69) extends those results to rectangular pulses. This result is also consistent with other theoretical work on oscillatory systems [39][56].

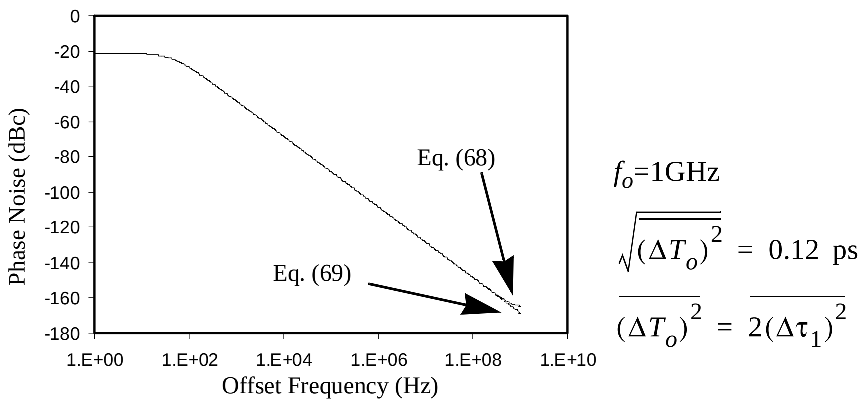

Fig. 45: Comparison of the phase noise predictions of (68) and (69) versus frequency. Design parameters are given in the inset of this figure.

A.2. Phase Noise with a Lorentzian Jitter Spectrum

A Lorentzian jitter spectrum is normally observed in oscillators, which have a dominant Lorentzian noise source and have poles only at frequencies considerably higher than the offset frequency at which we calculate phase noise (Appendix B). With this jitter spectrum, the jitter autocorrelation function is

$$\overline{(a_i - a_{i-1}) \cdot (a_j - a_{j-1})} = A_\theta e^{\frac{-|i-j|T_0}{\theta}} . \tag{70}$$

In this case, we calculate the phase noise using (66). This approach requires us to first calculate the variance of the duration of k consecutive periods, which can be written as

$$\sigma_{Tk}^2 = \overline{\left(\sum_{i=1}^{k} (a_i - a_{i-1})\right)^2} = \sum_{i=1}^{k}\sum_{j=1}^{k} \overline{(a_i - a_{i-1}) \cdot (a_j - a_{j-1})} . \tag{71}$$

Using (70) in (71) we get

$$\sigma_{Tk}^2 = kA_\theta + 2A_\theta \sum_{i=1}^{k} (k-i) e^{-\frac{iT_o}{\theta}} , \tag{72}$$

which after evaluating the summation, gives

$$\sigma_{Tk}^2 = C_\theta + D_\theta k + E_\theta e^{-\frac{kT_o}{\theta}} , \tag{73}$$

where

$$C_\theta = -2A_\theta \frac{e^{-\frac{T_o}{\theta}}}{\left(1 - e^{-\frac{T_o}{\theta}}\right)^2}, \tag{74}$$

$$D_\theta = A_\theta \left(1 + \frac{2e^{-\frac{T_o}{\theta}}}{\left(1 - e^{-\frac{T_o}{\theta}}\right)}\right), \tag{75}$$

and

$$E_\theta = 2A_\theta \frac{e^{-\frac{T_o}{\theta}}}{\left(1 - e^{-\frac{T_o}{\theta}}\right)^2}. \tag{76}$$

Using (73) in (66) we can calculate the PSD of the signal as

$$p(j\omega) = \frac{8}{\omega^2 T_o} \sum_{k=-\infty}^{\infty} e^{-\frac{\omega^2\left(C_\theta + D_\theta k + E_\theta e^{-\frac{kT_o}{\theta}}\right)}{2}} \cos \omega k T_o. \tag{77}$$

After expanding $\exp(-\omega^2 E_\theta \exp(-kT_o/\theta)/2)$ in a power series, (77) becomes

$$p(j\omega) = \frac{8}{\omega^2 T_o} \sum_{k=-\infty}^{\infty} e^{-\frac{\omega^2(C_\theta + D_\theta k)}{2}} \left(\sum_{k'=0}^{\infty} \left(-\frac{\omega^2}{2} E_\theta\right)^{k'} \frac{e^{-\frac{k'kT_o}{\theta}}}{k'!} \right) \cos \omega k T_o. \tag{78}$$

To simplify it further we change the order of summations to get

$$p(j\omega) = \frac{8}{\omega^2 T_o} e^{-\frac{\omega^2 C_\theta}{2}} \sum_{k'=0}^{\infty} \frac{\left(-\frac{\omega^2 E_\theta}{2}\right)^{k'}}{k'!} \sum_{k=-\infty}^{\infty} e^{-\frac{\omega^2}{2}\left(D_\theta + \frac{2k'T_o}{\omega^2\theta}\right)k} \cos \omega k T_o. \tag{79}$$

The inner summation represents a Lorentzian PSD shown in (69) with $\overline{T_{oeq}^2} = D_\theta + (2k'T_o)/(\omega^2\theta)$. We then see that the PSD of the signal with Lorentzian jitter spectrum is a summation of several Lorentzian functions:

$$p(j\omega) = e^{-\frac{\omega^2 C_\theta}{2}} \sum_{k'=0}^{\infty} \frac{\left(-\frac{\omega^2 E_\theta}{2}\right)^{k'}}{k'!} \frac{f_o^3\left(D_\theta + \frac{2k'T_o}{\omega^2\theta}\right)}{\left(\pi f_o^{\,3}\left(D_\theta + \frac{2k'T_o}{\omega^2\theta}\right)\right)^2 + (f-f_o)^2}. \quad (80)$$

which after normalization gives the phase noise as

$$PN(j\omega) = \frac{\sum_{k'=0}^{\infty} \frac{\left(-\frac{\omega^2 E_\theta}{2}\right)^{k'}}{k'!} \frac{f_o^3\left(D_\theta + \frac{2k'T_o}{\omega^2\theta}\right)}{\left(\pi f_o^{\,3}\left(D_\theta + \frac{2k'T_o}{\omega^2\theta}\right)\right)^2 + (f-f_o)^2}}{\sum_{k'=0}^{\infty} \frac{\left(-\frac{\omega^2 E_\theta}{2}\right)^{k'}}{k'!}}. \quad (81)$$

APPENDIX B:

ACCUMULATION OF JITTER WITH WHITE AND LORENTZIAN NOISE SOURCES

We can prove, in general, that cumulative jitter is linearly dependent upon the accumulation time if the following conditions are satisfied. First, all of the noise sources in the system should be white, and second, all poles of the system should be significantly beyond the offset frequency at which we calculate phase noise. The proof is based on elementary circuit theory. Consider an oscillator with P state variables and, therefore, P poles, the smallest of which is denoted by P_s. Also assume that there are several white noise sources in this system. We select the time interval T_T significantly larger than $1/P_s$ and much smaller than $1/\Delta f$ when $\Delta f = f - f_o$ is the offset frequency. Note that this is possible only if P_s is much larger than Δf as required above. Since T_T is much larger than all of the inverse pole frequencies in the system, the values of the state variables at time $2T_T$ are approximately independent of their values at time T_T. Thus, state variables are only a function of the behavior of noise sources in the time interval between T_T and $2T_T$. Since these sources are assumed to be white, their behavior between T_T and $2T_T$ is independent of their behavior between 0 and T_T. Thus the jitter, which is uniquely given by the value of the state variables at the end-points of the cycles, is mutually independent for different T_T-long intervals of time. For a total time of kT_T the cumulative jitter grows linearly with k and is k times the cumulative jitter in each of these intervals. The distribution of jitter inside each of these time intervals is insignificant for the phase noise at Δf because T_T is much smaller than $1/\Delta f$. We can then assume that the distribution of jitter inside each of these time intervals is uniform. With this assumption, jitter will grow linearly with time inside each T_T-long interval of time as well.

In many circuits, if the only noise source of the circuit is a Lorentzian noise and the lowest frequency pole is much higher than the offset frequency at which we calculate phase noise, the cycle-to-cycle jitter drops in a manner similar to a Lorentzian autocorrelation function. This is because in such conditions the period jitters in different periods of the oscillation are correlated mostly through the memory of the noise source which has a Lorentzian autocorrelation function. Thus the correlation between the jitter in different periods of oscillation will drop in a similar manner.

BIBLIOGRAPHY

[1] P. Gray and R Meyer, *Analysis and Design of Analog Integrated Circuits*, New York: Wiley, 1993.

[2] A. J. Scholten, L.F. Tiemeijer, R. van Langevelde, R. J. Havens, A. T. A. Zegers-van Duijnhoven and V. C. Venezia, "Noise modeling for RF CMOS circuit simulation," *IEEE Trans. Electron Devices*, vol. ED-50, pp. 618-632, Mar. 2003.

[3] J. B. Johnson, "Thermal agitation of electricity in conductors," *Physical Review*, vol. 119, pp. 97-109, July 1927.

[4] A. G. Jordan and N. A. Jordan, "Theory of noise in metal oxide semiconductor devices," *IEEE Trans. Electron Devices*, vol. ED-12, pp. 148-156, Mar. 1965.

[5] M. Shonji, "Analysis of high frequency thermal noise of enhancement mode MOS field-effect transistors," *IEEE Trans. Electron Devices*, vol. ED-13, pp. 520-524, June 1966.

[6] R. P. Jindal, "Hot-electron effects on channel thermal noise in fine-line NMOS field-effect transistors," *IEEE Trans. Electron Devices*, vol. ED-33, p. 1395-1397, Sep. 1986.

[7] A. A. Abidi, "High-frequency noise measurements on FET's with small dimensions," *IEEE Trans. Electron Devices*, vol. ED-33, p. 1801-1805, Nov. 1986.

[8] A. Papoulis, *Probability, Random Variables, and Stochastic Processes*, New York: McGraw-Hill, 1991.

[9] S. Kogan, *Electronic Noise and Fluctuations in Solids*, Cambridge: Cambridge University Press, 1996.

[10] H. Nyquist, "Thermal Agitation of Electric Charge in Conductors," *Physical Rev*iew, vol. 32, pp. 110-113, July 1928.

[11] F. Rief, *Fundamentals of Statistical and Thermal Physics*, McGraw-Hill Book Co., New York, 1965.

[12] R. C. Liu and Y. Yamamoto, "Suppression of quantum partition noise in mesoscopic electron

branching circuits," *Physical Review B*, vol. 49, pp. 10520-10532, Apr. 1994.

[13] R. C. Liu, B. Odom, Y. Yamamoto and S. Tarucha, "Quantum interference in electron collision," *Nature*, vol. 391, pp. 263-265, Jan. 1998.

[14] F. M. Klaasen and J. Prins, "Thermal noise of MOS transistors," *Philips Res. Reps.*, vol. 22 pp. 504-514, 1967.

[15] Y. P. Tsividis, *Operation and Modeling of the MOS Transistor*, New York: Wiley, 1987.

[16] A. van der Ziel, *Noise in Solid State Devices and Circuits*, New York: Wiley, 1986.

[17] W. Shockley, J. A. Copeland and R. P. James, "The impedance field method of noise calculation in active semiconductor devices," in *Quantum Theory of Atoms, Molecules and the Sold State*, Edited by Lowdin, pp. 537-563, Academic Press 1966.

[18] J. S. Goo, C. H. Choi, F. Danneville, E. Morifuji, H. S. Momose, Z. Yu, H. Iwai, T. H. Lee and R. W. Dutton, "An accurate and efficient high frequency noise simulation technique for deep submicron MOSFETs," *IEEE Trans. Electron Devices*, vol. ED-47, pp. 2410-2419, Dec. 2000.

[19] F. Danneville, H. Happy, G. Dambrine, J. -M. Belquin and A. Cappy, "Microscopic noise modeling and macroscopic noise models: how good a connection?" *IEEE Trans. Electron Devices*, vol. ED-41, pp.779-786, May 1994.

[20] F. Bonani, G. Ghione, M. R. Pinto and R. K. Smith, "An efficient approach to noise analysis through multidimensional physics-based models," *IEEE Trans. Electron Devices*, vol. ED-45, pp. 261-269, Jan. 1998.

[21] M. Lundstrom, *Fundamentals of Carrier Transport*, Cambridge: Cambridge University Press, 2000.

[22] L. M. Franca-Neto, "Noise in high electric field transport and low noise field effect transistor design: The Ergodic Method," *Ph.D. Dissertation, Department of Electrical Engineering, Stanford University*, May 1999.

[23] D. P. Triantis, A. N. Birbas and D. Kondis, "Thermal noise modeling for short-channel MOSFETs," *IEEE Trans. Electron Devices*, vol. ED-43, pp. 1950-1955, Nov. 1996.

[24] A. J. Scholten, H. J. Tromp, L. F. Tiemeijer, R. Van Langevelde, R. J. Havens, P. W. H. De Vreede, R. F. M. Roes, P. H. Woerlee, A. H. Montree, D. B. M. Klaassen, “Accurate thermal noise model for deep-submicron CMOS,” in *IEEE International Electron Device Meeting (IEDM) Dig. Tech. Papers*, Dec. 1999, pp. 155-158.

[25] C. H. Park and Y. J. Park, “Modeling of thermal noise in short-channel MOSFETs at saturation,” *Solid State Electronics*, vol. 44, pp. 2053-2057, Nov. 2000.

[26] G. Knoblinger, P. Klein and M. Tiebout, “A new model for thermal channel noise of deep-submicron MOSFETs and its application in RF-CMOS design,” *IEEE J. Solid-State Circuits*, vol. SSC-36, pp. 831-837, May 2001.

[27] C. H. Chen and M. J. Deen, “Channel noise modeling of deep submicron MOSFETs,” *IEEE Trans. Electron Devices*, vol. ED-49, pp. 1484-1487, Aug. 2002.

[28] G. Fiori and G. Iannaccone, “Modeling of ballistic nanoscale metal oxide semiconductor field effect transistors,” *Journal of Applied Physics*, vol. 81, pp. 3672-3674, Nov. 2002.

[29] A. Rahman, J. Guo, S. Datta and M. S. Lundstrom, “Theory of ballistic nanotransistors,” *IEEE Trans. Electron Devices*, vol. ED-50, pp. 1853-1864, Sep. 2003.

[30] B. J. Thompson, D. O. North and W. A. Harris, “Fluctuations in space-charge-limited currents at moderately high frequencies,” *Electron Tubes, RCA Review*, vol. 1 (1935-41), pp 58-160.

[31] R. C. Liu and Y. Yamamoto, “Conductance dependent suppression of current partition noise in mesoscopic electron branching circuits,” *Physica B*, vol. 210, pp. 37-42, Apr. 1995.

[32] C. W. J. Beenakker and M. Büttiker, “Suppression of shot noise in metallic diffusive conductors,” *Physical Review B*, vol. 46, pp. 1889-1892, July 1992.

[33] K. E. Nagaev, “Influence of electron-electron scattering on shot noise in diffusive contacts,” *Physical Review B*, vol. 52, pp. 4740-4743, Aug. 1995.

[34] V. I. Kozub and A. M. Rudin, “Shot noise in mesoscopic diffusive conductors in the limit of strong electron-electron scattering,” *Physical Review B*, vol. 52, pp. 7853-7856, Sep. 1995.

[35] C. Dekker, A. J. Scholten, F. Liefrink, R. Eppenga, H. van Houten and C. T. Foxon, “Spontaneous resistance switching and low-frequency noise in quantum point contacts,” *Physical Review Letters*, vol. 66, pp. 2148-2151, Apr. 1991.

[36] A. H. Steinbach, J. M. Martinis and M. H. Devoret, “Observation of hot-electron shot noise in a metallic resistor,” *Physical Review Letters,* vol. 76, pp. 3806-3809, May 1996.

[37] B. Grote, A. Takeuchi, “Noise analysis with Taurus-Device,” *TCAD Times*, Vol XII, no 1, p. 2, Winter 2001, Avant! Corp.

[38] M. Lundstrom, “Device physics at the scaling limit: what matters?” in *IEEE International Electron Device Meeting (IEDM) Dig. Tech. Papers*, Dec. 2003, pp. 33.1.1 - 33.1.4.

[39] A. Demir, A. Mehrotra and J. Roychowdhury, “Phase noise in oscillators: a unifying theory and numerical methods for characterization,” *IEEE Trans. Circuits and Syst. I*, vol. 47, pp. 655-674, May 2000.

[40] J. Rutman and F. L. Walls, “Characterization of frequency stability in precision frequency sources,” *Proceedings of the IEEE*, vol. **79**, pp. 952-960, June 1991.

[41] R. L. Stratonovich, *Topics in the Theory of Random Noise*. New York, NY: Science Publishers, Inc. 1967.

[42] W. F. Egan, *Frequency Synthesis by Phase Lock*, John Wiley and Sons 1981.

[43] A. A. Abidi and R. G. Meyer, “Noise in Relaxation Oscillators,” *IEEE J. Solid-State Circuits*, vol. 18, pp. 794-802, Dec. 1988.

[44] B. Oksendal, *Stochastic Differential Equations*, Springer-Verlag Berlin Heidelberg, 1998.

[45] B. Razavi, “A study of phase noise in CMOS oscillators,” *IEEE J. Solid-State Circuits*, vol. 31, pp. 331-343, Mar. 1996.

[46] J. G. Sneep and C. J. M. Verhoeven, “A new low-noise 100-MHz balanced relaxation oscillator,” *IEEE J. Solid-State Circuits*, vol. 25, pp. 692-698, Jun. 1990.

[47] F. Herzel, M. Pierschel, P. Weger, and M. Tiebout, “Phase noise in a differential CMOS voltage-controlled oscillator for RF applications,” *IEEE Trans. Circuits and Syst. II*, vol. CAS2-47, pp. 11-15, Jan. 2000.

[48] Y. P. Tsividis, *Operation and Modeling of MOS Transistors,* McGraw-Hill Companies, 1999.

[49] J. G. Maneatis and M. A. Horowitz, “Precise delay generation using coupled oscillators,” *IEEE J. Solid-State Circuits*, vol. 28, pp. 1273-1282, Dec. 1993.

[50] H Chang, X Cao, U. K. Mishra, and R. A. York, “Phase Noise in Coupled Oscillators: Theory and Experiment,” *IEEE Trans. Microwave Theory Thech.*, vol. MTT-45, pp. 604-615, May 1997.

[51] A. Hajimiri, S. Limotyrakis, and T. H. Lee, “Jitter and phase noise in ring oscillators,” *IEEE J. Solid-State Circuits*, vol. **34**, pp. 790-804, June 1999.

[52] R. F. Pierret, *Semiconductor Device Fundamentals*, Reading, Massachusetts: Addison-Wesley, 1996.

[53] B. Dierickx and E. Simoen, “The decrease of ‘random telegraph signal’ noise in metal-oxide-semiconductor field-effect transistors when cycled from inversion to accumulation,” *J. Appl. Phys.* **71** (4), 15 February 1992, pp. 2028-2029.

[54] I. Bloom and Y. Nemirovsky, “1/*f* noise reduction of metal-oxide-semiconductor transistors by cycling from inversion to accumulation,” *Appl. Phys. Lett.* **58** (15), 15 April 1991, pp. 1664-1666.

[55] F. Herzel and B. Razavi, “A study of oscillator jitter due to supply and substrate noise,” *IEEE Trans. Circuits and Syst. II*, vol. CAS2-46, pp. 56-62, Jan. 1999.

[56] F. X. Kaertner, “Determination of the correlation spectrum of oscillators with low noise,” *IEEE Trans. Microwave Theory Tech.*, vol. MTT-37, pp. 90-101, Jan. 1989.

[57] W. P. Robins, *Phase Noise in Signal Sources*. London, U.K.: Peter, 1991.

[58] T. H. Lee and A. Hajimiri, “Oscillator phase Noise: A tutorial,” *IEEE J. Solid-State Circuits*, vol. SSC-35, pp. 326-336, Mar. 2000.

[59] L. DeVito, J. Newton, R. Croughwell, J. Bulzacchelli, and F. Benkley, “A 52 MHz and 155 MHz clock-recovery PLL,” in *ISSCC Dig. Tech. Papers*, Feb. 1991, pp.142-143.

[60] I. A. Young, J. K. Greason, and K. L. Wong, “A PLL clock generator with 5 to 110 MHz of lock range for microprocessors,” *IEEE J. Solid-State Circuits*, vol. 27, pp. 1599-1607, Nov. 1992.

[61] C. Jungemann, B. Neinhus and B. Meinerzhagen, “Hierarchical 2-D DD and HD noise simulations of Si and SiGe devices. I. Theory,” *IEEE Trans. Electron Devices*, vol. ED-49, pp. 1250-1257, July 2002.

[62] C. Jungemann, B. Neinhus and B. Meinerzhagen, “Hierarchical 2-D DD and HD noise simulations of Si and SiGe devices. II. Results,” *IEEE Trans. Electron Devices*, vol. ED-49, pp. 1258-1264, July 2002.

[63] C. Jungemann, B. Neinhus, C. D. Nguyen, B. Meinerzhagen, R. W. Dutton, A. J. Schonten and L. F. Tiemeijer, “Hydrodynamic modeling of RF noise in CMOS devices,” in *IEEE International Electron Device Meeting (IEDM) Dig. Tech. Papers*, Dec. 2003, pp. 36.3.1 - 36.3.4.

[64] W. Shockley, “Currents to conductors induced by a moving point charge,” *Journal of Applied Physics*, vol. 9, pp. 635-636, Oct. 1938.

[65] S. Ramo, “Current induced by electron motion,” *Proceedings of the I.R.E.*, Sep. 1939, p. 584.

[66] N. Y. Kim, W. D. Oliver, Y. Yamamoto, J. Kong, and H. Dai, “Quantum Shot Noise Suppression in Single-Walled Carbon Nanotubes,” *Condensed Matter*/0311434, Nov. 2003.